

Instituto Tecnológico y de Estudios Superiores de Monterrey

Campus Monterrey

School of Engineering and Sciences



Differential Transcriptome and Lipidome Analysis of the Microalga
Desmodesmus abundans Under a Continuous Flow of Model Cement Flue
Gas in a Photobioreactor

A thesis presented by

Shirley María Mora Godínez

Submitted to the

School of Engineering and Sciences

in partial fulfillment of the requirements for the degree of

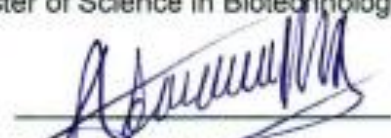
Master of Science

In Biotechnology

Monterrey Nuevo León, December 14th, 2018

Instituto Tecnológico y de Estudios Superiores de Monterrey
Campus Monterrey
School of Engineering and Sciences


The committee members, hereby, certify that have read the thesis presented by Shirley María Mora Godínez and that it is fully adequate in scope and quality as a partial requirement for the degree of Master of Science in Biotechnology,



Dr. Adriana Pacheco Moscoa
Tecnológico de Monterrey
School of Engineering and Sciences
Advisor



Dr. Carolina Senés Guerrero
Tecnológico de Monterrey
School of Engineering and Sciences
Advisor



Dr. Victor Treviño Alvarado
Tecnológico de Monterrey
School of Medicine
Committee Member



Dr. Rocio I. Díaz de la Garza
Tecnológico de Monterrey
School of Engineering and Sciences
Committee Member



Dr. Carlos E. Rodríguez López
John Innes Centre, Norwich
Biological Chemistry Department
Committee Member



Dr. Rubén Morales Menéndez
Associate Dean of Graduate Studies
School of Engineering and Sciences

Monterrey Nuevo León, December 14th, 2018

Declaration of Authorship

I, Shirley Maria Mora Godínez, declare that this thesis titled, "Differential transcriptome and lipidome analysis of the microalga *Desmodesmus abundans* grown under a continuous flow of model cement flue gas in a photobioreactor" and the work presented in it are my own. I confirm that:

- This work was done wholly or mainly while in candidature for a Master of Science degree at this University.
- Where any part of this thesis has previously been submitted for a degree or any other qualification at this University or any other institution, this has been clearly stated.
- Where I have consulted the published work of others, this is always clearly attributed.
- Where I have quoted from the work of others, the source is always given. With the exception of such quotations, this thesis is entirely my own work.
- I have acknowledged all main sources of help.
- Where the thesis is based on work done by myself jointly with others, I have made clear exactly what was done by others and what I have contributed myself.



Shirley María Mora Godínez

Monterrey Nuevo León, December 14th, 2018

©2018 by Shirley Maria Mora Godínez

All rights reserved

Dedication

To God, my family and friends, who have
been my support during this process

Acknowledgements

I would like to express my deepest gratitude first to God, for helping me to continue in adversity and for the infinite blessings. To my family, for always supporting me, for being the engine that pushes me to keep going.

To Dr. Adriana Pacheco, for her valuable support, guidance and time insight throughout this project, for being more than just an assessor and giving me her help whenever I needed it and in everything she could.

Thank you to the student Isis Castrejon for her infinite dedication, support, valuable time and friendship, her role in this project was remarkable, always giving the best of herself.

Thank you to my committee members for their collaboration in reviewing this work, to Dr. Carolina Senés and Dr. Carlos Rodríguez for their support and for answering my doubts during the development of the project. To Dr. Victor Treviño and Dr. Rocío Díaz for their valuable contributions.

I also thank you to Dr. Perla, Lic. Regina, Dr. Cristina Chuck and the student Maru Reyna for their collaboration.

I would like to thank you all my friends, who supported me during this process and always let me know that they are present when I most need them even through the distance.

To my colleagues at the FEMSA Biotechnology Center and master, for sharing pleasant moments, their friendship and support me in several things.

Finally, I thank to Tecnológico de Monterrey for the support on tuition and CONACyT for the support for living.

Differential transcriptome and lipidome analysis of the microalga *Desmodesmus abundans* grown under a continuous flow of model cement flue gas in a photobioreactor

by

Shirley María Mora Godínez

Abstract

Microalgae represent a potential strategy for flue gas mitigation as they capture CO₂ at high rates. Flue gases can also supply certain nutrients and, as a result, it can be valorized through biomass conversion into value-added compounds. The objective of this study was to characterize growth and analyze transcriptome, lipidome and cellular structure and composition of *Desmodesmus abundans* under continuous flow of cement model flue gas (MFG) in a 1 L photobioreactor using two strains adapted for nine years to atmospheres of 50% CO₂ and air, referred to as HCA (high CO₂ acclimated) and LCA (low CO₂ acclimated), respectively. Controls with the LCA strain were also evaluated in air, CO₂ and CO₂+cement kiln dust (CKD). Higher initial growth rates were observed with strain HCA; however, at the end of the run (5 days) similar biomass productivity was reached by the two strains (0.30-0.34 g d.w. L⁻¹ d⁻¹). As expected, the CO₂ control presented the highest growth rate (1.7-fold higher than under MFG), and when CKD was incorporated a slightly decreased (14 %) in growth was observed. Transcriptome analysis by RNA-seq, performed at day 4, resulted in a *de novo* assembly of 70 458 contigs with a N50 of 1 677 bp. Strain comparison under MFG resulted in 16 435 up-regulated and 4 219 down-regulated genes for strain HCA. Most of these genes were related with nucleotide, amino acid and carbon metabolisms; specifically, C3 and C4 cycle, glycolysis and gluconeogenesis, and TCA cycle, where almost all the contigs were up-regulated. In accordance, cell component GO terms up-regulated were in cell wall, chloroplast and photosystems. Likewise, starch and TAG metabolism were up-regulated. Cell structure analysis by SEM and TEM showed that most cells of both strains under MFG were unicellular contrary to typical *Desmodesmus* morphology; under air, some cells still preserved a grouping morphology. Strains cell size under MFG was similar (17-37 μm²), while under air cells were significant smaller (7-13 μm²). Both strains under MFG possessed high content of starch granules, a disorganized chloroplast and several lipid bodies, while a thicker cell wall was only observed in strain HCA. Biomass composition at the end of the run (day 5) showed no differences in proximate analysis between strains under MFG. A 1.8 to 2-fold higher protein

content in strain LCA was found in complete medium (BG-11) than under MFG (BG-11-N-S). Under MFG, LCA presented the highest starch content (47.2 ± 22.3 % d.w) followed by HCA (23.1 ± 4.5 % d.w). On the contrary, HCA showed a higher content of pigments compared to LCA but the highest values were found in the control with only CO₂. Lipidome analysis resulted in 663 detected features. Under MFG no many differences were found between strains by day 5; however, clear differences were observed at day 4 when both strains were in exponential growth. Particularly, 12 glycerolipids (GL) and 18 glycerophospholipids (GP) increased, and 27 GL and 3 GP decreased in HCA compared LCA. Still, most differences were found when strain LCA under MFG was compared with CO₂+CKD (incomplete vs complete culture medium) that showed changes in GL (42 increased and 27 decreased) and GP (58 increased and 42 decreased), possibly attributed to low N in MFG. The results presented in this study show significant differences between strains HCA and LCA under MFG. However, most differences were observed at the transcriptome level (day 4), while biomass production was comparable at the end of the experimental period (day 5). Morphological changes appeared to be induced by the high CO₂ condition at the moment of growth, with no significant differences between acclimated strains, except for a thicker cell wall in the HCA strain. Overall, both strains presented a high content of starch that represents a high value compound under MFG. Further studies could contemplate continuous cultures under MFG with longer experimental periods (>5 days) to validate differences between strains. Also, explore differences between strains at the genome level such as synonymous mutation rates by sequencing and studies of epigenetic changes. Additionally, metabolome and proteome analysis to better understand differences under the different control conditions.

Key words: Microalgae, *Desmodesmus*, flue gas, cement kiln dust, transcriptome, biomass composition, lipidome, cell morphology

List of Figures

Figure 1. CO ₂ concentration mechanism reported for <i>Chlamydomonas reinhardtii</i> (Moroney and Ynalvez, 2007). PM: plasmatic membrane. CE: chloroplast envelope. TM: thylakoidal membrane.	9
Figure 2. Schematic of experimental conditions and controls using <i>D. abundans</i> strains high CO ₂ acclimated (HCA) and low CO ₂ acclimated (LCA) enriched for nine years under atmospheres of 50% CO ₂ and air.	23
Figure 3. Pipeline of the <i>de novo</i> transcriptome analysis of <i>D. abundans</i> under a model cement flue gas.	28
Figure 4. Arithmetic (a) and semi-log (b) representation of growth curves of <i>D. abundans</i> strains HCA and LCA under MFG and controls with LCA strain under air, CO ₂ and CO ₂ +CKD	53
Figure 5. pH (a), dCO ₂ (b) and dO ₂ (c) during culture of <i>D. abundans</i> strains HCA and LCA under MFG and controls with LCA strain under air, CO ₂ and CO ₂ +CKD	54
Figure 6. Sulfate (a), nitrate (b) and nitrite (c) in solution during culture of <i>D. abundans</i> strains HCA and LCA under MFG and controls with LCA strain under air, CO ₂ and CO ₂ +CKD	55
Figure 7. NO _x (a) and SO _x (b) utilization efficiencies of <i>D. abundans</i> strains HCA and LCA under MFG and controls with LCA strain under air, CO ₂ and CO ₂ +CKD in a 1 L column photobioreactor with continuous flow (0.05 vvm), 24 °C, 80-90 μmol PAR-photons m ⁻² s ⁻¹ and 24 h light.	56
Figure 8. BLAST results of the assembled transcriptome using two databases created with the BLAST top-hit species reported for two chlorophyte microalgae, <i>Scenedesmus acutus</i> (Sirikhachornkit <i>et al.</i> , 2018) and <i>Dunaliella tertiolecta</i> (Shin <i>et al.</i> , 2015, Rismani-Yazdi <i>et al.</i> , 2011).	57
Figure 9. Transcriptome analysis of <i>D. abundans</i> strains HCA and LCA grown under MFG (n=3). a) Principal component analysis, b) Heatmap of DEGs (adjusted <i>p.value</i> <0.01, log ₂ FC >2) gradient color represents change in contig expression (red: up-regulated, green: down-regulated), c) Volcano plot of log ₂ fold change against -log ₁₀ (adjusted <i>p.values</i>) and d) Venn Diagram of DEGs	58

Figure 10. Multilevel pie charts of GO annotation enrichment of DEGs (adjusted $p.value < 0.01$, $|\log_2 FC| > 2$) found in *D. abundans* strain HCA against LCA grown under MFG (n=3). a) biological process, b) molecular function and c) cellular component.59

Figure 11. KEGG categories and subcategories of DEGs (adjusted $p.value < 0.01$, $|\log_2 FC| > 2$) found in *D. abundans* strain HCA against LCA grown under MFG (n=3). Only KEGG categories with contig count ≥ 2 are shown. a) Nucleotide metabolism and b) Energy, lipid, carbohydrate, amino acid metabolisms, and other pathways.60

Figure 12. One carbon pool by folate metabolism. a) Pathways showing up and down-regulated enzyme contigs in HCA compared with LCA, red and green arrows indicate up- and down-regulation, respectively, and b) contig ID, $\log_2 FC$ and adjusted $p.values$ for enzyme contigs. ...61

Figure 13. Pyrimidine metabolism described in plants. Red color indicates up-regulated and green down-regulated contigs in HCA strain compared with LCA strain under MFG (Figure adapted from Zrenner *et al.*, 2006). Numbers correspond to enzymes in the list.62

Figure 14. Purine metabolism described in plants. Red color indicates up-regulated contigs in HCA strain compared with LCA strain under MFG (Figure adapted from Zrenner *et al.*, 2006). Numbers correspond to enzymes in the list.63

Figure 15. Proposed diagram of pathways involved in central carbon metabolism based on the transcriptome of *D. abundans* grown under model flue gas after nine years of acclimation under 50% CO₂ and air (HCA and LCA strains)..64

Figure 16. Contigs annotated as cell component GO terms of cell wall, chloroplast and photosystems. $\log_2 FC$ distribution of HCA vs LCA of cell components from a) cell wall, b-d) chloroplast parts and e-f) photosystems.65

Figure 17. $\log_2 FC$ distribution of HCA vs LCA of contigs annotated as cell nitrogen compound transport GO terms.65

Figure 18. Starch metabolism. a) Starch anabolism and catabolism showing up and down-regulated enzyme contigs in HCA compared with LCA, red arrow indicates up-regulation, and b) contig ID, $\log_2 FC$ and adjusted $p.values$ for enzyme contigs.66

Figure 19. Final pathway steps of TAGs biosynthesis. a) TAGs synthesis showing up and down-regulated enzyme contigs in HCA compared with LCA, red arrow indicates up-regulation, and b) contig ID, log ₂ FC and adjusted <i>p.values</i> for enzyme contigs.	67
Figure 20. Transcriptome analysis of <i>D. abundans</i> controls with LCA strain under air, CO ₂ and CO ₂ +CKD (n=2-3). a) Principal component analysis and b) heatmap of DEGs (adjusted <i>p.value</i> <0.01, log ₂ FC >2).....	68
Figure 21. Volcano plot of log ₂ FC against the -log ₁₀ (adjusted <i>p.values</i>) of the transcriptome analysis of <i>D. abundans</i> controls with LCA strain under air, CO ₂ and CO ₂ +CKD.....	69
Figure 22. Multilevel pie charts of the GO annotation enrichment of DEGs (adjusted <i>p.value</i> <0.01, log ₂ FC >2) found in <i>D. abundans</i> control with strain LCA grown under MFG compared with an air atmosphere (n=3). a) biological process, b) molecular function and c) cellular component...70	
Figure 23. Scanning electron micrographs of <i>D. abundans</i> strains. (a-b) HCA strain grown under MFG, (c-d) LCA strain grown under MFG and (e-f) LCA strain grown under air. Magnitude: 1000X (a,c,e), 2000X (b,d) and 2500X (f).....	94
Figure 24. Transmission electron micrographs of <i>D. abundans</i> strains. (a-c) HCA strain grown under MFG, (d-f) LCA strain grown under MFG and (g-i) LCA strain grown under air..	95
Figure 25. Protein fractions of <i>D. abundans</i> strains HCA and LCA under MFG determined by Osborne solubility method.....	95
Figure 26. Starch content of <i>D. abundans</i> strains HCA and LCA under MFG and controls with LCA strain under air, CO ₂ and CO ₂ +CKD.....	96
Figure 27. Chlorophyll <i>a</i> and <i>b</i> , and carotenoids content of <i>D. abundans</i> strains HCA and LCA under MFG and controls with LCA strain under air, CO ₂ and CO ₂ +CKD	96
Figure 28. Untargeted of <i>D. abundans</i> strains HCA and LCA under MFG and controls with LCA strain under air, CO ₂ and CO ₂ +CKD in a 1 L column photobioreactor with continuous flow (0.05 vvm), 24 °C, 80-90 μmol PAR-photons m ⁻² s ⁻¹ and 24 h light. a) Sample lipid extract content, b) principal component analysis of features detected in samples and c) scatter plots between sample comparisons..	97

Figure 29. Total identified lipidic features and cured lipid category level assignation after alignment and gap filling of <i>D. abundans</i> strains HCA and LCA under MFG and controls with LCA strain under air, CO ₂ and CO ₂ +CKD in a 1 L column photobioreactor with continuous flow (0.05 vvm), 24 °C, 80-90 μmol PAR-photons m ⁻² s ⁻¹ and 24 h light.....	98
Figure 30. Differential lipidome analysis of <i>D. abundans</i> strains HCA and LCA under MFG and controls with LCA strain under air, CO ₂ and CO ₂ +CKD	98
Figure 31. Cloud plots representing molecules with significant changes when comparing HCA->MFG vs LCA->MFG (b), LCA->MFG vs LCA->air (c) and LCA->MFG vs LCA->CO ₂ +CKD (d), dots placed in negative m/z represent lipids decreasing, bigger dots indicate higher log ₂ FC and transparency represents less significance.....	99
Figure 32. Glycerolipid and glycerophospholipid changes between strains HCA and LCA under MFG by the 4 day of growth in a 1 L column photobioreactor.....	100
Figure 33. Glycerophospholipid class distributions of <i>D. abundans</i> strains HCA and LCA under MFG, and controls with LCA strain in MFG vs air, and MFG vs CO ₂ +CKD.....	101
Figure 34. Characterization of glycerophospholipids by number of carbons (a-b) and unsaturations (c) significantly decreasing and increasing between experimental group comparison.	102
Figure 35. Characterization of glycerolipids TAG and DAG by number of carbons (a and c) and unsaturations (b and d) significantly decreasing (left) and increasing (right) between experimental group comparison.	103
Figure A. 1. Dissolved sulfate (a), nitrate (b), nitrite (c) and dCO ₂ in BG-11-N-S during aeration with model flue gas (MFG) for 5 d. MFG composition balanced with dry air (v/v) was 25% CO ₂ , 700 ppm NO and 100 ppm SO ₂ . 150 ppm of CKD was added each 24 h.....	109
Figure A. 2. Sample RNA electrophoresis using the Agilent 2100 Bioanalyzer.....	110
Figure A. 3. Sample library electrophoresis after adapter ligation and purification.....	111
Figure A. 4. Sample library size distribution used for RNA-seq.	112

Figure A. 5. Results of the sequencing run (81 bp paired-end) using a MiSeq Illumina sequencer.
a) Reads per sample passing filter (PF), b) nucleotide intensity by cycle, c) QScore distribution
and d) cluster density passing filter (green box plot).....114

Figure A. 6. Results of the sequencing run (300 bp paired-end) using a MiSeq Illumina sequencer.
a) Reads per sample passing filter (PF), b) nucleotide intensity by cycle, c) QScore distribution
and d) cluster density passing filter (green box plot).....115

Figure A. 7. Sample paired read mapping to the *de novo* transcriptome of *D. abundans* using
CLC Workbench Genomics 11.0.....117

List of Tables

Table 1. Culture conditions for experimental and control runs in photobioreactor.	23
Table 2. Equations and units for biomass productivity, CO ₂ fixation rate, total soluble CO ₂ and CO ₂ utilization efficiency (Jiang <i>et al.</i> , 2013).....	25
Table 3. Growth parameters of <i>D. abundans</i> strains HCA and LCA under MFG and controls with AIR strain under air, CO ₂ and CO ₂ +CKD	46
Table 4. Summary of results of the sequencing run (81 bp paired-end) for differential transcriptome analysis using a MiSeq Illumina sequencer.	46
Table 5. Statistics results of the <i>de novo</i> transcriptome assembly of <i>D. abundans</i> using CLC Genomics Workbench 11.0 program.....	47
Table 6. Statistics of completeness of the <i>de novo</i> transcriptome of <i>D. abundans</i> based on the Benchmarking Universal Single-Copy Orthologous (BUSCO) using the eukaryotic lineage dataset ^a	47
Table 7. Contig ID, log ₂ FC and adjusted <i>p.value</i> of DEGs codifying for enzymes in purine and pyrimidine metabolisms from pathways shown in Figures 13 and 14.	48
Table 8. Contig ID, log ₂ FC and adjusted <i>p.value</i> of DEGs codifying for enzymes in central carbon metabolism from pathways shown in Figure 11	49
Table 9. Log ₂ FC and adjusted <i>p.value</i> of the top-hit GO terms in biological process, molecular function and cellular component categories of <i>D. abundans</i> controls with LCA strain under MFG, CO ₂ and CO ₂ +CKD vs air.....	51
Table 10. Cell diameter, area and cell wall thickness of <i>D. abundans</i> strains HCA and LCA under MFG and controls with LCA strain under air, CO ₂ and CO ₂ +CKD.	92
Table 11. Biomass composition of <i>D. abundans</i> strains HCA and LCA under MFG and controls with LCA strain under air, CO ₂ and CO ₂ +CKD	92

Table 12. Ratio of chlorophyll <i>a</i> and <i>b</i> and ratio of total carotenoids and total chlorophyll <i>D. abundans</i> strains HCA and LCA under MFG and controls with LCA strain under air (0.04% CO ₂), 25% CO ₂ and 25% CO ₂ +CKD in a.	93
Table A. 1. RNA quantification and quality parameters.....	110
Table A. 2. Average size and concentration of libraries used to normalize and pool libraries..	113
Table A. 3. Summary of results of the sequencing run (300 bp paired-end) for differential transcriptome analysis using a MiSeq Illumina sequencer.	114
Table A. 4. Species protein sequences used to generate the two databases for transcriptome BLAST analysis.....	116
Table A. 5. Sample paired read mapping to the <i>de novo</i> transcriptome of <i>D. abundans</i> using CLC Workbench Genomics 11.0.....	117

Contents

Abstract	v
List of Figures	vi
List of Tables	vii
1. Introduction	2
2. Theoretical Framework	5
2.1 Global warming	5
2.1 Cement industry	6
2.2 Microalgae	6
2.2.1 Photosynthesis	7
2.2.2 CO ₂ concentration mechanisms (CCM)	8
2.3 Bioremediation of flue gas using microalgae	9
2.4 Transcriptomics in microalgae	10
2.5 Lipid metabolism in microalgae	11
2.5.1 Fatty acids biosynthesis and catabolism	11
2.5.2 Triacylglycerols (TAGs) biosynthesis	12
2.6 Applications of microalgae biomass	13
3. Justification, hypothesis and objectives	15
3.1 Justification	15
3.2 Hypothesis	15
3.3 Objectives	15
3.3.1 General objective	15
3.3.2 Specific objectives	16
4. Study 1: Transcriptome analysis of the microalga <i>Desmodesmus abundans</i> under a continuous flow of model cement flue gas in a photobioreactor	18
4.1 Introduction	19
4.2 Methods	20

4.2.1	Microalga and culture conditions.....	20
4.2.2	Cement model flue gas (MFG) and cement kiln dust (CKD).....	20
4.2.3	Microalga growth under model cement flue gas	21
4.2.4	Growth kinetics and specific growth rate	23
4.2.5	pH, dO ₂ and dCO ₂ analysis	24
4.2.6	Chemical analysis of NO ₂ ⁻ , NO ₃ ⁻ and SO ₄ ²⁻ in solution	24
4.2.7	Determination of CO ₂ , NO and SO ₂ assimilation	24
4.2.8	Statistical analysis	25
4.2.9	RNA extraction.....	25
4.2.10	RNA-seq library construction	26
4.2.11	Transcriptome <i>de novo</i> assembly and functional annotations	26
4.2.12	Differential expression analysis.....	27
4.3	Results.....	28
4.3.1	Microalga growth under MFG and CO ₂ utilization efficiency	28
4.3.2	NO _x and SO _x assimilation.....	30
4.3.3	<i>de novo</i> transcriptome assembly and functional annotation	31
4.3.4	Differentially expressed genes under continuous cement flue gas and nine years of strain enrichment under 50% CO ₂ and air atmospheres.....	32
4.3.5	Differentially expressed genes of <i>D. abundans</i> strain LCA with different components of the model cement flue gas	35
4.4	Discussion	36
4.4.1	Microalga growth under cement model flue gas	36
4.4.2	<i>de novo</i> transcriptome assembly and functional annotations	39
4.4.3	Differentially expressed genes under continuous cement flue gas and nine years of strain enriched in 50% CO ₂ and air atmospheres.....	39
4.4.4	Differentially expressed genes of <i>D. abundans</i> strain LCA with different components of the model cement flue gas	43
4.5	Conclusions	44

Tables and figures.....	46
5. Study 2: Biomass composition and lipidome analysis of the microalga <i>Desmodesmus abundans</i> under a continuous flow of model cement flue gas in a photobioreactor	72
5.1 Introduction.....	73
5.2 Materials and methods.....	74
5.2.1 Microalga and culture conditions.....	74
5.2.2 Microalga growth under model cement flue gas	75
5.2.3 Scanning electron microscopy (SEM) and transmission electron microscopy (TEM)	76
5.2.4 Proximate analysis of microalgae biomass	77
5.2.5 Starch content determination	77
5.2.1 Pigment content determination	77
5.2.2 Statistical analysis	78
5.2.3 Lipidome analysis	78
5.3 Results.....	80
5.3.1 Cell morphology and structure	80
5.3.2 Biomass composition	81
5.3.3 Starch content.....	82
5.3.4 Chlorophyll and carotenoid content.....	82
5.3.5 Lipidome changes of <i>D. abundans</i> under model cement flue gas	82
5.4 Discussion	84
5.4.1 Morphological and structural changes.....	84
5.4.2 Biomass composition	85
5.4.1 Lipidome changes of <i>D. abundans</i> under model cement flue gas	88
5.5 Conclusions	91
Tables and figures.....	92
6. Conclusions	105

6.1	Further studies.....	106
Appendix A		108
6.2	Theoretical dissolved gases.....	108
Appendix B		110
6.3	RNA quality and quantification	110
6.4	RNA-seq library construction	111
6.5	Sequencing results	114
Appendix C		116
6.6	<i>de novo</i> assembly and functional annotations.....	116
Bibliography		118
Curriculum Vitae		130

Chapter 1

Introduction

Chapter 1

1. Introduction

Global warming has emerged as a consequence of increased greenhouse gas (GHG) emissions. CO₂ is the major contributor to this problematic as it represents around 82 % of GHG. The principal industrial sectors contributing CO₂ are the combustion of fossil fuels for energy generation and the cement industry (Shahzad, 2015, WMO and GAW, 2017). Cement manufacturing contributes to global emissions by 6, 2.5 and 1 % of CO₂, NO_x and SO_x, respectively (WBCSD, 2012). Because the accelerated increase of atmospheric CO₂, implementation of biological mitigation systems and renewable energies that replace fossil fuels is a worldwide necessity (Cuellar-Bermudez *et al.*, 2014; Lara *et al.*, 2016).

Microalgae are the only photosynthetic microorganism with the capacity to directly use CO₂ from industrial combustion gases with fixation rates by dozens of times higher than terrestrial crops, which makes them a good alternative for mitigation systems (Fan *et al.*, 2015). Also, other GHGs such as NO_x and SO_x are oxidized in solution to nitrite, nitrate and sulfate and can be assimilated by microalgae (Van Eynde *et al.*, 2016).

Therefore, combustion gases from industries can be used as a nutrient source for microalgae culture, valorizing their fixation through biomass conversion and obtaining compounds of high commercial value such as antioxidants, pigments, proteins, carotenoids, polysaccharides, triglycerides, fatty acids, vitamins, carbohydrates and others (Cheban *et al.*, 2015; Ohse *et al.*, 2014; Duong *et al.*, 2015; Ghosh *et al.*, 2016). One of the major interests in microalgae biomass is based on their potential for biofuel production as biodiesel from lipids or bioethanol from starch fermentation (Bertozzini *et al.*, 2011; Sun *et al.*, 2018). Biofuels obtained from biomass contribute around 10% of the energy demand in the world and are a better alternative because they are carbon neutral, CO₂ generated during combustion is equal or less than the CO₂ captured by microalgae (Perrineau *et al.*, 2014). Using microalgae for biofuel production, average yields can be 10 to 20 times higher than from vegetable oils or oleaginous seeds (Ghosh *et al.*, 2016).

Some advantages in using microalgae over other biological systems are high growth rate, capability to grow in waste water and other low-cost culture media, high biomass productivity up to 75 tons per hectare per year in open bioreactors and cultivation in non-arable lands, therefore, no competition with food production (González-Lopez *et al.*, 2011; Bertozzini *et al.*, 2011; Oshe

et al., 2014; Duong *et al.*, 2015). Also, once a product of interest has been extracted, byproducts like protein, pigments and other compounds can also be harvest from the remaining biomass (Garibay-Hernandez *et al.*, 2009).

Despite microalgae high growth rates and accumulation of macromolecules of interest as lipids and starch, production at large-scale is still not profitable. For economic and environmental feasibility, it is necessary to optimize microalgae characteristics in order to increase biomass productivity in terms of byproducts of interest (Rismani-Yazdi *et al.*, 2011). In particular, when using flue gas as a source of CO₂, it is imperative to understand and associate microalgae response to high CO₂ and other gas components (NO_x and SO_x) at the genome level in order to elucidate biosynthetic pathways, regulatory mechanisms and, potentially, manipulate the processes of CO₂ capture and pathways involve in value-added compound generation (Shin *et al.*, 2015). Next generation sequencing (NGS) has allowed microalga transcriptome studies as this technology can be implemented even when the genome of the organism under study is unknown (Conesa *et al.*, 2016). From these studies several new genes have been identified, such as genes of carbonic anhydrases and regulators of the CO₂ concentration mechanism (Valenzuela *et al.*, 2012).

The microorganism in study, *Desmodesmus abundans* (strain RSM, UTEX no.2976), is an environmental microalga isolated in 2008 by our group from a river in Monterrey, Nuevo León, México (Lara-Gil *et al.*, 2014). The strain has been maintained under high CO₂ (i.e., 50% v/v CO₂) and low CO₂ (i.e., 0.04% CO₂, an air atmosphere) for nine years, which gave rise to the two strains evaluated in this study referred to as high CO₂ acclimated (HCA) and low CO₂ acclimated (LCA), respectively. Lara-Gil *et al.* (2014 and 2016) demonstrated that *D. abundans* tolerates, grows and uses components from cement flue gas as a nutrient source by a supply scheme of 24 h cycles of flue gas and by regulating the pH of the culture medium with cement kiln dust (CKD), another component of cement flue gas. In the present study, one of the main objectives is to scale-up the system and supply a continuous flow of cement flue gas using a 1 L column photobioreactor. Microalgae growth, transcriptome, lipidome and cellular structure and composition would be evaluated using the two strains adapted to atmospheres of 50% CO₂ and air.

Chapter 2

Theoretical Framework

Chapter 2

2. Theoretical Framework

2.1 Global warming

Global warming is referred to as the increase in temperature of the atmosphere and oceans, this problematic has emerged as a consequence of greenhouse gas (GHG) emissions (Shahzad, 2015, WMO and GAW, 2017). Typically, when the sunlight reaches the Earth; clouds, atmospheric particles, reflective ground and ocean surfaces send back to the space near 30 % of infrared rays, the rest is absorbed by oceans, air and land and, as a result, the Earth warms up nourishing life. Nowadays, a large amount of infrared radiation is absorbed by GHG in the atmosphere and radiated back to the Earth surface increasing global warming (Shahzad, 2015).

The major GHG are carbon dioxide, methane, ozone, water vapor and other gases (Dincer *et al.*, 2013; Shazad, 2015). Some of the principal factors that have contributed to the increase of GHG emissions are the growing population, agricultural practices, use of fertilizers, higher land use and deforestation, industrialization and energy obtained from fossil fuel, among others (Dincer *et al.*, 2013; Shazad, 2015, WMO and GAW, 2017). The energy sector that depends fossil fuel combustion contributes to around 68 % of total GHG. The demand for energy increases with economic growth and development, in 2014 global primary energy supply was 150 % more than in 1971, which relies mainly on fossil fuels (IEA, 2016).

CO₂ is the major contributor to global warming since it represents around 82 % of GHG. The concentration of atmospheric CO₂ in the pre-industry (1750) age was 278 ppm; but in 2016 increased by 145 % reaching 403.3 ± 0.1 ppm. Combustion of fossil fuels for energy generation and the cement industry are the principal contributors worldwide, the amount of CO₂ from these sectors in 2015 was of 9.8±0.5 PgC (WMO and GAW, 2017). NOAA (2018) reported an Annual Greenhouse Gas Index (AGGI) in 2017 of 1.41, which showed an increase of 40% since 1990 (26 years), in contrast from 1750 to 1990 (in 240 years) AGGI increased from 0 to 1, reflecting an accelerated increment in GHG.

2.1 Cement industry

Cement manufacturing is the second contributor of GHG worldwide, responsible for 6, 2.5 and 1 % of CO₂, NO_x and SO_x, respectively (WBCSD, 2012). CO₂ is released in the calcination process of limestone, combustion of fuels in the kiln and energy generation (Worrell *et al.*, 2001). Considering the combustion emissions, cement industry contributes with 8% (i.e. 33 billion tons CO₂ in 2010) of the global emission of CO₂, where the coal and natural gas are responsible of 40 and 20 %, respectively; and the remaining comes from transport of raw material and electricity consumed by cement production process (PBL, 2011; WBCSD, 2012). Specifically, in this sector Mexico by 2016 presented the fourteen position among the countries that most contribute to CO₂ emissions, with 17 MtCO₂ (GCA, 2017). CEMEX (2011) reported 41.4 million metric tons CO₂ per 64 million metric tons of cement. Flues gas is compound by 20-25% CO₂ and the rest approximately 101.6 million metric tons to SO_x, NO_x and particulate solid material (Cuellar-Bermudez *et al.*, 2015).

Cement kiln dust is generated in calcination process in around 15-20% per ton of cement (Van Oss and Padovani, 2003). The emission of this pollutant has decreased thanks to improvements in design and operation, among them the use of modern de-dusting equipment. Other components in cement flue gases can be trace metal (Hg, Cd, Sb, As, Pb, Cr, Co, Cu, Mn, Ni and V) which are present in raw material and fuels usually in very low concentrations, and organic micro-pollutants such as polychlorinated dibenzodioxins, dibenzofurans and biphenyls; and polycyclic aromatic hydrocarbons (WBCSD, 2012).

2.2 Microalgae

Microalgae are photosynthetic microorganisms present in almost all habitats of the planet as important constituents of ecosystems, including aquatic bodies like freshwater, marine water and brackish systems; some species can grow on land and are found from hot to very cold temperatures (Oshe *et al.*, 2014; Duong *et al.*, 2015; Ghosh *et al.*, 2016). These microorganisms present several advantages over other biological systems, such as a rapid growth with a duplication time lesser than one day, capacity to grow in waste water and other cheap culture media, possess photosynthetic rates higher than plants and produce biomass rich in protein, lipids, carbohydrates, pigments and other relevant molecules (Bertozzini *et al.*, 2011; Oshe *et al.*, 2014; Duong *et al.*, 2015; Fan *et al.*, 2015; Sun *et al.*, 2018;). Among the photosynthetic organisms, microalgae represent a source of biomass with high potential since they are highly

productive microorganisms, achieving up to 75 tons of biomass per hectare per year in open bioreactors (González-Lopez *et al.*, 2011).

2.2.1 Photosynthesis

Photosynthesis is the metabolic process in which light energy is transformed into chemical energy by the oxidation of water to produce NADPH and ATP, this is known as oxygenic photosynthesis. The process is accomplished in the chloroplast thylakoid membrane, where four multi-subunit membrane-protein complexes catalyze a series of reactions, these are photosystem II and I, cytochrome (cyt) b6f complex and ATP synthase (Nelson and Yocum, 2006). Photosystem II (PSII) and I (PSI) participate in generating a redox potential from the oxidation of water, in this process light energy from two photons is absorbed by antenna pigments and transferred to the reaction centers (PSII and PSI), which allows electron transfer from water to NADP⁺ producing NADPH. Cytochrome (cyt) b6f complex mediates the electron transport between PSII and PSI and converts the redox energy into part of the proton gradient. The proton motive force (pmf) caused is approached by ATP synthase to generate ATP (Nelson and Yocum, 2006; Martínez, 2012). NADPH and ATP are then used by the cell to fix and reduce CO₂ to organic carbon (Gowik and Westhoff, 2011).

In microalgae, CO₂ fixation has been reported to be accomplished by the Calvin-Benson-Bassham cycle (C3) and Hatch-Slack cycle (C4). In C3 cycle, CO₂ capture is catalyzed by ribulose-1,5-bisphosphate carboxylase oxygenase (Rubisco) (Sun *et al.*, 2018). In this process, Rubisco catalyzes the carboxylation of ribulose-1,5-bisphosphate (molecules of 6 C) and originates two molecules of 3-phosphoglycerate (3PGA) (molecules of 3 C), then these molecules are reduced to glyceraldehyde-3-phosphate by consuming two NADPH and three ATPs (Gowik and Westhoff, 2011).

However, Rubisco affinity for CO₂ is low. Under atmospheric conditions, the enzyme uses only 25 % of the catalytic carboxylase capacity since the concentration of dissolved CO₂ is less than the *K_m* (constant of enzyme affinity for substrate). At the same time, atmospheric O₂ competes for the active site of Rubisco, which can also act as an oxygenase. This is known as photorespiration in which fixed CO₂ is released and energy is consumed. Therefore, many microalgae have developed the C4 mechanism, in which photosynthetic carboxylation is improved and photorespiration is reduced by increasing the flow of CO₂ to Rubisco that works more efficiently at high CO₂ concentrations (Moroney and Ynalvez, 2007; Martínez, 2012; Sun *et al.*,

2016). The C4 mechanism is conducted in the cytosol and mitochondria. The initial fixation of CO₂ is catalyzed by the enzyme phosphoenolpyruvate carboxylase (PPC), which forms oxaloacetate (OAA) from CO₂ and phosphoenolpyruvate (PEP). OAA is metabolized to malate, and then decarboxylated to increase the CO₂ concentration around Rubisco. The initial substrate (PEP) of the C4 cycle is obtained from pyruvate by dikinase orthophosphate (PPDK) (Wang et al., 2012; Sun *et al.*, 2016,).

2.2.2 CO₂ concentration mechanisms (CCM)

Carbon dioxide concentration mechanisms have an important role in microalgae photosynthesis process, mainly in C3 cycle for the proper functioning of Rubisco. These mechanisms appear to be regulated according to the availability of CO₂ in the medium, at low CO₂ CCMs are up-regulated, while at high concentration are suppressed (Ramanan *et al.*, 2012; Pessarakli, 2016).

Microalgae can capture different forms of inorganic carbon (Ci) from the medium. In an aquatic environment, and depending on pH, CO₂ or HCO₃⁻ may exist. In an acid pH, most of the Ci is in the form of CO₂, while in an alkaline pH HCO₃⁻ is the major species. A CCM has been reported for the model green algae *Chlamydomonas reinhardtii* (Fig. 3). The mechanism is divided into two phases; a first phase, involves the uptake of CO₂ and HCO₃⁻ from the environment and their release into the chloroplast. Different isoforms of carbonic anhydrase (CA) enzymes participate in this phase, which are in the periplasmic space (CAH1) and cytoplasm (CAH9). In addition, it is hypothesized that there are HCO₃⁻ transporters and CO₂ channels in the plasma membrane and chloroplast envelope (Moroney and Ynalvez, 2007).

The second phase involves the generation of high concentrations of HCO₃⁻ in the chloroplast stroma, using the pH gradient across the thylakoid membrane. In this phase, participate CAs from chloroplast stroma (CAH6) and thylakoid lumen (CAH3), as well as an HCO₃⁻ transporter. This allows to reach high concentrations of CO₂ in the pyrenoid, where Rubisco is located and stimulate the carboxylase activity of the enzyme (Moroney and Ynalvez, 2007; Pessarakli, 2016).

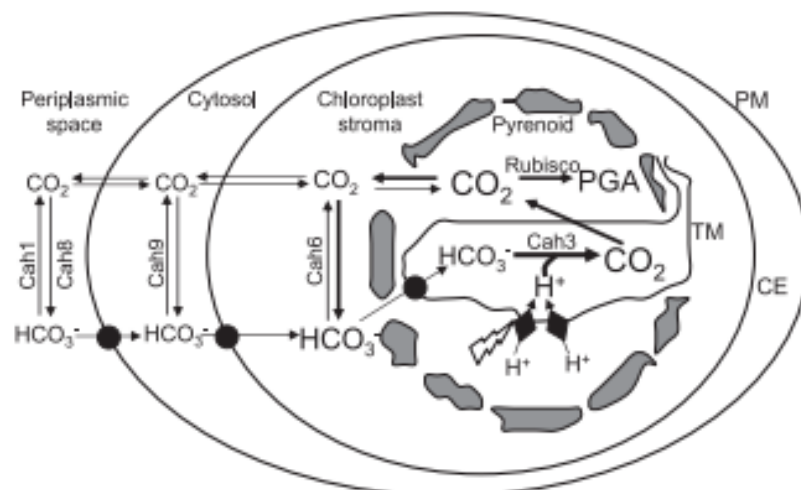


Figure 1. CO₂ concentration mechanism reported for *Chlamydomonas reinhardtii* (Moroney and Ynalvez, 2007). PM: plasmatic membrane. CE: chloroplast envelope. TM: thylakoidal membrane.

2.3 Bioremediation of flue gas using microalgae

Because microalgae are the only photosynthetic microorganism with the capacity to directly use CO₂ from industry combustion gases represent a potential biomitigation strategy for GHG (Cuellar-Bermudez *et al.*, 2014; Lara *et al.*, 2016). Therefore, the use of flue gas as a nutrient source for microalgae and their conversion into valuable products is feasible (Solovchenko *et al.*, 2013; Cuellar-Bermudez *et al.*, 2015; Fan *et al.*, 2015)

Several studies using high CO₂ have been performed for different microalgae species. An example is *Desmodesmus sp.* than under 20 % CO₂ showed two times higher growth rates than under air condition (Solovchenko *et al.*, 2015). Similarly, *Scenedesmus bajacalifornicus* growing in a range of 5 to 25 % CO₂, showed the highest CO₂ fixation rate and biomass productivity at 15 % CO₂ (Patil and Kaliwal, 2017). *Dunaliella salina* and *Chlorella sorokiniana* were also able to grow under high CO₂ (10 %) and increased their lipid content (Muradyan *et al.*, 2004; Sun *et al.*, 2016). *Chlorella pyrenoidosa* grew under CO₂ concentrations from 1 to 20%, showing the highest biomass and lipid productivities under 5% CO₂ (Fan *et al.*, 2015).

Flue gas from cement industry, additionally to CO₂ contains other gases such as NO_x and SO_x, which represent a nutrient source of N and S. In solution they are oxidized to nitrite/nitrate and sulfate and can be assimilated by microalgae (Van Eynde *et al.*, 2016). However, changes in pH because of SO₂ in solution can form bisulfite in low-buffered media, causing a decrease in pH as low as 2-3 and affect microalgae growth. Despite of this drastic changes, culture of different

species of microalgae under optimized conditions using cement flue gas has been reported (Jiang *et al.*, 2013; Talec *et al.*, 2013; Olofsson *et al.*, 2015; Lara-Gil *et al.*, 2016).

Different strategies to control culture pH have been developed. Among them, the use of cement kiln dust (CKD) as a buffering agent, which is a flue gas component represents a no cost strategy that solves a disposable problem for the cement industry (Lara-Gil *et al.*, 2014 and 2016). Tolerance to 10-20 % CO₂, 100-500 ppm NO and 100 ppm SO₂ was observed for *Scenedesmus dimorphus*, and when CaCO₃ was used to control pH, growth in a simulated flue gas (15% CO₂, 300 ppm NO and 400 ppm SO₂) was possible with high biomass production (Jiang *et al.*, 2013). Olofsson *et al.* (2015) cultured *Tetraselmis sp.* and *Skeletonema marioni* under a real mix of cement flue gas and found that it was not toxic for any of these species, besides found a high biomass quality with 20-30 % d.w. lipids, 20-28 % d.w. protein and 15-30 % d.w. carbohydrates. Tolerance to flue gas has also been observed in *Desmodesmus armatus*, which was grown under 15% CO₂, 200 ppm NO and 100 ppm SO₂ and pH was control with phosphate buffer (Guo *et al.*, 2017). Likewise, *Chlorella sorokiniana* presented a high tolerance to a simulated flue gas (18 % CO₂, 300 ppm NO₂ and 140 ppm SO₂), however pH was not control resulting in a decrease of 27 % in growth rate (Camargo and Lombardi, 2017).

Experiments with culture media without N and S source have been realized to evaluate NO and SO₂ as nutrient sources by Lara-Gil *et al.* (2016) and Aslam *et al.* (2017), where in both cases microalgae, *Desmodesmus abundans* (from the present study) and *Desmodesmus spp.* achieved to grow when pH was controlled. Nitrogen and sulfur are essential nutrients for protein synthesis and microalga growth (Perrineau *et al.*, 2014). Aslam *et al.* (2017) cultured a microalgae community under a 100% flue gas from an unfiltered coal-fired power plant. For a better adaptation of microalgae to NO_x and SO_x, culturing by increasing from 10 to 100% flue gas and controlling pH with phosphate buffer were performed, once microalgae diversity decreased *Desmodesmus spp.* was the most representative species.

2.4 Transcriptomics in microalgae

Although microalgae have shown to grow at high rates and accumulate valuable products as lipids and starch under high CO₂, production at large-scale is still not profitable. This is because cultivation and biomass harvest are still highly costly (Shin *et al.*, 2015). For economic and environmental viability, it is necessary to optimize microalga characteristics in order to increase the biomass productivity in terms of byproducts (Rismani-Yazdi *et al.*, 2011). To look for possible

solutions, first must be understood and associate the response of the microalga to high CO₂ and other conditions at the genome level in order to elucidate biosynthetic pathways, regulatory mechanisms and, potentially, manipulate the processes of CO₂ capture and pathways involve in value-added compound generation (Shin *et al.*, 2015).

This knowledge can be generated through next generation sequencing (NGS) of microalga transcriptome under certain condition of interest (for example, high CO₂). NGS allows to study differentially expressed genes related to different catabolic and anabolic pathways, and can be correlated with physiological effect under different growth conditions. This technology is useful when the genome of the organism under study is unknown (Conesa *et al.*, 2016), principally because there are few sequenced genomes of microalgae. Thus, environmental organisms can be analyzed quickly allowing to evaluate potential byproducts of interest, for example, neutral lipids for the generation of biodiesel (Rismani-Yazdi *et al.*, 2011). However, even between phylogenetically close microalgae high genetic variability exists (Yeh *et al.*, 2017), which makes difficult identification of several important genes.

Valenzuela *et al.* (2012) mention that thanks to NGS, transcriptomics studies have been carried out in which new genes have been identified, such as several genes of carbonic anhydrases and regulators of the CO₂ concentration mechanism in microalgae. Most of transcriptome analysis have been related with growth conditions of low and high CO₂, and replete and deplete nutrients and the effect in lipid metabolism (Rismani-Yazdi *et al.*, 2011; Perrineau *et al.*, 2014; Shin *et al.*, 2015; Mansfeldt *et al.*, 2016; Sun *et al.*, 2016; Huang *et al.*, 2017; Sirikhachornkit *et al.*, 2018).

2.5 Lipid metabolism in microalgae

Lipid metabolism in microalgae is similar to plants; particularly, fatty acid and triglycerides synthesis. Homology in sequence and biochemical similarity in some genes and enzymes of the lipid synthesis pathways between plants and microalgae has been demonstrated (Garibay-Hernández, 2009).

2.5.1 Fatty acids biosynthesis and catabolism

Synthesis of fatty acids in microalgae occurs in the chloroplast, where acetyl-CoA is used as precursor to produce saturated palmitic acid (C16:0) and acyl carrier protein (C18:0-ACP). Acetyl-CoA can be obtained from two processes, the direct catalysis of pyruvate by the plastid-localized pyruvate dehydrogenase complex (PDC) that links glycolysis and lipid biosynthesis pathways in

the plastid. The other mechanism is an indirect regeneration from the imported cytosolic acetate, in which pyruvate is converted to acetate by pyruvate carboxylase and aldehyde dehydrogenase, and then the acetate is transported to chloroplast and transfer into acetyl-CoA (Sun *et al.*, 2016). Fatty acid biosynthesis starts with the formation of malonyl-CoA from acetyl-CoA and bicarbonate, this reaction is catalyzed by acetyl-CoA carboxylase. Malonyl is transferred to an acyl-carrier protein (ACP) to obtain malonyl-ACP by malonyl-CoA ACP transacylase enzyme. For fatty acid elongation, malonyl-ACP enters into a series of carbon chain condensation reactions to generate fatty acids of 16 and 18 carbon, where acyl ACP (or acetyl-CoA) are the acceptors and the process is catalyzed by the multiple isoforms of ketoacyl-ACP synthase (KAS) (Rismani-Yazdi *et al.*, 2011; Sun *et al.*, 2016). For the synthesis of unsaturated fatty acids, a double bond is introduced to the acyl group esterified to ACP by the enzyme acyl-ACP desaturase (AAD) (Rismani-Yazdi *et al.*, 2011).

The fatty acid catabolic pathway is called β -oxidation. A process where four enzymes are involved; acyl-coA oxidase (AOx), enoyl-CoA hydratase (ECH), 3-hydroxyacyl-CoA dehydrogenase (CHAD) and acetyl-CoA acyltransferase (ACAT). In this process, cleavage of two carbons from the acyl chain occurs in each cycle by the action of the mentioned enzymes. The acetyl-CoA obtained can be used to produce energy for the cell via the citrate cycle (Rismani-Yazdi *et al.*, 2011).

2.5.2 Triacylglycerols (TAGs) biosynthesis

Triglycerides (TAG) biosynthesis occurs in the cytosol and endoplasmic reticulum (Garibay-Hernández *et al.*, 2009). The precursors for TAG biosynthesis are glycerol-3-phosphate (G-3-P), and acyl-CoA, where G-3-P is produced in the glycolysis or by the action of the enzyme glycerol kinase (GK) on free glycerol; and the acyl-CoA is generated via esterification of fatty acids to coenzyme A (Rismani-Yazdi *et al.*, 2011; Sun *et al.*, 2016)

In the TAG biosynthesis, first occur two sequential esterification of acyl chains from acyl-CoA to positions 1 and 2 of G-3-P, catalyzed by glycerol-3-phosphate O-acyltransferase (GPAT) and 1-acyl-glycerol-3-phosphate O-acyltransferase (AGPAT), respectively. This step results in the generation of phosphatidic acid (PA), that is a key intermediate in the biosynthesis of glycerolipids (Niu *et al.*, 2013). Then the phosphate group is removed from PA by the enzyme phosphatide phosphatase (PP) and diacylglycerol (DAG) is produced. DAG is also an essential intermediate in the biosynthesis of phosphatidylcholine (PC) and phosphatidylethanolamine (PE) A (Rismani-

Yazdi *et al.*, 2011). Then, the next reaction consists in the acetylation of DAG at the position 3 using an acyl donor to generate TAG. Two enzymes appear be responsible of this reaction, the first enzyme is diacylglycerol O-acyltransferase (DGAT), which uses acyl-CoA as an acyl-donor and is probably the principal. The second enzyme is phospholipid: diacylglycerol acyltransferase (PDAT), which uses phospholipids as acyl donors (Rismani-Yazdi *et al.*, 2011)

2.6 Applications of microalgae biomass

Algal biomass contains value-added compounds such as a high protein content, essential amino acids, lipids like fatty acids and TAGs, carbohydrates, pigments, carotenoids, antioxidants, enzymes, polymers, toxins and sterols, among others (Cheban *et al.*, 2015; Ohse *et al.*, 2014; Duong *et al.*, 2015; Ghosh *et al.*, 2016). For this reason and considering the advantages over other biological systems, there is a great interest in their use in the food industry, in agriculture as fertilizers and as third generation biofuels (Ghosh *et al.*, 2016; Sun *et al.*, 2018).

One of the major interests in microalgae biomass is to produce biofuels. Because of fossil fuel depletion and environmental problems such as climate change and global warming as consequence of the increasing emission of GHG, countries have dedicated their efforts to investigate new renewable energy alternatives (Bertozzini *et la.*, 2011; Cuellar-Bermudez *et al.*, 2015; Ghosh *et al.*, 2016). Biofuels obtained from biomass contribute around 10% of the energy demand in the world and are a better alternative because they are not toxic, are carbon neutral, the CO₂ generated during combustion is equal or lesser than the captured by microalgae, and is biodegradable (Perrineau *et al.*, 2014). Microalgae represent a potential source of third-generation biofuel production for their high lipid content and high productivity. The neutral lipids are accumulated in large amounts, from 25 to 50% of dry weight, mainly in form of triacylglycerol (TAG) (Chen, 2011). Using microalgae for biofuel production, the average yield of biofuel can be from 10 to 20 times higher than the yield obtained from vegetables oils or oleaginous seeds (Ghosh *et al.*, 2016).

Likewise, microalgae can be used for bioethanol production since the biomass can provides high content of carbohydrate polymers such as polysaccharide, starch and cellulose for saccharification or degradation of bioethanol. An advantage of their used instead of plants is the low or absence content of lignin making easier the degradation of cellulose and hemicellulose (Sun *et al.*, 2018).

An advantage of the use of microalgae instead of plants for biofuel production is that they are cultivated in non-arable land, therefore, these systems do not affect food supply (Bertozzini *et al.*, 2011). Also microalgae cultures are not affected by weather seasonality as occurs with plants, the lipid composition can be manipulated in function of growth conditions, sub-products such as protein, carbohydrates, pigments, and other compounds, can be obtained once the lipids have been extracted; at the same time this technology can be coupled with mechanisms of CO₂ mitigation from industrial emissions and presented biodiesel productivities higher than plants with rates of 12000-20000 L/ha/year, while this value in plants are from 446 L/ha/year in soybean to 5950 L/ha/year in palm (Garibay-Hernandez *et al.*, 2009).

Microalgae also offer a wide range of value-added bioactive compounds, such as polyunsaturated fatty acids (PUFAs) such as docosahexaenoic acid (DHA), eicosapentaenoic acid (EPA) and arachidonic acid (AA), which have important physiological functions, preventing high cholesterol, myocardial infarction and improving high blood pressure (Niu *et al.*, 2013). Marine oil derived long-chain n-3 fatty acids such as C18:4 has shown being effective in health benefits in humans related to cardiovascular disease (Yao *et al.*, 2015). The algal biomass is used as animal feed, in diets of juvenile fish, crab, shellfish rotifer and cladoceran because of their high bioactive compounds (Li *et al.*, 2014). Also, this is considered a potential source to replaced conventional feed supplements for aquaculture because their high lipid and protein content (Sun *et al.*, 2018).

Glycolipids have different biological applications like antiviral, antitumor, anti-inflammatory, and immune-suppressive activities. For example, phytosterol has shown beneficial health effects, including cholesterol-lowering activity. Besides, chlorophylls are natural food coloring agents and valuable bioactive compounds that present antimutagenic activity and other health benefits (Yao *et al.*, 2015). TAGs and starch can be used as precursors for production of other bio-based products such as plastics, cosmetics, and surfactants (Rismani-Yazdi *et al.*, 2011).

Chapter 3

3. Justification, hypothesis and objectives

3.1 Justification

As a first approach in this study, transcriptome analysis of the enriched microalga strains (high CO₂ acclimated – HCA and low CO₂ acclimated - LCA) will allow to characterize differential response of *Desmodesmus abundans* under continuous cement flue gas and after nine years of enrichment under atmospheres of 50% CO₂ and air. Thus, pathways related with CO₂ fixation could be elucidated as a strategy to adapt or tolerate high CO₂. In addition, biosynthesis pathways of value-added compounds such as lipids and starch can be identified to proposed biomass byproducts during flue gas mitigation. In parallel, biomass composition and lipidome analysis will be performed to validate and characterize potential byproducts. With this study, we pretend to propose an optimized and profitable mitigation system that possesses high fixation rates of flue gas, high biomass productivity and generation of value-added compounds. At the same time, the *de novo* transcriptome of *D. abundans* would function as a platform for other studies as this species has not been previously characterized.

3.2 Hypothesis

The adaptation or tolerance of *D. abundans* to high CO₂ and other flue gas components after nine years of acclimation to atmospheres of 50% CO₂ and air, involves changes in gene expressions and metabolic profiles that can be measured by transcriptome and lipidome analysis, as well as cellular structure and composition.

3.3 Objectives

3.3.1 General objective

Characterize growth and analyze transcriptome, lipidome and biomass composition of the microalga *Desmodesmus abundans* grown under continuous flow of model cement flue gas in a 1 L column photobioreactor using the strains acclimated for nine years to 50% CO₂ and air atmospheres, with the purpose of optimize CO₂ capture and propose high value byproducts.

3.3.2 Specific objectives

1. Establish culture conditions for *D. abundans* strains in a 1 L column photobioreactor using a continuous flow of model cement flue gas as a nutrient source in an incomplete culture medium (BG11-N-S).
2. Characterize growth kinetics and utilization efficiencies of CO₂, NO_x and SO_x of *D. abundans* strains grown under an optimum supply of model cement flue gas in a 1 L column photobioreactor.
3. Establish differential transcriptome changes of *D. abundans* strains acclimated for nine years to 50% CO₂ and air, and grown under optimum conditions in a 1 L photobioreactor with model cement flue gas.
4. Characterize cellular structure and composition of *D. abundans* strains grown under optimum conditions in a 1 L photobioreactor with model cement flue gas by scanning and transmission electron microscopy (SEM and TEM), proximal analysis and pigment and starch quantification.
5. Characterize the lipidome of *D. abundans* strains grown under optimum conditions in a 1 L photobioreactor with model cement flue gas by HPLC-TOF MS.

Chapter 4

Study 1: Transcriptome analysis of the microalga *Desmodesmus abundans* under a continuous flow of model cement flue gas in a photobioreactor

Chapter 4

4. Study 1: Transcriptome analysis of the microalga *Desmodesmus abundans* under a continuous flow of model cement flue gas in a photobioreactor

Abstract

Microalgae represent a potential strategy for flue gas mitigation as they capture CO₂ at high rates. Flue gases can also supply certain nutrients and, as a result, it can be valorized through biomass conversion into value-added compounds. The objective of this study was to characterize growth and the transcriptome of *Desmodesmus abundans* under an optimized supply scheme of continuous flow of cement model flue gas, using BG-11-N-S, in photobioreactor using two strains adapted for nine years to 50% CO₂ (HCA strain) and air (LCA) atmospheres. Controls with the HCA strain were also evaluated in air, CO₂ and CO₂+cement kiln dust (CKD). Higher initial growth rates were observed with HCA strain; however, at the end of the run (5 days) similar biomass productivity was reached by the two strains (0.30-0.34 g d.w. L⁻¹ d⁻¹). As expected, the CO₂ control presented the highest growth rate (1.7-fold higher than MFG), and when CKD was incorporated a slightly decreased (14 %) in growth was observed. Transcriptome analysis by RNA-seq was performed at day 4, resulting in a *de novo* assembly of 70 458 contigs with a N50 of 1 677 pb N50. Strain comparison under MFG resulted in 16 435 up-regulated and 4 219 down-regulated genes for HCA strain. Most of these genes were related with nucleotide, amino acid and carbon metabolisms; specifically, C3 and C4 cycle, glycolysis and gluconeogenesis, and TCA cycle, where almost all the contigs were up-regulated. In accordance, cell components GO terms up-regulated were in cell wall, chloroplast and photosystems with 7, 30 and 63 contigs, respectively. Likewise, starch and TAG metabolism were up-regulated in HCA strain. Control comparisons with strain LCA revealed that under MFG compared to air differences were related to down-regulation of photosynthesis genes. The results presented here show significant differences between strains HCA and LCA under MFG. Most of differences were observed at transcriptome level in central carbon metabolisms, TAG and starch metabolism and cellular component related with photosynthesis and cell wall and but not in growth. Further studies under flue gas using continuous cultures with longer experimental period than 5 days could validate differences in growth and transcriptome between strains HCA and LCA.

Key words: Microalgae, *Desmodesmus*, flue gas, cement kiln dust, transcriptomic

4.1 Introduction

CO₂ is the major contributor of greenhouse gases (GHG) since it represents around 82 %. Atmospheric CO₂ increased in a 145% of the pre-industry (1750) age, reaching 403.3 ± 0.1 ppm. Combustion of fossil fuels and cement industry are the principal sectors responsible of this increased (Shahzad, 2015, WMO and GAW, 2017). Cement manufacturing, being the second sector that most contribute to global GHG emissions, provides 6%, 2.5% and 1% of CO₂, NO_x and SO_x, respectively (WBCSD, 2012). Because the accelerated increase of CO₂ the implementation of biological mitigation systems and renewable energies is necessary. Particularly, microalgae represent an attractive strategy since they are the only photosynthetic microorganism with the capacity to directly use CO₂ from combustion gases of industry with CO₂ fixation rates by dozens higher than terrestrial crops (Cuellar-Bermudez *et al.*, 2014; Fan *et al.*, 2015; Lara *et al.*, 2016).

Flue gas from cement industry can be used as nutrient sources for microalgae culture, valorizing their fixation through biomass conversion and obtaining compounds of high commercial value such as antioxidants, pigments, proteins, carotenoids, polysaccharides, triglycerides, fatty acids, vitamins, carbohydrates and other (Cheban *et al.*, 2015; Ohse *et al.*, 2014; Duong *et al.*, 2015; Ghosh *et al.*, 2016). Despite microalgae present high growth rates and accumulate lipids and starch under high concentrations of CO₂, and other flue gases the production at large-scale is still not profitable. To established economic and sustainable systems more metabolic mechanisms must be elucidated and correlated to microalga response to high CO₂ and other components of flue gas, and potentially, manipulate the processes of CO₂ capture and pathways involve in value-compound generation (Shin *et al.*, 2015).

This knowledge can be generated through new generation sequencing (NGS) of microalga transcriptome under certain condition of interest (for example, high CO₂), since this technology can be implemented even when the genome of the organism under study is unknown (Conesa *et al.*, 2016). NGS allows to determine differential expression genes related with different pathways, and then be correlated with physiological effect under the different growth conditions. Thus, environmental organisms little studied can be analyzed quickly allowing to evaluate the potential in obtaining bioproducts of interest, for example, neutral lipids for the generation of biodiesel (Rismani-Yazdi *et al.*, 2011). Most of transcriptome analysis have been related with growth conditions of low and high CO₂; and replete and deplete nutrients, as well as their effect in lipid metabolism (Rismani-Yazdi *et al.*, 2011; Perrineau *et al.*, 2014; Shin *et al.*, 2015; Mansfeldt *et al.*,

2016; Sun *et al.*, 2016; Huang *et al.*, 2017; Sirikhachornkit *et al.*, 2018). However, even between close phylogenetically microalgae exist a high genetic variation (Yeh *et al.*, 2017), which makes difficult the identification of several important genes.

The microorganism in study, *Desmodesmus abundans* (strain RSM, UTEX no.2976), is an environmental microalga isolated in 2008 by our group from a river in Monterrey, Nuevo León México (Lara-Gil *et al.*, 2014). The strain has been maintained under high CO₂ concentrations, 25 and 50% CO₂, and air for nine years. Lara-Gil *et al.* (2014 and 2018) demonstrated that *D. abundans* can tolerate, grow and used components from cement flue gas as nutrient sources by a supply scheme of 24 cycles of flue gas. In the present study, the growth and transcriptome of the microalga *Desmodesmus abundans* under an optimize supply scheme of continuous flow of cement flue gas in a 1 L column photobioreactor was analyzed, using the strains adapted for nine years to 50% CO₂ and air atmospheres.

4.2 Methods

4.2.1 Microalga and culture conditions

Desmodesmus abundans strain RSM (UTEX 2976) was isolated from an environmental sample collected in 2008 by our research group from a freshwater river (pH 7.4) in the city of Monterrey, Nuevo Leon, Mexico. The strain was isolated after sample enrichment under an atmosphere of 25% CO₂ (Lara-Gil *et al.*, 2014). In addition, *D. abundans* has been maintained for around nine years under atmospheres of air (0.04% CO₂) and 50% CO₂ in 125 mL flasks containing 20 mL of BG-11 medium, pH 7.4 (UTEX 2009). Cultures were maintained every 10 d in batch and the pH was not controlled during growth. Enriched CO₂ atmospheres were obtained by using rubber stoppers and removing with a 60 mL syringe the corresponding volume of air from the headspace and adding the same volume of 99.9% (v/v) CO₂ (AOC Mexico, NL, Mexico). Cultures were incubated at 25 ± 2 °C, 60-70 μmol PAR photons m⁻² s⁻¹ of continuous light, and 110 rpm agitation using an orbital shaker. For experimentation, *D. abundans* acclimated to atmospheres of 50% CO₂ and air were studied and referred to as strains HCA (high CO₂ acclimated) and LCA (low CO₂ acclimated), respectively.

4.2.2 Cement model flue gas (MFG) and cement kiln dust (CKD)

Simulated model flue gas (MFG) components represented exhaust gas from a modern cement plant with a desulfurization system; concentrations used approximate maximum reported values

(WBSCD, 2012; LRTAP and EEA, 2016). Hence, the model cement flue gas consisted of 250 000 ppm CO₂, 700 ppm NO and 100 ppm SO₂ (in v/v). Independent mass flow meters were used to aerate each gas to a principal line, balanced with dry air, and delivered to the photobioreactor at a flow rate of 49 mL min⁻¹ (0.05 vvm). Two Smart-Trak 2 Series 100 (Sierra Instruments, Monterrey, CA, USA) were used for CO₂ and extra dry air, and two Side-Trak Series 840 for NO and SO₂. The gas mixture was filtered at the reactor inlet with 0.2 µm PTFE membranes (Corning, NY, USA). CO₂ (99.9%) was purchased from AOC Mexico (NL, Mexico) and extra dry air, 1.29% v/v NO (balance with N₂) and 0.352% v/v SO₂ (balance with N₂) were provided by Praxair Mexico (NL, Mexico).

Cement kiln dust (CKD) was also considered as a component of the flue gas and was used as a strategy to control culture pH (Lara-Gil *et al.*, 2014 and 2016). CKD was collected from a local cement plant in Hidalgo (NL, Mexico) and sterilized by thinly spreading 150 mg into a polystyrene weighing dish and exposing it to UV light for 30 min under a laminar flow cabinet. CKD was delivered to the bioreactor (150 ppm) daily by dissolving 150 mg in 11 mL of fresh culture media (see Section 4.2.3).

4.2.3 Microalga growth under model cement flue gas

D. abundans was cultured in a 1 L customized column photobioreactor (6 cm diameter, 45 cm height) with 980 mL working volume at 25 ± 2 °C and continuous illumination. Temperature was controlled by a water jacket made of glass covering the column and the illumination by four external fluorescent lamps (4000 K cool white, Philips) placed around the column, which provided 80-90 µmol PAR-photons m⁻² s⁻¹ to the interior of the vessel. Gas was supplied to the reactor at a continuous flow of 49 mL min⁻¹ (0.05 vvm) by a sparger stone at the bottom of the column and axis with metal meshes of 1 mm distributed each 5 cm and covering the entire diameter of the bioreactor were used for gas retention.

For experimentation, culture medium without nitrogen and sulfur (BG-11-N-S) was used to evaluate the potential of the cement flue gas as nutrient source of N and S. Therefore, NaNO₃ and MgSO₄·6H₂O were replaced with NaCl and MgCl₂·6H₂O, respectively, to provide the same Mg and Na concentration and preserve the conductivity of the medium. Before microalga inoculation under model flue gas, 580 mL of BG-11-N-S with 150 mg of CKD were aerated with flue gas for 4 h to provide N and S and avoid microalga starvation. During this period of time, flue gas consisted of 35-40% NO and SO₂ concentration (i.e., 233 ppm NO and 40 ppm SO₂), and

25% CO₂. Then, 400 mL of medium containing the inoculum was added and, from this moment on, an acclimation period of 24 h was conducted under the same flue gas conditions. After the acclimation period, gas concentrations were set to the simulated cement flue gas (25% CO₂, 700 ppm NO, 100 ppm SO₂) and 150 ppm w/v of CKD was added every 24 h. Initial biomass concentration in the bioreactor was normalized to Abs_{750 nm} 0.13 ± 0.02 (0.15 ± 0.05 g d.w. L⁻¹) of an active $\frac{3}{4}$ log phase culture. These were previously grown in 500 mL flasks containing 75 mL of BG-11 medium and 25 mL of inoculum ($\frac{3}{4}$ log phase) for a final work volume of 100 mL, and 50% CO₂ and air (0.04% CO₂) atmosphere were supplied according to the strain (See section 4.2.1) used. Before normalization, the inoculum was harvest by centrifugation (5000 rpm, 15 min, 4°C) and the pellet washed with the experimental medium (BG-11-N-S) for MFG runs.

Experiments under MFG were conducted with the strains HCA and LCA to compare strains differential responses to flue gas after nine years of enrichment (Fig. 2, Table 1). In addition, the LCA strain was used to analyze the effect of MFG main components. Control runs in complete culture medium (BG-11) contemplated aeration with only air, 25% CO₂ and 25% CO₂+CKD, in order to assess the effect of CO₂, CKD and the source of N and S. In the control CO₂+CKD, the addition of CKD was performed as in the MFG experiments (i.e., 150 ppm every 24 h). To maintain experimental culture pH in the controls, as with the supply of MFG, the initial pH of BG-11 medium was adjusted to 6.2 using a phosphate buffer (pH 6.2). All runs were sampled every 24 h by removing 11 mL of the culture and centrifuged (5000 rpm, 5 min, 4°C) to generate a cell pellet that was used to determine biomass productivity and the supernatant was collected for chemical analysis, as described in the next sections.

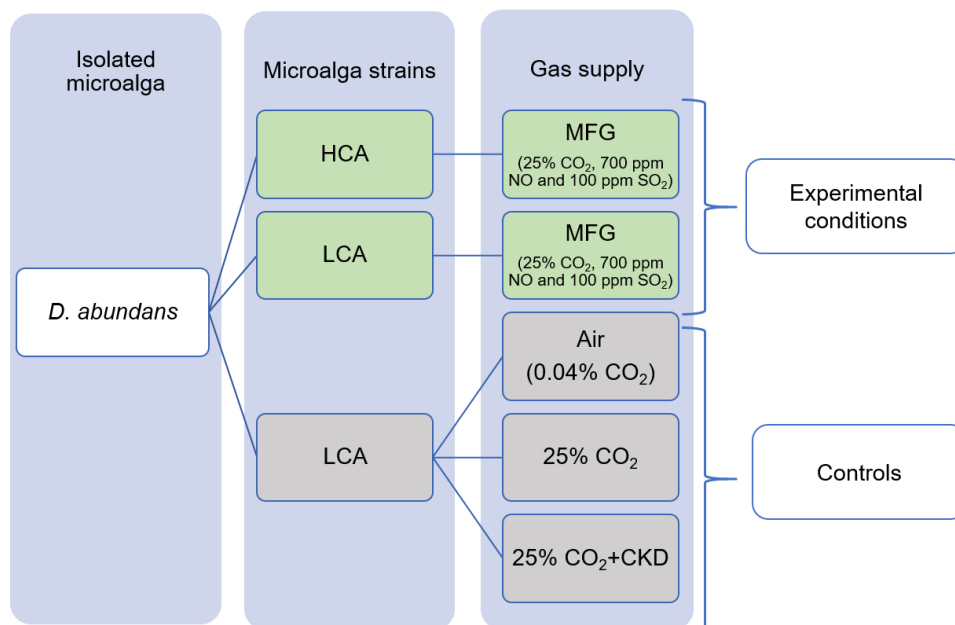


Figure 2. Schematic of experimental conditions and controls using *D. abundans* strains high CO₂ acclimated (HCA) and low CO₂ acclimated (LCA) enriched for nine years under atmospheres of 50% CO₂ and air.

Table 1. Culture conditions for experimental and control runs in photobioreactor.

Microalga strain	Gas supply	pH control method (6-7)	Culture medium	Objective
HCA	MFG	CKD	BG-11-N-S	Differential response of the strains and MFG effect
LCA	MFG	CKD	BG-11-N-S	
LCA	Air	KH ₂ PO ₄	BG-11	Low CO ₂ concentration
LCA	25% CO ₂	KH ₂ PO ₄	BG-11	High CO ₂ concentration
LCA	25% CO ₂ +CKD ^a	CKD+KH ₂ PO ₄	BG-11	CKD effect, and N and S source

Each run contemplated 3-6 independent replicates. HCA: high CO₂ acclimated. LCA: low CO₂ acclimated. MFG: model flue gas. CKD: cement kiln dust.

^a 150 ppm every 24 h as for MFG.

4.2.4 Growth kinetics and specific growth rate

Cell growth was assessed daily during the experimental period by sampling 11 mL of the bioreactor and determining optical absorbance at 680 and 750 nm ($Abs_{680\text{ nm}}$ and $Abs_{750\text{ nm}}$), and direct cell counting under the microscope using a Neubauer hematocytometer. Absorbance was

measured under the linear range of 0.5-1.5 using a GENESYS 10S UV-VIS spectrophotometer (Thermo Scientific, DE, USA).

Growth kinetics were determined according to the model $\ln(X/X_0)$ vs time, where X is the biomass obtained per day and X_0 the biomass at the start of bioreactor run, from here the slope in exponential growth phase corresponds to specific growth rate (Becker, 1994).

4.2.5 pH, dO_2 and dCO_2 analysis

Culture pH, dissolved O_2 (dO_2) and dissolved CO_2 (dCO_2) were determined daily, in a 2 mL sample from the bioreactor using a pH sensor (Model Z001023551, AppliSens®, Scheidam, Holland), dO_2 sensor (Model Z010023525, AppliSens®, Scheidam, Holland) and Carbon Dioxide Gas-Sensing Electrode (Van London-pHoenix Co., TX, USA). For dCO_2 measurements, 2 mL of the sample were added to a 15 mL Falcon tube containing 200 μ L of ionic strength adjuster solution (Cat. No.C021S01, London-pHoenix Co., TX, USA). Readings were taken once stabilized.

4.2.6 Chemical analysis of NO_2^- , NO_3^- and SO_4^{2-} in solution

Nitrite, nitrate and sulfate in solution were monitored daily during the experiment following standard methods for water and wastewater analysis (APHA-AWWA-WEF, 2012): 4500- NO_2^- B Colorimetric Method, 4500- NO_3^- B Ultraviolet Spectrophotometric Screening Method and 4500- SO_4^{2-} E Turbidimetric Method, respectively.

4.2.7 Determination of CO_2 , NO and SO_2 assimilation

To determine carbon assimilation, biomass concentration (d.w. $g L^{-1}$) was measured daily from 11 mL of sample that were centrifuged (see Section 4.2.3), the pellet stored at $-80^\circ C$ for at least 24 h, lyophilized for 48 h and quantified by weight. CO_2 utilization efficiency was calculated accordingly to equations described by Jiang *et al.*, 2013 (Table 2). N and S fixation rates were estimated according to biomass productivity, considering microalgae elemental composition, $CO_{0.48}H_{1.83}N_{0.11}P_{0.01}S_{0.01}$ (Radmann *et al.*, 2011).

In table 2, biomass productivity (P) was determined considering initial (X_0) and maximum X_{max} biomass concentrations and change in time (Δt). CO_2 fixation rate (Fc) considered the P, a 50% as carbon content of microalga dry biomass; and the carbon and CO_2 molecular weights (12 and 44 g/mol). Finally, the utilization efficiency (Ec) was calculated utilizing the Fc and only theoretical

soluble CO₂ fraction during the elapsed time (SC), which was estimated using the flux (0.05 vvm), corresponding gas concentration and solubility in water (Appendix A, Table A.1).

Table 2. Equations and units for biomass productivity, CO₂ fixation rate, total soluble CO₂ and CO₂ utilization efficiency (Jiang *et al.*, 2013).

Parameter	Equation	Units
Biomass productivity (P)	$P = \frac{\Delta X}{\Delta t} = \frac{X_{\max} - X_0}{\Delta t}$	g d.w. L ⁻¹ d ⁻¹
CO ₂ fixation rate (Fc)	$F_c = \frac{P \times 50\%}{12} + 44$	g CO ₂ L ⁻¹ d ⁻¹
CO ₂ utilization efficiency (Ec)	$E_c = \frac{F_c}{M_c} \times 100\%$	%

4.2.8 Statistical analysis

One-Way Analysis of Variance (ANOVA) was performed to compare group means of the different set of data using Minitab® 18 (Minitab Inc., PA, USA). Differences among groups were assessed with Tukey's HSD test. An alpha of 0.05 was used for all tests.

4.2.9 RNA extraction

A sample (7 mL) of the bioreactor at day 4 was centrifuged (5000 rpm, 5 min, 4°C) to generate a pellet that was frozen in liquid nitrogen and stored at -80 °C until RNA extraction. Cell lysis of 60-80 mg of frozen pellet was performed using lysis matrix E (MP Biomedicals, CA, USA), 1 mL of lysing buffer (RNeasy Plant Mini Kit; Qiagen, USA) and the FastPrep®-24 Homogenizer (MP Biomedicals, CA, USA) set at 6 m s⁻¹ for 40 s. The mixture was centrifugated at 12000 rpm for 10 min and the supernatant retrieved. RNA was extracted using the RNeasy Plant Mini Kit (Qiagen, USA).

RNA quality and quantity were evaluated by agarose gel electrophoresis, Nanodrop 1000 spectrophotometer (Thermo Scientific, USA) and the Agilent 2100 Bioanalyzer (Agilent, USA). Quality parameters evaluated were: rRNA Ratio [28s/18s] ≥1, OD 260/280 ≥1.9, OD 260/230 ≥1.5 and RNA Integrity number (RIN) >7-8, as described by Johnson *et al.*, 2012.

4.2.10 RNA-seq library construction

A total of 12 samples with three replicates for MFG experiments with HCA and LCA strains and two replicates for control runs (air, CO₂ and CO₂+CKD) were used to generate cDNA libraries using 500 ng of total RNA and following the TruSeq RNA Sample Prep v2 LS Protocol (Illumina, CA, USA). Pool libraries were normalized to 11 pM and 1% v/v of 11 pM PhiX sequencing control was added. Two paired-end sequencing runs were performed (2x306 bp and 2x81 bp) using the MiSeq Reagent Kit v3 on the MiSeq Sequencer (Illumina, USA). For *de novo* transcriptome assembly both runs were used that resulted in 2.75 and 5.44 Gbp of information, respectively (Appendix B, Fig. A.5-A.6). Then, the 2x81 bp run (5.44 Gbp) was utilized for differential expression analysis which corresponded to 65 957 802 reads passing filter, a %Q30 \geq of 92.18 and an error rate of 0.036% (Table 4).

4.2.11 Transcriptome *de novo* assembly and functional annotations

The transcriptome analysis pipeline is presented in figure 3. The protocol contemplates raw data trimming, *de novo* assembly, assessment of the assembled transcriptome, annotation of the contigs and differential expression analysis. Reads from 81 bp paired-end and 300 bp paired-end libraries were used for the transcriptome assembly. Data processing and *de novo* assembly were performed using CLC Workbench Genomics 11.0 (Qiagen, USA). Sequencing QC reports were generated to assess raw data quality. Adaptors and low-quality reads were removed using Trim Reads tool, trimmed reads were merged and used for *de novo* assembly. The parameters for the assembly were: for word and bubbled size were used the values assigned by default (24 and 50, respectively), a penalty value of 3 for mismatch, deletion and insertion costs; 200 bp as minimum contig length, 0.5 for length fraction and 0.95 of similarity fraction. The *de novo* transcriptome was evaluated according to the read percentage mapping back to the assembly and N₅₀ length statistics obtained from CLC Workbench Genomics, the completeness was assessed using BUSCO program (Benchmarking Universal Single-Copy Orthologs) (Simão *et al.*, 2015) against the eukaryotic lineage dataset (303 BUSCOs from 100 species) and redundant contigs were determined utilizing CD-HIT-EST program (Huang *et al.*, 2010) for sequence identities of 95 and 100%. Gene ontology terms were assigned with Blast2GO 5 (Conesa *et al.*, 2005) and genes were classified as encoding cellular components, proteins with molecular functions, or proteins involved in biological processes.

For BLAST, first a data base with the BLAST top-hit species reported for a phylogenetically close microalga, *Scenedesmus acutus*, plus *Arabidopsis thaliana* and *Scenedesmus quadricauda* (Sirikhachornkit *et al.*, 2018) and a second data base using the BLAST top-hit species for *Dunaliella tertiolecta* (Shin *et al.*, 2015, Rismani-Yazdi *et al.*, 2011) plus other algae, bacteria and plants, were created and used for BLAST process. All the species included in each data base are shown in (Appendix C, Table A.4). Then, contigs still without results were blasted utilizing the non-redundant protein data base from NCBI (<ftp://ftp.ncbi.nlm.nih.gov/blast/db/FASTA/nr.gz>). Finally, Enzyme code (EC) and Biochemical pathway were assigned using KEGG Pathway maps (Kanehisa and Goto, 2000).

4.2.12 Differential expression analysis

The reads quantification and differential expression genes analysis were performed using CLC Workbench Genomics 11.0. The trimmed paired reads from each individual growth condition were mapped against the *de novo* transcriptome and quantified using the RNA-seq Analysis tool, default parameters were used. Expression tracks obtained from quantification step were used to identify differentially expressed genes (DEGs) among experimental groups. The Differential Expression for RNA-seq tool fits a Generalized Linear Model (GLM) using the Wald test and assumes a Negative Binomial distribution for the read count, and the *p.values* are corrected by false discovery rate (FDR) using Benjamini and Hochberg's method (Benjamini and Hochberg, 1995). Threshold values of $FDR < 0.01$ and a $|\text{Log}_2(\text{fold change})| > 2$ were set to defined DEGs. To visualize DEGs, volcano plots, heatmap and clustering plots were generated.

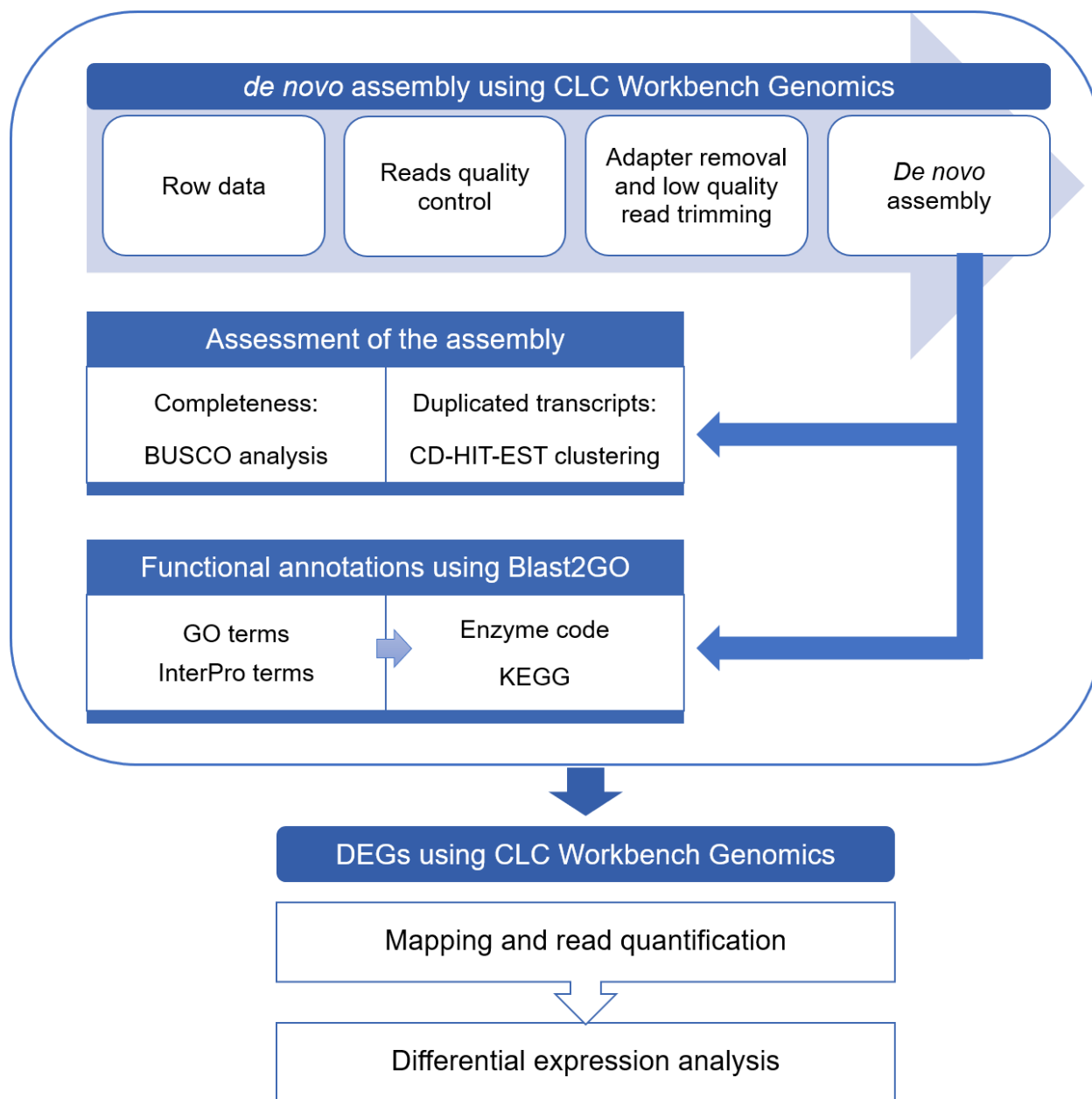


Figure 3. Pipeline of the *de novo* transcriptome analysis of *D. abundans* under a model cement flue gas.

4.3 Results

4.3.1 Microalga growth under MFG and CO₂ utilization efficiency

As a first approach to evaluate the capability of the microalga strains to use a continuous flow of flue gas as a nutrient source, *D. abundans* strains HCA and LCA were grown under MFG using an incomplete medium (BG-11-N-S) and compared to controls (Fig. 4a-b). After the acclimation period (24 h), all treatments started to grow exponentially, except for the control under air where

a lag phase was evident until 96 h. The strain HCA in MFG grew at a higher rate from the start of the run compared to strain LCA; however, strain LCA reached similar biomass production by the end of the experimental period when HCA was already entering into the stationary phase. As expected, controls in complete medium, where only the LCA strain was used, reached the highest cell concentrations under 25% CO₂ only followed by 25% CO₂+CKD control, whereas inferior growth was observed under an air atmosphere (0.04% CO₂).

Maximum specific growth rates between strains under MFG did not show significant differences with values of 0.79 ± 0.14 and 0.65 ± 0.13 d⁻¹ for strain HCA and LCA, respectively (Tukey' HSD test, $\alpha=0.05$) (Table 3). Control runs with the LCA strain showed that a higher growth rate was observed with only CO₂ (1.7-fold higher) compared to MFG experiment and that the presence of CKD reduced the rate by 14 % (Tukey' HSD test, $\alpha=0.05$). Concerning biomass productivity, a similar trend was observed among treatments, except for the control in an air atmosphere that showed the highest growth rate but did not produced compared biomass in the experimental period. Strains under MFG produced between 0.30-0.34 g d.w. L⁻¹ d⁻¹. As expected, under CO₂ only the highest biomass was produced (0.53 g d.w. L⁻¹ d⁻¹) but when CKD was incorporated a significant decrease of 34 % was observed (Tukey' HSD test, $\alpha=0.05$). There were no differences in productivity between treatments under MFG and CO₂+CDK in incomplete and complete culture medium, respectively.

CO₂ fixation rate based on biomass productivity was 0.55-0.63 g CO₂ L⁻¹ d⁻¹ for both strains under MFG, which corresponded to a CO₂ utilization efficiency of 2.03-2.34 % (Table 3). The control with only CO₂ showed the highest fixation rate (0.97 ± 0.08 g CO₂ L⁻¹ d⁻¹) with a utilization efficiency of 3.61 % (Tukey' HSD test, $\alpha=0.05$). However, there were no significant differences in CO₂ utilization efficiencies for all runs, except for the control under an air atmosphere that presented the highest efficiency (100%) with the lowest fixation rate (0.09 g CO₂ L⁻¹ d⁻¹).

During the photobioreactor runs, pH, dCO₂ and dO₂ were monitored through time (Fig. 5). Because pH under MFG experiments was controlled between 6.0-6.5 by incorporating CKD (150 ppm d⁻¹), in control runs phosphate buffer (pH 6.2) was used. Initial pH, after 4 h of aeration and before inoculation, for all runs was between 5.7 and 6.4 (Fig. 5a). When the total amount of flue gas was supplied to the system, after the 24 h acclimation period, pH was not affected allowing microalga growth and the pH to gradually increase to around 6.4. Both strains under MFG showed similar pH patterns. Maximum final pH (7.14 ± 0.23) was observed in the control under an air atmosphere followed by the CO₂ controls (Fig.5a).

As expected, continuous aeration of 25% CO₂ in the photobioreactor under MFG increased dCO₂ to a maximum average of 30-32 % by day 5 (Fig. 5b). Controls with CO₂ exhibited final values between 35-36 % dCO₂. Also, dO₂ accumulated during the run after dilution by 25% CO₂. For MFG runs, maximums reached 102 and 127 % dO₂ for strains HCA and LCA, respectively; while controls were between 89-122 % dO₂ (Fig. 5c).

4.3.2 NO_x and SO_x assimilation

Dissolved NO_x and SO_x compounds in the culture medium were monitored during microalga growth under MFG (incomplete medium) and the controls (complete medium) (Fig. 6). Under MFG, nitrogen concentration from dissolved NO₃⁻-N and NO₂⁻-N was detectable at the beginning of the experimental period (0.6 and 0.5 mg L⁻¹ of NO₃⁻-N and NO₂⁻-N, respectively), after 4 h of bubbling NO abiotically. These values reached 19 and 118 mg L⁻¹ when in abiotic conditions showing flue gas can provide NO₃⁻-N and NO₂⁻-N as nutrient sources (Fig. A.1). However, the NO_x concentration was lower in MFG runs than the supply in complete medium (354 ± 21 mg L⁻¹) by 60% at the end of run.

In abiotic conditions, after 24 h and before a 100% NO was supplied to the system, differences between strains were evident. NO₃⁻-N and NO₂⁻-N accumulated under growth of the strain LCA to day 3, contrary to strain HCA (Fig. 6a-b). In strain LCA values reached 9 ± 1 and 42 ± 5 mg L⁻¹ of NO₃⁻-N and NO₂⁻-N, respectively, and then decreased to 0.1 ± 0.0 and 0.06 ± 0.83 mg L⁻¹ by day 4. For strain HCA, only NO₃⁻-N increased with time to 0.98 ± 0.16 mg L⁻¹ (Fig. 6a-b). Control runs showed initial NO₃⁻-N values that corresponded to the original culture medium recipe (354 ± 21), which decreased with time to a final concentration of 299 ± 5, 109 ± 12 and 218 ± 1 mg L⁻¹ for air, CO₂ and CO₂+CKD controls, respectively (Fig. 6a). NO₂⁻-N in control runs was minimal and increased with time for CO₂ and CO₂+CKD to around 3 mg L⁻¹, while the control under air increased during the last day of the run to 2 ± 1 mg L⁻¹ (Fig. 6b).

Dissolved SO₄²⁻ under MFG was also detected from the beginning of the experimental period and accumulated with time to 219 ± 33 and 207 ± 35 mg L⁻¹ for strain HCA and LCA, respectively (Fig. 6c). As expected, controls consumed sulfate provided by the culture medium (88 ± 4) to 53 ± 10 and 0.13 ± 0.93 mg L⁻¹ under air and CO₂, respectively. The CO₂+CKD control also showed increments in sulfate concentration up to 164 ± 6 mg L⁻¹ by day 3, after three additions of CKD, and decreased to 89 ± 3 mg L⁻¹ by day 5.

NO_x and SO_x fixation rates were determined based on biomass productivity (Fig.7). Both strains under MFG presented NO_x fixation rates around 0.06-0.07 g L⁻¹ d⁻¹, which corresponded to 95-100% assimilation efficiency (Fig. 7a). Statistical differences were found among controls in complete BG-11 (Tukey' HSD test, $\alpha=0.05$), the CO₂ control presented the highest fixation rate (0.11 ± 0.01 g L⁻¹ d⁻¹) followed by the CO₂+CKD (0.07 ± 0.01 g L⁻¹ d⁻¹) and the air atmosphere (0.01 ± 0.00 g L⁻¹ d⁻¹). Similarly, there were no differences in SO_x fixation rates between strains under MFG (Tukey' HSD test, $p.value=0.05$), with values around 0.005-0.0062 g L⁻¹ d⁻¹. In addition, the same pattern was observed for the controls in complete medium, where CO₂ had the highest efficiency and air the lowest efficiency, with an average of 0.0097 and 0.0009 g L⁻¹ d⁻¹, respectively.

4.3.3 *de novo* transcriptome assembly and functional annotation

A total of 72 766 244 trimmed reads from both sequencing runs (2x81 and 2x306 bp) were used to assemble the *de novo* transcriptome using CLC Genomics Workbench 11.0 program. Transcriptome assembly resulted in 70 458 contigs with an average length of 881 bp and a 50th percentile (N50) of 1 677 bp (Table 5). In addition, completeness of the transcriptome was assessed with the BUSCO program and the eukaryotic lineage dataset (Table 5). A total of 277 out of 303 BUSCOs (91.4 %) were obtained from the assembled transcriptome, which were characterized by 236 complete (77.9 %) and 41 fragmented (13.5 %) BUSCOs.

Overall alignment rates of 91-92 % were obtained when the individual samples were mapped to the assembled transcriptome using only data of the 2x81 bp run (Appendix C, Table A.6). The proportion of redundant contigs determined in the CD-HIT-EST Program was 0.37 % and 0.01 % with a similarity of 95 % and 100 %, respectively (data not shown).

For transcriptome annotation, two databases were created with the BLAST top-hit species reported for phylogenetically close microalgae and other relevant organisms (Appendix C, Table A.5). The first database constructed with *Scenedesmus acutus* BLAST top-hit (Sirikhachornkit *et al.*, 2018) plus *S. quadricauda* and *Arabidopsis thaliana* resulted in 3048 hits, with most hits corresponding to *Monoraphidium neglectum*, *Chlamydomonas reinhardtii* and *Volvox carteri f. nagariensis* (Fig. 8a). In the second analysis, based on *Dunaliella tertiolecta* (Shin *et al.*, 2015, Rismani-Yazdi *et al.*, 2011), other algae, bacteria and plants; 3711 hits were obtained, where *Raphidocelis subcapitata*, *Chlamydomonas eustigma* and *Gonium pectoral* contained the most hits (Fig. 8b).

4.3.4 Differentially expressed genes under continuous cement flue gas and nine years of strain enrichment under 50% CO₂ and air atmospheres

As a first overview of gene expression of *D. abundans* strains under MFG, a principal component analysis (PCA) is shown in Figure 9a. Strains HCA and LCA were separated into two groups by component 1, explaining 67.1 % of data variability. In the case of the LCA strain, the component 2 (10.8 %) divided among replicates. Differential expression analysis showed that strain HCA under MFG presented 16 435 up-regulated genes and 4 219 down-regulated genes when compared to strain LCA (adjusted $p.value < 0.01$, $|\log_2 FC| > 2$). The heatmap in Figure 9b reflects this finding by the normalized expression level of each sample and DEG. Also, it showed hierarchical clustering of two groups that corresponded to the replicates of each strain. The volcano plot visualized the dispersion of $p.values$ and $\log_2 FC$ of all contigs, most DEGs with the highest significance were located at positive $\log_2 FC$ of 2-8 (Fig. 9c). Additionally, of the 20 653 DEGs obtained when comparing the two strains under MFG, only 42 of these were also present when comparing growth conditions (i.e., under MFG or an air atmosphere) of the LCA strain (Fig 10d). The latter comparison only showed 120 DEGs.

Differentially expressed contigs were analyzed and enriched with Gene Ontology (GO) terms using Blast2Go, resulting in 15 509 genes annotated with GO terms, while 5 055 contigs (24 %) remained without annotation. From DEGs with GO terms, 6 608, 5 081 and 3 820 were classified as genes participating in biological process, with molecular function and as cellular components, respectively (Fig. 10). The enrichment of GO terms, showed that top most genes for biological process are part of oxidation-reduction process (6 %), cellular response to stimulus (6 %) and regulation of cellular process (6 %); for molecular function corresponded to genes related with oxidoreductase activity (16%), protein binding (15 %) and ATP binding (8 %); and for cellular component to integral component of membrane (28 %), plasma membrane (5 %) and chloroplast stroma (4 %) (Fig. 10a-c).

After GO term annotation, enzyme code and biochemical pathways were assigned to DEGs according to KEGG categories and subcategories (Fig. 11). The category with more DEGs was the nucleotide metabolism with 384 up-regulated and 137 down-regulated genes (Fig.11a), followed by carbohydrate, amino acid, energy and lipid metabolism (Fig.11b). Most DEGs in these pathways were up-regulated representing 81.5 % of the contigs (733 of 899).

In energy metabolism, carbon fixation pathways of phototrophs and prokaryotes changed the most with 30 up-regulated genes in HCA strain, while in lipid metabolism the least differences were found with 8 and 2 up-regulated genes for glycerolipid and fatty acid metabolism, respectively. Within carbohydrate metabolism, the top-hit pathways with more DEGs were pyruvate metabolism (34 up and 4 down-regulated), glycolysis/gluconeogenesis (28 up and 3 down-regulated) and the citrate cycle (22 up and 4 down-regulated). Also, amino acid metabolism was mainly up-regulated. Specifically, in glycine, serine and threonine metabolism, being the most changing, showed 21 contigs up-regulated and only 1 down-regulated. For phenylalanine, tyrosine and tryptophan biosynthesis; cysteine and methionine metabolism; and arginine and proline metabolism, 11-13 and 0-1 contigs were up- and down-regulated, respectively. Whereas in valine, leucine and isoleucine degradation pathway 5 contigs were up-regulated. DEGs from some other specific pathways were also found, among them porphyrin and chlorophyll metabolism, aminoacyl-tRNA biosynthesis; and ubiquinone and other terpenoid quinone biosynthesis, with 14-16 up-regulated contigs.

DEGS of carbon pool by folate and nucleotide

Contigs from one carbon by folate metabolism were found up-regulated in HCA strain compared with LCA strain under MFG, by the enzymes phosphoribosylglycinamide formyltransferase, methylenetetrahydrofolate dehydrogenase (NADP⁺) and aminomethyltransferase (MTHFD), while the enzyme Methylenetetrahydrofolate reductase (NADPH) (MTHFR) was down-regulated with -3.91 log₂FC (Fig. 12). Nucleotide metabolism scheme are the reported for plants, from these most of contigs in pyrimidine and purine were up-regulated in the strain HCA (Fig. 13-14, Table 7). In purine metabolism all the enzymes were up-regulated with log₂FC between 7.15 and 13.35. Pyrimidine metabolism were up-regulated by 2.0 to 13.45 log₂FC, however contigs down-regulated were found with -2.1 to -7.34 log₂FC, these contigs codify for three enzymes, nucleoside diphosphate kinase (NDK), uracil phosphoribosyltransferase (UPRT) and nucleoside triphosphate phosphatase .

DEGs of carbon metabolism

Transcriptome analysis revealed that several enzymes of the central carbon metabolism were up-regulated (Fig. 15 and Table 8). In the Calvin-Beson-Bassham cycle (C3), phosphoglycerate kinase (PGK) and two glyceraldehyde-3-PO₄ dehydrogenases (EC: 1.2.1.12 and EC: 1.2.1.59)

were up-regulated with \log_2FC of 3 to 4 and a transketolase with 13.37 \log_2FC . Up-regulated enzymes in the Hatch-Slack cycle (C4) were phosphoenolpyruvate carboxylase (PPC), aspartate aminotransferase (AAT) and pyruvate-orthophosphate dikinase (PPDK) with 12.1 to 12.8 \log_2FC and malate dehydrogenase (decarboxylating) with 9.7 \log_2FC ; while malate dehydrogenase (NADP+) enzyme (1.1.1.82 EC) showed two isoforms with contrary expression (i.e., 12.27 and -7.28 \log_2FC , respectively). In addition, most enzymes involved in glycolysis, gluconeogenesis and the Krebs cycle (TCA cycle) were up-regulated. Likewise, three enzymes responsible for the conversion of pyruvate to malonyl-CoA; pyruvate dehydrogenase E1 and E2 components (PDCs) and acetyl-CoA carboxylase (ACC) were also up-regulated.

DEGs of cellular components and nitrogen compound transport

GO term enrichment identified several contigs codifying for cellular components of the cell wall, chloroplast and photosystems (Fig. 16). A total of 14 contigs were assigned to cell wall components, of these 7 genes were up-regulated and 7 down-regulated (Fig. 16a). However, fold change of up-regulated genes (\log_2FC 7 to 14) were higher than down-regulated genes (\log_2FC -2 to -7). DEGs of chloroplast components (stroma, envelope and thylakoid membrane) consisted of around 30 to 40 up- and down-regulated genes, with up-regulation in the range of 8 to 14 \log_2FC and down-regulation of -2 to -8 (Fig. 16b-d). For photosystem I, 48 DEGs were determined of which 28 were up-regulated and 20 down-regulated, and for photosystem II 57 DEGs were observed, 35 up-regulated and 22 down-regulated (Fig. 16e-f). As described for the other cellular components, up-regulation was more pronounced than down-regulation with \log_2FC values of 11-14 and 8-14 for photosystem I and II, respectively, and down-regulation of -2 to -8 (Fig. 16e) and -2 to -7 (Fig. 16f). Differential expression analysis showed 140 up-regulated contigs related with nitrogen compound transport up-regulated in HCA strain compared with LCA, and \log_2FC of 2.7 to 15 were observed. Also, some 65 down-regulated contigs with -2.4 to -9.5 \log_2FC were found (Fig. 17).

DEGs of starch anabolism and catabolism

Key enzymes involved in starch anabolism and catabolism were also found to be up-regulated (Fig. 18). In starch anabolism, these enzymes were ADP glucose phosphorylase, UDP-glycogen synthase and 1,4- α -glucan branching enzyme, and in starch catabolism α -amylase, β -amylase, glycogen phosphorylase and 4- α -glucanotransferase. All enzymes presented \log_2FC of 15.51 (Fig. 18b).

DEGs of TAG biosynthesis

Final steps of TAG biosynthesis were observed up-regulated (Fig. 19) by the enzymes glycerol kinase, glycerol-3-PO₄ acyltransferase, 1-acylglycerol-3-PO₄ acyltransferase and diacylglycerol acyltransferase. Also, enzymes related with TAGs degradation were up-regulated; triacylglycerol lipase and diacylglycerol kinase. Expression level changes were between 7.5 and 10.9 log₂FC for contigs of enzymes in TAG synthesis, and 10.71 and 11.57 for enzymes of TAG degradation (Fig. 19b).

4.3.5 Differentially expressed genes of *D. abundans* strain LCA with different components of the model cement flue gas

The effect of different components of the flue gas was evaluated using only the strain LCA. High variability among replicates was observed in the growth condition MFG, air and 25% CO₂, which was evident in the grouping of the principal component 1 (Fig. 20a). However, principal component 2 clearly separates the air atmosphere condition from the other high CO₂ conditions. The normalized expression levels visualized in the heatmap showed that when *D. abundans* strain LCA was grown under air, most DEGs appeared to have higher expression levels than under high CO₂ conditions (Fig. 20b). Also, an air atmosphere was hierarchically clustered with a higher distance from the rest of the groups.

Strain LCA grown under MFG presented 120 DEGs compared with the growth condition under an air atmosphere, of these, 42 genes were up-regulated and 78 down-regulated (adjusted *p.value*<0.01, |log₂ FC|>2) (Fig. 21a). The same strain under 25% CO₂ only compared to the air condition presented 54 DEGs (28 up-regulated and 26 down-regulated genes) and under 25% CO₂+CKD 58 DEGs (39 up-regulated and 19 down-regulated genes) (Fig. 21b-c). Additionally, a comparison between MFG and 25% CO₂+CKD was performed to analyze the effect of the source of N and S since incomplete and complete media were used, respectively. This analysis resulted in only two significant DEGs (Fig. 21d). As shown in the Venn Diagram, the different growth conditions compared to an air atmosphere shared only 24 DEGs (Fig. 21e). DEGs of the MFG condition shared 25 contigs (21 %) with CO₂ only and 12 (10 %) with CO₂+CKD.

DEGs from MFG compared to the air control (120 contigs) were further analyzed and enriched with Gene Ontology (GO) terms using Blast2Go. This analysis showed a total of 83 contigs annotated with GO terms and 37 unknowns. Genes participating in biological process (n=25), molecular function (n=23) and cellular component (n=24) were identified (Fig. 22). The top

biological process GO terms with more contigs were protein-chromophore linkage (17% of contigs), photosynthetic electron transport in photosystem II (10%), protein phosphorylation (10%) and acyl carnitine transport (10%) (Fig. 22a). In molecular function category, most contigs corresponded to genes involved with ATP binding (13%), protein binding (11%) and chlorophyll binding (11%) (Fig. 18b). With 43% of contigs, cellular component-related genes were associated with integral component of membrane (Fig. 22c).

Differential expression in \log_2FC with their respective *p.value* for the different GO terms are shown in Table 9. Most of contigs in MFG compared with air were down-regulated, including all the GO terms already mentioned for biological process category and molecular function. The latter presented two contigs up-regulated in protein binding Go term with 3.19 and 4.39 \log_2FC . In cellular component, GO terms of photosystem I, plastoglobuli, cell wall, proton-transporting ATP synthase complex-catalytic core E(1), respiratory chain complex III and integral component of membrane were analyzed, where also almost all the contigs were down-regulated with \log_2FC in a range of -2.51 to -11.96; with an exception of a contig in integral component of membrane with 2.7 \log_2FC . When these GO terms were analyzed in CO₂ vs air similar expressions were observed, two contigs related with protein phosphorylation, one of acyl carnitine transport, three of ATP binding and another in photosystem I GO terms were significantly down-regulated, while two contigs in protein binding and one in integral component membrane were up-regulated. In CO₂+CKD vs air comparison, most of the GO terms showed here looked down-regulated, however only one contig for protein-chromophore linkage, one for protein phosphorylation, one for acyl carnitine transport, five for ATP binding and one related with chlorophyll binding and photosystem I were significant.

4.4 Discussion

4.4.1 Microalga growth under cement model flue gas

As a first approach to characterize *D. abundans* strain, which was acclimated for nine years under an atmosphere of 50% CO₂ and air, and their capability to grow under continuous cement flue gas and use it as a nutrient source, we evaluated growth under controlled laboratory conditions. Results showed that both strains were able to grow under MFG with similar biomass productivities. However, strain HCA presented a higher specific growth rate at the start of run and entered stationary phase before strain LCA (Fig. 4).

In MFG condition, pH was successfully controlled in a range of 6-6-5 by adding CKD (Fig. 5a). At low pH microalgae presents difficulties to tolerate flue gas, under a pH lower than 5 most SO_x are in form of bisulfate. When this is assimilated by microalgae is converted to SO_4^{2-} forming oxidative species that can damage membranes and pigments, and the inhibit the growth (Yan *et al.*, 2004; Lara *et al.*, 2014). Therefore, previous works have shown that the pH control is an important factor to increase microalga tolerance to flue gas, being the use of phosphate buffer and CaCO_3 some of the implemented methods (Jiang *et al.*, 2013; Guo *et al.*, 2017; Aslam *et al.*, 2017). However, these strategies compromise the simplicity and economy of the system (Lara *et al.*, 2016). Because CKD represent a buffering agent of no cost that is generated as industrial waste in calcination process in cement production (Van Oss and Padovani, 2003), this has been used to control pH (Talec *et al.*, 2013; Lara *et al.*, 2014 and 2016).

As expected, continuous dCO_2 increase to a maximum average of 30-32 % by day 5 (Fig. 5b); under a 6-7 pH range most of Ci is in form of HCO_3 and only a smaller part as CO_2 , both forms can be capture by microalga (Moroney and Ynalvez, 2007). Dissolved O_2 reached 102 and 127 % for strains HCA and LCA under MFGs, respectively; while controls were between 89-122 % dO_2 (Fig. 5c). In experiments with CO_2 , where dO_2 was diluted by 25% CO_2 values were as high as or higher than in air control, evidencing a high dO_2 production that can be correlated with a higher biomass production since it is released in photosynthesis process (Nelson and Yocum, 2006).

NO_x and SO_x are part of cement flue gas in variable composition (WBCSD, 2012). Diverse studies have demonstrated the viability of their use as N and S sources in microalgae culture (Lara-Gil *et al.*, 2014 and 2016; Aslam *et al.*, 2017). The growth of strain HCA in MFG correlates with less dissolved nitrate and nitrite in culture medium, because N is required for *de novo* protein synthesis during growth (Ito *et al.*, 2013, Duong *et al.*, 2015), explaining also the notable decreased of nitrate and nitrite during the fastest growth rate period (from day 3 to 4) of the LCA strain (Fig. 6). Microalga growth under the designed condition could be limited by several factors such as light, bioreactor agitation system (bubble), temperature and other since the growth and metabolism is highly affected when is grown under different culture conditions (Cheban *et al.*, 2015; Perrineau *et al.* 2014). An optimal condition of these factors and where nitrogen is not limited could show a higher more notable characteristic between the strains HCA and LCA.

D. abundans strains HCA and LCA under MFG showed a high tolerance to CO_2 , with fixation rates of 0.55-0.63 $\text{g CO}_2 \text{ L}^{-1} \text{ d}^{-1}$ (Table 3). NO_x and SO_x fixation rates based on biomass productivity considering microalga elemental composition (i.e. $\text{CO}_{0.48}\text{H}_{1.83}\text{N}_{0.11}\text{P}_{0.01}\text{S}_{0.01}$) were

obtained (Van Den Hende *et al.*, 2012). Both strains, HCA and LCA, under MFG presented NO_x and SO_x fixation rates around 0.06-0.07 and 0.005-0.006 g L⁻¹ d⁻¹, respectively; thus, these values represented assimilation efficiencies of 95-100 and 33-38% of N and S supplied by MFG, respectively (Fig. 7). Cement flue gas represents a potential nutrient source for microalgae culture, Van Eynde *et al.* (2016) explains that NO and SO₂ are oxidized to sulfate and nitrite in aerobic conditions and then can be used for microalgae. These components together with CO₂ could be use directly from industry combustion gases and converted to valuable bioproducts. Different studies have been realized with microalgae using flue gases, where microalgae tolerate, grow and generate bio-compounds of industrial interest (Olofsson *et al.*, 2015; Cuellar-Bermudez *et al.*, 2015; Camargo and Lombardi, 2017; Guo *et al.*, 2017, García-Cubero *et al.*, 2017; Aslam *et al.*, 2017.)

Control LCA grown in air had an adaptation phase of 4 d with the lowest biomass production, which could be attributable to low-CO₂ given that the control with 25% CO₂ presented one day adaptation phase with the highest biomass productivity (Fig. 4, Table 3). Patil and Kaliwal (2017) also reported similar when *Scenedesmus bajacalifornicus* was grown under continuous flux of 25% CO₂ respect to air (0.04% CO₂). Moreover, when CKD was incorporated to CO₂, biomass productivity decreased by 34%, which could be caused by CKD toxicity. Talec *et al.* (2013) reported a toxicity of 680 mg L⁻¹ for four species, among them two chlorophytes, where there was an immediate effect in biomass decrease. For the strain in this study, *D. abundans*, Lara *et al.* (2016) observed that when microalgae entered to stationary phase 450 ppm CKD had been incorporated. In the present study *D. abundans* showed a high tolerance to CKD since for day 5, 750 mg L⁻¹ had been incorporated to the system, and an exponential phase was still observed (Fig. 4). Even under MFG, CKD was enough to control pH and the microalga was capable to grow, which makes CKD a good strategy to control pH when a continuous flow of MFG.

The control with CO₂ and CKD, where S and N are supplied by the medium and differs only from MFG experiment in this, achieved 3.15 times more biomass and a significant higher growth rate (1.5-fold) than LCA strain in MFG. Despite there were no difference in biomass productivity (Table 3), which could be because part of the metabolism was shifted to a higher synthesis of storage compound caused by the low N concentrations in MFG condition (Ito *et al.*, 2013, Perrineau *et al.*, 2014, Shin *et al.*, 2015) than in complete medium (354 ± 21). After 4 h of bubbling NO abiotically only 1.1 mg L⁻¹ of NO_x at start of run was found, reaching a maximum value of 137 mg L⁻¹ NO_x by day 5 (Appendix A. Fig. A.1). Van Den Hende *et al.* (2012) mentioned that the solubility of NO is low in water, and is consider a limiting step, however could be increased by using used chelators.

4.4.2 *de novo* transcriptome assembly and functional annotations

The assembly of the transcriptome resulted in 70 458 contigs with an average length of 881 bp and a 50th percentile (N50) of 1 677 bp (Table 5). Completeness of the *de novo* transcriptome was 91.4 % based on BUSCOs analysis and overall read alignment rates of samples were 91-92 % (Table 6). According to Honass *et al.* (2016), the above criteria is the best metric combination to assess the quality of a *de novo* transcriptome assembly.

Transcriptome annotations using BLAST top-hit species reported for the phylogenetically close microalga *Scenedesmus acutus* (Sirikhachornkit *et al.*, 2018), *Arabidopsis thaliana* and *Scenedesmus quadricauda* resulted in 3048 hits, from this analysis the BLAST top-hit species to *D. abundans* transcriptome were *Monoraphidium neglectum*, *Chlamydomonas reinhardtii* and *Volvox carteri f. negariensis* (Fig. 8). Sirikhachornkit *et al.* (2018) reported the same species as the three top-hits for *S. acutus*. However, in the present study, 77.5% lower number of hits was obtained than for *S. acutus* considering only the three BLAST top-hit species. In a second BLAST, including *D. tertiolecta* (Shin *et al.*, 2015, Rismani-Yazdi *et al.*, 2011), other algae, bacteria and plants; 3711 hits were obtained with *Raphidocelis subcapitata*, *Chlamydomonas eustigma* and *Gonium pectorale* being the three top-hit species.

The two BLAST top-hit species *R. subcapitata* and *M. neglectum* are from Selenastraceae family (Suzuki *et al.*, 2018), while *D. abundans* is part of Scenedesmaceae family, but all within Sphaeropleales order (Hegewald and Braband, 2017). The results could suggest a higher genetical similitude with Selenastraceae rather than species from same family such as *Scenedesmus quadricauda*, *Scenedesmus vacuolatus* and *Scenedesmus sp.* FKBP, whose protein sequences were also included in database and only 4, 4 and 2 hits were obtained respectively. When Chen *et al.* (2017) analyzed the transcriptome of *Desmodesmus sp.* found that the best hit sequences did not correspond from chlorophyta species, being this the only study of the transcriptome or genome of *Desmodesmus*.

4.4.3 Differentially expressed genes under continuous cement flue gas and nine years of strain enriched in 50% CO₂ and air atmospheres

At day 4 of continuous flow of MFG, *D. abundans* enriched strains showed 20 653 DEGs (adjusted $p.value < 0.01$, $|\log_2 FC| > 2$) (Fig. 8). Surprisingly, more changes were found between strains HCA and LCA under the same growth condition (MFG), than the controls of the LCA strain grown under MFG and an air atmosphere, where only 120 DEGs were observed. Between strains under MFG

a total of 16 435 DEGs were up-regulated and 4 219 down-regulated. DEGs were classified as genes with molecular function (6 608), followed by biological process (5 055) and cellular component category (3 820) (Fig. 10). An overall higher expression of strain HCA compared to strain LCA could be because it possesses an upper level of basal expression and/or a higher capacity to respond to stress conditions, as a result of acclimation to high CO₂ atmospheres for nine years. In the studied system, stress might have been imposed by a continuous supply of 25% CO₂, an incomplete culture medium (BG11-N-S) where N and S were supplied by NO and SO₂ in the MFG, and the daily incorporation of CKD (150 ppm). In MFG experiments, lower NO_x concentrations than in complete medium (354 ± 21) were found, with only 1.1 mg L⁻¹ of NO_x at start of run after 4 h of bubbling NO abiotically and a maximum value of 137 mg L⁻¹ NO_x by day 5 (Appendix A. Fig. A.1), then N could be considered a limiting nutrient.

The superior adaptability of HCA strain to this condition is reflected in the several up-regulated pathways compared with strain LCA (Fig. 11). First, DEGs related with microalgae growth such as nucleotide metabolism with the higher number of DEGs, amino acid metabolism, aminoacyl-tRNA biosynthesis pathway were major up-regulated, suggesting a higher proliferation (Shin *et al.*, 2015). Three enzymes from one carbon pool (C1) by folates were up-regulated and one down-regulated, this metabolism has been reported to be important in nucleotide synthesis, growth stimulation and generation of reducing power (Fan *et al.*, 2014) (Fig. 11,12). The other most changes pathways were from carbohydrate and energy metabolism (Fig. 11). In particular, central carbon metabolism, starch anabolism and catabolism, and TAG biosynthesis showed highly expressed genes (up to log₂FC 15.51) (Fig. 15, 18-19, Table 8).

Nitrogen and sulfur are essential nutrients for protein biosynthesis, lipids, chlorophyll, photosystem proteins and other central intermediates. Usually under nitrogen limitation, microalgae appear to degrade macromolecules, as well as chlorophyll, carotenoids and thylakoid membranes, at the same time growth is retarded and storage compounds start to accumulate (Min *et al.*, 2016; Huang *et al.*, 2017; Sun *et al.*, 2018). Despite the limited nitrogen, both strains manage to grow under MFG with no difference in biomass productivity (Table 3) but strain HCA initiated with higher growth rates, this could be caused by a higher facility of adaptation of this strain. During growth, N levels in solution for strain HCA remained low (less than 1 mg L⁻¹) compared to strain LCA (Appendix A, Fig. A.1), this can be related with the 140 up-regulated contigs found in nitrogen compound transport with higher log₂FC (3-14) than the down-regulated (-2 to -9 log₂FC) (Fig. 17). Valenzuela *et al.* (2012) observed a high number of up-regulated

contigs for nitrate, ammonium and urea and suggests that it could represent a strategy to scavenge nitrogen from the medium.

Carbon metabolism

Several catabolic steps in carbon metabolism were up-regulated in HCA strain compared with LCA strain under MFG (Fig. 15, Table 8). In the C3 cycle enzymes PGK and two glyceraldehyde 3-PO₄ dehydrogenases showed 3-4 log₂FC, while transketolase presented 13.4 log₂FC. Also, several enzymes in the C4 cycle were up-regulated, PPC, AAT and PPKD with 12.1-12.8 log₂FC and malate dehydrogenase (MDH) (decarboxylating) with 9.7 log₂FC. PPC is a light-dependent enzyme that converts phosphoenolpyruvate to oxaloacetate by fixation of CO₂ and is normally overexpressed under high light. MDH catalyzes the conversion of oxaloacetate to malate, which is a reversible reaction. Oxaloacetate is a substrate used in gluconeogenesis, urea cycle, amino acid synthesis and TCA cycle. Pyruvate from malate conversion, can be then transformed to acetyl-CoA (Shin *et al.*, 2015).

Additionally, most enzymes of glycolysis and gluconeogenesis, and TCA cycle were up-regulated (Fig. 15, Table 8). Sun *et al.* (2016) also observed up-expressed genes for TCA cycle and carbohydrate metabolism when *Chlorella sorokiniana* was cultured under high CO₂. The up-regulation in glycolysis under N starvation was observed for *Scenedemus acutus* (Sirikhachornkit *et al.*, 2018). The acetyl-CoA obtained from glycolysis or C4 cycle can enter to TCA cycle to produce NADH that allowed ATP synthesis by oxidative phosphorylation; also, the intermediates (2-oxoglutarate, succinyl CoA, fumarate and oxaloacetate) can be used in amino acid metabolism, while the intermediate malate can be converted to pyruvate and then used in FA synthesis (Sun *et al.*, 2016). Since most of DEGs here were up-regulated, a co-regulation of all these pathways under this specific condition was evident, where HCA strain had a clear more active metabolism than LCA strain. Similarly, Shin *et al.* (2015) observed similar expression patterns of all these pathways when grown under *Nannochloropsis gaditana* under nitrogen deprivation, but in that case most of genes were down-regulated.

Cellular components

Components of the cell wall, chloroplast and photosystems are of interest to understand *D. abundans* strains adaptation to high CO₂. DEGs of cell wall components (14 in total) were half up-regulated (log₂FC 7 to 14) and half down-regulated (log₂FC -2 to -7) (Fig. 16). Cell components related to photosynthesis (chloroplast stroma, envelope and thylakoid membrane) also showed a

similar pattern, 31-42 DEGs with up-regulation in the range of 8 to 14 \log_2 FC and down-regulation of -2 to -8 (Fig. 16e-g). These results can be correlated with a high flux of carbon since photosynthesis is the process that provide the NAPH and ATP necessary to capture CO₂ via C3 cycle (Gowik and Westhoff, 2011).

Photosynthesis performed in the chloroplast by photosystem II and I catalyzed the oxidation of water, reduction of NADP and synthesis of ATP (Nelson and Yocum, 2007). These photosystems presented 28 DEGs up-regulated and 20 down-regulated for photosystem I and 35 DEGs up-regulated and 22 down-regulated for photosystem II (Fig. 16b). Up-regulation showed higher fold changes (8-14 \log_2 FC) than down-regulated genes (-2 to -8 \log_2 FC). Photosystem II has been reported to be highly sensible to stress conditions, when *Chlorococcum littorale* and *Chlorella sp.* growing under 3% CO₂ were transferred to low-CO₂ (0.04%) and to extremely high-CO₂ (40%), a PI/PII ratio increased (Miyashi *et al.*, 2003). The over-regulation of the two photosystems in strain 5HCA, suggests higher tolerance to the new growth condition of continuous flow of MFG, even when N and S were provided by NO and SO₂ from flue gas.

Starch and lipid metabolism

Enzymes of starch anabolism and catabolism, as well as TAG synthesis and degradation were up-regulated in the strain HCA under MFG compared to the strain LCA (Fig. 18-19). In starch anabolism, ADP glucose phosphorylase, UDP-glycogen synthase and 1,4- α -glucan branching enzyme were up-regulated (15.5 FC), and in starch catabolism α -amylase, β -amylase, glycogen phosphorylase and 4- α -glucanotransferase (15.5 FC). Min *et al.* (2016) observed that *Dunaliella tertiolecta* when depleted of nitrogen accumulated starch corresponding to up-regulation of genes in starch biosynthesis and at the same time TCA cycle was up-regulated, revealing an active interchange of carbon skeletons for anabolic and catabolic processes. Similarly, in this study genes from starch and TCA cycle were up-regulated for HCA strain, probably because a higher CO₂ flux.

In lipid metabolism, three enzymes responsible for the conversion of pyruvate to malonyl-CoA (Fig. 15, Table 8), a precursor for fatty acid biosynthesis (Sun *et al.*, 2016), were up-regulated in strain HCA. These enzymes were pyruvate dehydrogenase E1 and E2 components (PDCs) and acetyl-CoA carboxylase (ACC). Acetyl-CoA from catalysis of pyruvate by PDC links glycolysis with lipid biosynthesis pathways, then ACC catalyzes conversion to malonyl-CoA, being these the first steps for *de novo* FA biosynthesis (Sun *et al.*, 2016). Because of the low concentration of N

in the medium, acetyl-CoA that is normally used to support algal growth by entering the TCA cycle under nitrogen-replete conditions could be relocated to the chloroplast to generate storage compounds (Perrineau *et al.*, 2014). Also, under high CO₂ it has been observed that the flux of acetyl-CoA increases resulting in lipid accumulation (Valenzuela *et al.*, 2012; Sun *et al.*, 2016). In concordance, enzymes from final steps of TAG biosynthesis were up-regulated (7.5-10.9 log₂FC) in the strain HCA (glycerol kinase, glycerol-3-PO₄ acyltransferase, 1-acylglycerol-3-PO₄ acyltransferase and diacylglycerol acyltransferase) (Fig. 19). Several studies have reported accumulation of TAGs in microalgae when grown under nutrient limitations (Valenzuela *et al.*, 2012; Perrineau *et al.*, 2014; Mansfeldt *et al.*, 2016; López *et al.*, 2015). Likewise, some species have shown an increase in lipid content under high CO₂, it is hypothesized that a higher carbon flux occurs into TAGs (Sun *et al.*, 2016).

Moreover, enzymes related with glycerolipid degradation were up-regulated, triacylglycerol lipase and diacylglycerol kinase, with log₂FC of 11.57 and 10.71, respectively (Fig. 19b). Lipases can be found at membranes and lipid droplets, their function is to cleave FAs from glycerol in TAG molecules, then the degradation of FA to acetyl-CoA occurs, and acetyl-CoA enters the glyoxylate cycle and gluconeogenesis (Kong *et al.*, 2018). These pathways were also up-regulated in strain HCA (Fig. 15). The lipid accumulation in *S. acutus* under N starvation has been suggested that occurred for inhibition of TAG turnover by the down-regulation of TAG and DAG lipases (Sirikhachornkit *et al.* 2018). Despite the efforts to understand microalgae lipid catabolism much is still unknown, as well as enzymes identity (Kang *et al.*, 2018).

4.4.4 Differentially expressed genes of *D. abundans* strain LCA with different components of the model cement flue gas

The effect of individual components of cement flue gas was evaluated using only the LCA strain under air, 25% CO₂ and CO₂+ CKD gas supply. When MFG condition was compared with air 120 DEGs were found, of which 42 genes were up-regulated and 78 down-regulated. Of these only 83 contigs were annotated, the top biological process GO terms were protein-chromophore linkage (17% of contigs), photosynthetic electron transport in photosystem II (10%), protein phosphorylation (10%) and acyl carnitine transport (10%) (Fig. 18a). In molecular function category, most of contigs corresponded to genes involved with ATP binding (13%), protein binding (11%) and chlorophyll binding (11%) (Fig. 18b). With 43% of contigs, cellular component-related genes were associated with integral component of membrane (Fig. 18c).

Some contigs were annotated with more than one GO term, even among categories. Most of DEGs related with these GO terms were down-regulated in MFG compared with air, expression levels were from -2.51 to -11.96 log₂FC, with exception of two contigs up-regulated in protein binding and one in integral component membrane. Under CO₂ two contigs related with protein phosphorylation, one with acyl carnitine transport, four with ATP binding, and another in photosystem I were down-regulated. Similarly, in CO₂+CKD growth condition, only one contig for protein-chromophore linkage, one for protein phosphorylation, one for acyl carnitine transport, five for ATP binding and one related with chlorophyll binding and photosystem I were significantly down-regulated. These results could suggest that LCA strain in air, was probably under a higher stress condition.

Despite the extremely differences in growth conditions, among air (0.04% CO₂) compared with a continuous flow of 25% CO₂, the limited-N in MFG versus experiments with complete medium (100% and 60% lower by 0 and 5 d in abiotic conditions) or CKD addition; no many differences were found in enzymes and other proteins. This could be first for the high variability in transcriptome and microalgae response between replicates, and also because LCA strain was stressed by bioreactor conditions like agitation, light and other, making difficult to notice differences at transcriptome level, even when microalgae presented differential growth rates and biomass productivities.

4.5 Conclusions

D. abundans strains HCA and LCA tolerated, grew and used cement flue gas components (CO₂, NO_x, SO_x) as a nutrient source. Addition of CKD effectively controls system pH under model cement flue gas, representing a low-cost strategy to increase microalga tolerance. *de novo* transcriptome assembly revealed that *D. abundans* is more similar to the family Selenastraceae than Scenedesmaceae; however, this analysis was based on available data still poor in comparison with the high diversity of microalgae. Transcriptome changes in strain HCA compared with strain LCA under MFG were related with a probably higher flux of carbon that activated all central carbon metabolism pathways. In addition, TAG and starch catabolism and anabolism were both expressed and up-regulated. Characteristic features of adaptation or tolerance to high CO₂ might be related to: nitrogen transporters, active synthesis of essential macromolecules for growth (nucleotides and amino acids) and cellular components of cell wall and the photosynthetic apparatus. In particular, it appears, as nitrogen transporters between strains possess different substrate affinities or gene regulators as in the LCA strain dissolved N accumulated to day 4 but

not in the HCA strain. DEGs related with photosynthesis in the LCA strain under MFG compared with air were down-regulated, while in the control with CO₂ were down-regulated (low FC), suggesting a stress condition for the LCA strain in air since this culture presented almost no growth (long adaptation phase).

Differences between strains were not evident based on growth but transcriptome analysis revealed important differences at day 4. However, as both produced the same biomass at the end of the experimental period (5 days) could imply that either strain adapts to MFG eventually. Further studies to evaluate the LCA strain after growth for more than 5 days could validate the differences in expression of HCA.

Tables and figures

Table 3. Growth parameters of *D. abundans* strains HCA and LCA under MFG and controls with AIR strain under air, CO₂ and CO₂+CKD in a 1 L column photobioreactor with continuous flow (0.05 vvm), 24 °C, 80-90 μmol PAR-photons m⁻²s⁻¹ and 24 h light.

Strain-> Gas supply	Culture medium	Maximum specific growth rate (d ⁻¹)	Productivity (g d.w. L ⁻¹ d ⁻¹)	CO ₂ fixation rate (g CO ₂ L ⁻¹ d ⁻¹) ^a	CO ₂ utilization efficiency (%)
HCA->MFG	BG-11-N-S	0.79 ± 0.14 ^{CD}	0.30 ± 0.04 ^B	0.55 ± 0.09 ^B	2.03 ± 0.33 ^B
LCA->MFG	BG-11-N-S	0.65 ± 0.13 ^D	0.34 ± 0.06 ^B	0.63 ± 0.10 ^B	2.34 ± 0.38 ^B
LCA->Air	BG-11	1.33 ± 0.19 ^A	0.05 ± 0.00 ^C	0.09 ± 0.01 ^C	100.00 ± 16.92 ^A
LCA->CO ₂	BG-11	1.11 ± 0.03 ^{AB}	0.53 ± 0.00 ^A	0.97 ± 0.08 ^A	3.61 ± 0.30 ^B
LCA->CO ₂ +CKD	BG-11	0.95 ± 0.03 ^{BC}	0.35 ± 0.07 ^B	0.65 ± 0.12 ^B	2.40 ± 0.44 ^B

^a Based on biomass productivity accordingly to equations of Jian *et al.* (2013). HCA: high CO₂ acclimated. LCA: low CO₂ acclimated. MFG: model flue gas. CKD: Cement kiln dust. MFG composition in dry air was (v/v): 25% CO₂, 700 ppm NO and 100 ppm SO₂. 150 ppm w/v CKD were added every 24 h for MFG and CO₂+CKD runs. CO₂ condition represents 25% CO₂. Values represent average ± SD (n=3-6). Means not connected by the same letter are significantly different (Tukey' HSD test, α=0.05, n=3-6).

Table 4. Summary of results of the sequencing run (81 bp paired-end) for differential transcriptome analysis using a MiSeq Illumina sequencer.

Parameter	Value
Yield (Gbp)	5.44
%≥Q30	92.18
Error rate (%)	0.036
Reads passing filter (PF)	65 957 802
Cluster density (k mm ⁻²)	1933

Table 5. Statistics results of the *de novo* transcriptome assembly of *D. abundans* using CLC Genomics Workbench 11.0 program.

Assembly output	Value
Total number of contigs	70 458
Min length (bp)	200
Max length (bp)	15 389
Average length (bp)	881
Standard deviation (bp)	1096
Median length (bp)	420
Total bases in contigs (bp)	62 071 384
Number of contigs < 500 bp	40 076
Number of contigs > or = 500 bp	30 382
Number of contigs > or = 1,000 bp	17 492
Number of contigs > or = 2,000 bp	7 894
Number of contigs > or = 5,000 bp	972
Number of contigs > or = 10,000 bp	27
N50 (bp)	1 677
Contigs in N50	60 352
GC content	55.6%

Table 6. Statistics of completeness of the *de novo* transcriptome of *D. abundans* based on the Benchmarking Universal Single-Copy Orthologous (BUSCO) using the eukaryotic lineage dataset ^a.

BUSCO statistics	Value ^b
Complete BUSCOs	236 (77.9%)
Complete-single-copy BUSCOs	110 (36.3%)
Complete-duplicated BUSCOs	126 (41.6%)
Fragmented BUSCOs	41 (13.5%)
Missing BUSCOs	26 (8.6%)

^aIncludes 100 species and 303 BUSCOs. ^bIn parenthesis, percentage of BUSCOs in the assembled transcriptome.

Table 7. Contig ID, log₂FC and adjusted *p.value* of DEGs codifying for enzymes in purine and pyrimidine metabolisms from pathways shown in Figures 13 and 14.

Metabolism	Enzyme		Contig ID	Log ₂ FC	Adjusted <i>p.value</i>	
	Name	KEGG ID				
Purine metabolism	GAR synthase (GARS)	6.3.4.13	3878	13.35	4.2E-07	
	GAR transformylase (GART)	2.1.2.2	30909	7.26	7.9E-03	
	AIR synthase (AIRS)	6.3.3.1	3878	13.35	4.2E-07	
	Adenylosuccinate lyase (ASL)	4.3.2.2	1647	12.98	8.2E-07	
	AICAR tranformylase/IMP cyclohydrolase (ATIC)	2.1.2.3	3805	11.60	0.0E+00	
		3.5.4.10	3805	11.60	0.0E+00	
	Adenylosuccinate synthase (ASS)	6.3.4.4	10167	7.15	9.5E-03	
	Adenylate kinase (AMK)	2.7.4.3	18709	7.58	6.9E-03	
	AMP deaminase (AMPD)	3.5.4.6	6488	12.16	4.4E-06	
	IMP dehydrogenase (IMPDH)	1.1.1.205	12059	10.48	8.3E-05	
	GMP synthase (GMPS)	6.3.5.2	2525	12.50	2.2E-06	
	Adenosine phosphorylase (Ade Pase)	2.4.2.1	6691	11.74	1.1E-05	
	Inosine–guanosine phosphorylase (PNPase)	2.4.2.1	6691	11.74	1.1E-05	
	Hypoxanthine–guanine phosphoribosyltransferase (HGRT)	2.4.2.8	13678	10.50	3.1E-13	
	Allantoinase, allantoin amidohydrolase (ALNase)	3.5.2.5	16406	10.55	7.2E-05	
	Ureidoglycolate lyase	4.3.2.3	1550	10.95	5.3E-15	
	Allantoin deaminase	3.5.3.9	10436	7.78	5.3E-03	
	Pyrimidine metabolism	Aspartate transcarbamoylase (ATCase)	2.1.3.2	16065	11.74	9.6E-06
		Dihydroorotase (DHOase)	3.5.2.3	10943	9.46	5.5E-04
		Orotate phosphoribosyltransferase (OPRTase)	2.4.2.10	11848	11.97	6.7E-06
Orotidine 5-phosphate decarboxylase (ODCase)		4.1.1.23	11848	11.97	6.7E-06	
Nucleoside diphosphate kinase (NDK)		2.7.4.6	10503	-5.56	1.4E-09	
CTP synthase		6.3.4.2	6431	7.96	3.5E-03	
Apyrase (Apy)		3.6.1.5	21904	8.74	1.2E-03	
Uridine/cytidine kinase (UK)		2.7.1.48	8762	12.25	3.5E-06	
Uracil phosphoribosyltransferase (UPRT)		2.4.2.9	2335	-7.34	8.6E-03	
PRPP synthase (PRS)		2.7.6.1	2620	13.45	3.6E-07	
Cytidine deaminase (CDA)		3.5.4.5	22501	8.49	1.7E-03	
β-ureidopropionase (PYD3)		3.5.1.6	32212	-3.64	2.3E-03	
Nucleoside triphosphate phosphatase		3.6.1.15	n=326 ^a	(2.0 to 15.3) ^b	- ^c	
	n=131		(-2.1 to -8.7)	-		

^aNumber of contigs that codified for this enzyme. ^bRange of log₂FC for contigs. ^cNot shown but significant (adjusted *p.value*<0.01) for all contigs.

Table 8. Contig ID, log₂FC and adjusted *p.value* of DEGs codifying for enzymes in central carbon metabolism from pathways shown in Figure 11

Pathway	Enzyme		Contig ID	Log ₂ FC	Adjusted <i>p.value</i>
	Name	KEGG ID			
C3 cycle	Phosphoglycerate kinase (PGK)	2.7.2.3	2951	3.13	2.4E-05
	Glyceraldehyde 3-PO ₄ dehydrogenase (GAPDH)	1.2.1.12	6541	4.01	1.7E-05
	Glyceraldehyde-3-PO ₄ dehydrogenase (NAD(P)+)	1.2.1.59	6541	4.01	1.7E-05
	Transketolase	2.2.1.1	1029	13.37	0.0E+00
C4 cycle	Phosphoenolpyruvate carboxylase (PPC)	4.1.1.31	3593	12.14	0.0E+00
	Aspartate aminotransferase (AAT)	2.6.1.1	24779	7.63	5.4E-03
	Malate dehydrogenase (NADP+)	1.1.1.82	791	-7.28	9.6E-03
			792	12.27	3.6E-06
	Malate dehydrogenase (decarboxylating)	1.1.1.39	14288	9.73	2.7E-04
	Pyruvate, orthophosphate dikinase (PPDK)	2.7.9.1	240	12.71	0.0E+00
Photosynthesis	Cytochrome b6-f complex iron-sulfur subunit (petC)	1.10.9.1	585	12.76	0.0E+00
Glycolysis	Hexokinase	2.7.1.1	15592	11.62	1.3E-05
	Glucokinase	2.7.1.2	1004	11.19	0.0E+00
	Fructose-1,6-bisphosphatase (FBP)	3.1.3.11	22041	8.31	2.4E-03
	6-phosphofructokinase (PFK)	2.7.1.11	2327	11.01	5.3E-15
	Fructose-bisphosphate aldolase, class I (ALDO)	4.1.2.13	9904	7.99	2.2E-08
	Glyceraldehyde 3-PO ₄ dehydrogenase (GAPDH)	1.2.1.12	6541	4.01	1.7E-05
	Glyceraldehyde-3-PO ₄ dehydrogenase (NAD(P)+)	1.2.1.59	6541	4.01	1.7E-05
	Phosphoglycerate kinase (PGK)	2.7.2.3	2951	3.13	2.4E-05
	Phosphopyruvate hydratase	4.2.1.11	581	13.45	0.0E+00
	Pyruvate kinase	2.7.1.40	31.66	13.27	4.4E-07
	Glyceraldehyde-3-PO ₄ dehydrogenase (NADP+) ₂	1.2.1.9	6099	10.70	5.3E-05
	Aldose 1-epimerase	5.1.3.3	5237	10.28	4.2E-13
	Glucose-6-PO ₄ 1-epimerase	5.1.3.15	1486	11.65	0.0E+00
	Pyruvate -> Malonyl CoA	Pyruvate dehydrogenase E1 component (PDC1)	1.2.4.1	7776	8.40
Pyruvate dehydrogenase E2 component (PDC2)		2.3.1.12	1304	11.77	9.0E-06
Acetyl-CoA carboxylase (ACC)		6.4.1.2	4849	14.06	6.8E-08
TCA cycle	Citrate synthase (CS)	2.3.3.1	8208	14.63	1.8E-08
	ATP citrate synthase (ATP-CS)	2.3.3.8	2563	11.11	0.0E+00
	Aconitate hydratase (ACH)	4.2.1.3	627	12.48	0.0E+00
	Isocitrate dehydrogenase (NAD+)(IDH)	1.1.1.41	2685	14.21	5.1E-08
	Isocitrate dehydrogenase (IDP)	1.1.1.42	4326	14.05	7.0E-08
	2-oxoglutarate dehydrogenase component E1 (AKGDH)	1.2.4.2	8241	2.93	1.1E-05
	2-oxoglutarate dehydrogenase component E2	2.3.1.61	5128	11.90	0.0E+00
	Succinyl-CoA synthetase (ADP-forming) (SCS)	6.2.1.4	10503	-5.56	1.4E-09

Succinyl-CoA synthetase (GDP-forming) (SCS)	6.2.1.5	3096	12.53	0.0E+00
Succinate dehydrogenase (SDH)	1.3.5.1	1489	15.08	6.1E-09
Fumarate hydratase	4.2.1.2	8205	10.58	7.0E-14
Malate deshydrogenase (MDH)	1.1.1.37	6546	11.42	0.0E+00
		13194	11.41	1.7E-05
		1893	-5.57	1.3E-09
		1894	11.80	0.0E+00
		19790	12.22	4.4E-06
Phosphoenolpyruvate carboxykinase (GTP) (PEP)	4.1.1.32	3593	12.14	0.0E+00
		3594	-6.79	1.2E-07
		8893	8.44	1.9E-03
		955	13.65	0.0E+00
		956	-10.79	8.4E-05
Phosphoenolpyruvate carboxykinase (ATP) (PEPCK (ATP))	4.1.1.49	8893	8.44	1.9E-03

Table 9. Log₂FC and adjusted p.value of the top-hit GO terms in biological process, molecular function and cellular component categories of *D. abundans* controls with LCA strain under MFG, CO₂ and CO₂+CKD vs air.

Go term category	Go term	Contig ID	LCA->MFG vs LCA->Air		LCA->CO ₂ vs LCA->Air		LCA->CO ₂ +CKD vs LCA->Air	
			Log ₂ FC	Adjusted p.value	Log ₂ FC	Adjusted p.value	Log ₂ FC	Adjusted p.value
Biological process	Protein-chromophore linkage	16633	-4.55	1.4E-05	-2.42	2.2E-01	-3.99	2.4E-03
		8987	-3.99	5.9E-05	3.07	2.3E-01	-3.07	3.1E-02
		29484	-3.73	8.9E-03	0.2	1.0E+00	-3.25	1.8E-01
		5897	-3.66	8.6E-04	0.4	1.0E+00	-3.6	1.3E-02
		11309	-2.51	2.4E-03	1.9	3.5E-01	-2.07	1.6E-01
	Photosynthetic electron transport in photosystem II	29484	-3.73	8.9E-03	0.2	1.0E+00	-3.25	1.8E-01
		5897	-3.66	8.6E-04	0.4	1.0E+00	-3.6	1.3E-02
		11309	-2.51	2.4E-03	-1.93	3.5E-01	-2.07	1.6E-01
	Protein phosphorylation	24354	-5.86	3.6E-12	-5.14	0.0E+00	-4.34	4.3E-06
		108	-3.85	6.8E-04	-2.98	1.2E-01	-2.7	1.9E-01
		32079	-3.75	5.5E-05	-3.39	7.1E-03	-2.48	2.1E-01
	Acyl carnitine transport	26557	-8.76	0.0E+00	-7.9	0.0E+00	-5.88	1.3E-10
		14944	-8.13	2.9E-11	0.4	1.0E+00	-4.43	2.1E-02
		14943	-4.65	8.0E-05	0.25	1.0E+00	0.22	1.0E+00
	Molecular function	ATP binding	54834	-11.96	0.0E+00	-9.63	0.0E+00	-8.88
54835			-6.42	1.5E-03	2.9	3.4E-02	-5.27	4.1E-03
54835			-6.42	1.5E-03	2.9	3.4E-02	-5.27	4.1E-03
24354			-5.86	3.6E-12	-5.14	1.3E-07	-4.34	4.3E-06
24354			-5.86	3.6E-12	-5.14	1.3E-07	-4.34	4.3E-06
25661			-4.04	6.6E-03	1.63	1.0E+00	-7.62	8.1E-01
25661			-4.04	6.6E-03	1.63	1.0E+00	-7.62	8.1E-01
108			-3.85	0.0E+00	-2.98	1.2E-01	-2.7	1.9E-01
Protein binding		32079	-3.75	0.0E+00	-3.39	7.1E-03	-2.48	2.1E-01
		8987	-3.99	5.9E-05	-2.57	2.3E-01	-3.07	3.1E-02
		9359	-3.86	5.9E-05	-2.9	8.1E-02	-0.89	1.0E+00
		29484	-3.73	8.9E-03	0.2	1.0E+00	-3.25	1.8E-01
		15631	3.19	2.7E-05	3.22	3.8E-04	2.57	2.7E-02
		15344	4.39	1.6E-03	4.98	8.6E-04	3.01	4.6E-01
		Chlorophyll binding	16633	-4.55	1.4E-05	-2.42	2.2E-01	-3.99
8987	-3.99		5.9E-05	-2.57	2.3E-01	-3.07	3.1E-02	
29484	-3.73		8.9E-03	0.2	1.0E+00	-3.25	1.8E-01	
5897	-3.66		8.6E-04	0.4	1.0E+00	-3.6	1.3E-02	
11309	-2.51		2.4E-03	-1.93	3.5E-01	-2.07	1.6E-01	
Photosystem I	49925	-6.33	0.0E+00	-5.72	9.8E-09	-7.3	3.1E-11	

		16633	-4.55	1.4E-05	-2.42	2.2E-01	-3.99	2.4E-03
	Plastoglobule	25661	-4.04	6.6E-03	1.63	1.0E+00	-7.62	8.1E-01
	Cell wall	8987	-3.99	5.9E-05	-2.57	2.3E-01	-3.07	3.1E-02
	Proton-transporting ATP synthase complex, catalytic core F(1)	29484	-3.73	8.9E-03	0.2	1.0E+00	-3.25	1.8E-01
Cellular component	Respiratory chain complex III	43109	-3.5	4.7E-03	4.78	3.8E-01	-5.95	3.4E-02
		54834	-11.96	0.0E+00	-9.63	0.0E+00	-8.88	0.0E+00
		26557	-8.76	0.0E+00	-7.9	0.0E+00	-5.88	1.3E-10
		14944	-8.13	2.9E-11	0.4	1.0E+00	-4.43	2.1E-02
	Integral component of membrane	54835	-6.42	1.5E-03	2.9	3.4E-02	-5.27	4.1E-03
		5897	-3.66	8.6E-04	0.4	1.0E+00	-3.6	1.3E-02
		45668	-3.13	3.8E-03	2.73	1.0E+00	0.22	1.0E+00
		11309	-2.51	2.4E-03	-1.93	3.5E-01	-2.07	1.6E-01
		5282	2.7	3.5E-03	3.02	4.8E-03	2.55	5.7E-02

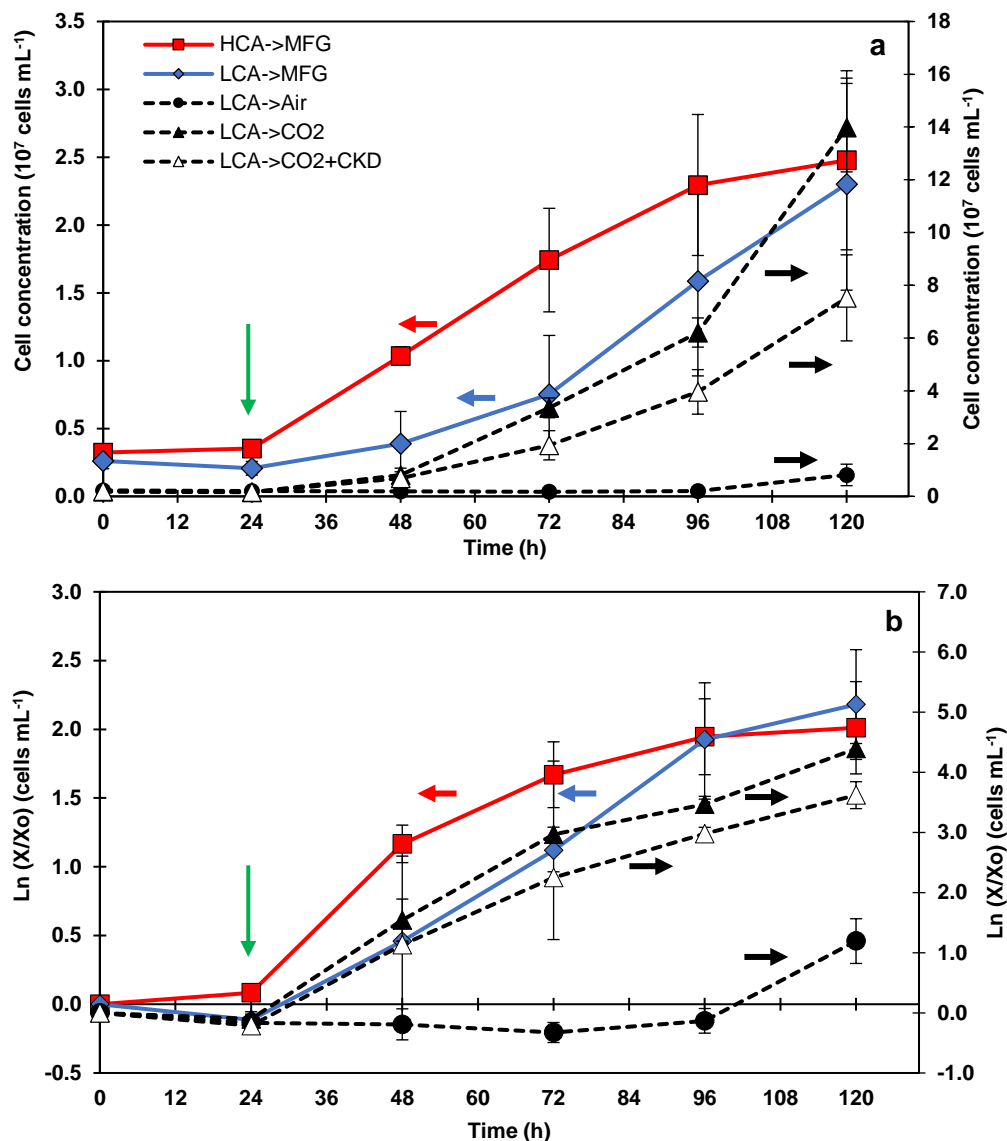


Figure 4. Arithmetic (a) and semi-log (b) representation of growth curves of *D. abundans* strains HCA and LCA under MFG and controls with LCA strain under air, CO₂ and CO₂+CKD in a 1 L column photobioreactor with continuous flow (0.05 vvm), 24 °C, 80-90 μmol PAR-photons m⁻²s⁻¹ and 24 h light.

HCA: high CO₂ acclimated. LCA: low CO₂ acclimated. MFG: model flue gas. CKD: Cement kiln dust. MFG composition in dry air was (v/v): 25% CO₂, 700 ppm NO and 100 ppm SO₂. 150 ppm w/v CKD were added every 24 h for MFG and CO₂+CKD runs. CO₂ condition represents 25% CO₂. Values represent average ± SD (n=3-6). Green arrow indicates addition of total NO_x and SO_x after 24 h acclimation period at 40% concentration. 100% of dO₂ is equal to atmospheric O₂ (21%). Time 0 h corresponds to values after 4 h of aeration before culture inoculation.

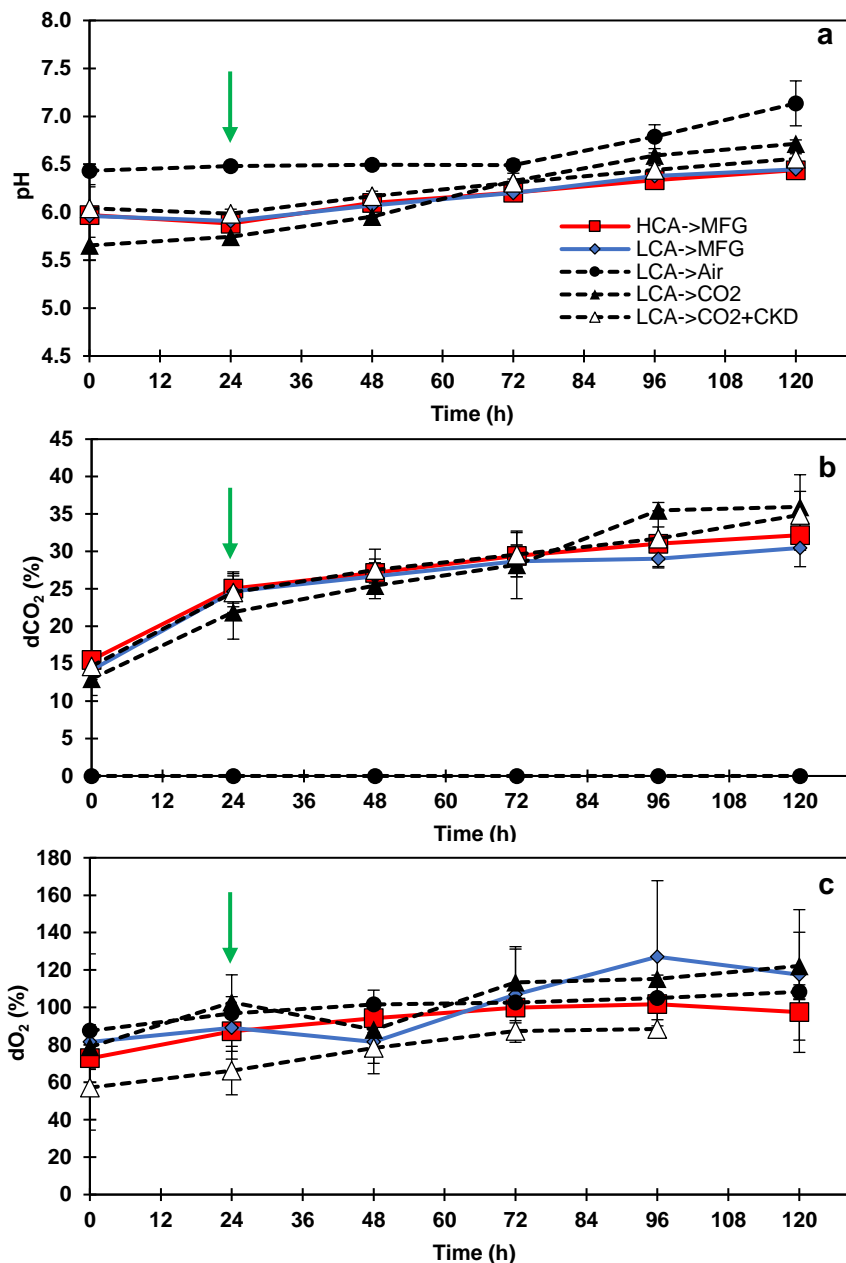


Figure 5. pH (a), dCO₂ (b) and dO₂ (c) during culture of *D. abundans* strains HCA and LCA under MFG and controls with LCA strain under air, CO₂ and CO₂+CKD in a 1 L column photobioreactor with continuous flow (0.05 vvm), 24 °C, 80-90 μmol PAR-photons m⁻²s⁻¹ and 24 h light.

HCA: high CO₂ acclimated. LCA: low CO₂ acclimated. MFG: model flue gas. CKD: Cement kiln dust. MFG composition in dry air was (v/v): 25% CO₂, 700 ppm NO and 100 ppm SO₂. 150 ppm w/v CKD were added every 24 h for MFG and CO₂+CKD runs. CO₂ condition represents 25% CO₂. Values represent average ± SD (n=3-6). Green arrow indicates addition of total NO_x and SO_x after 24 h acclimation period at 40% concentration. 100% of dO₂ is equal to atmospheric O₂ (21%). Time 0 h corresponds to values after 4 h of aeration before culture inoculation.

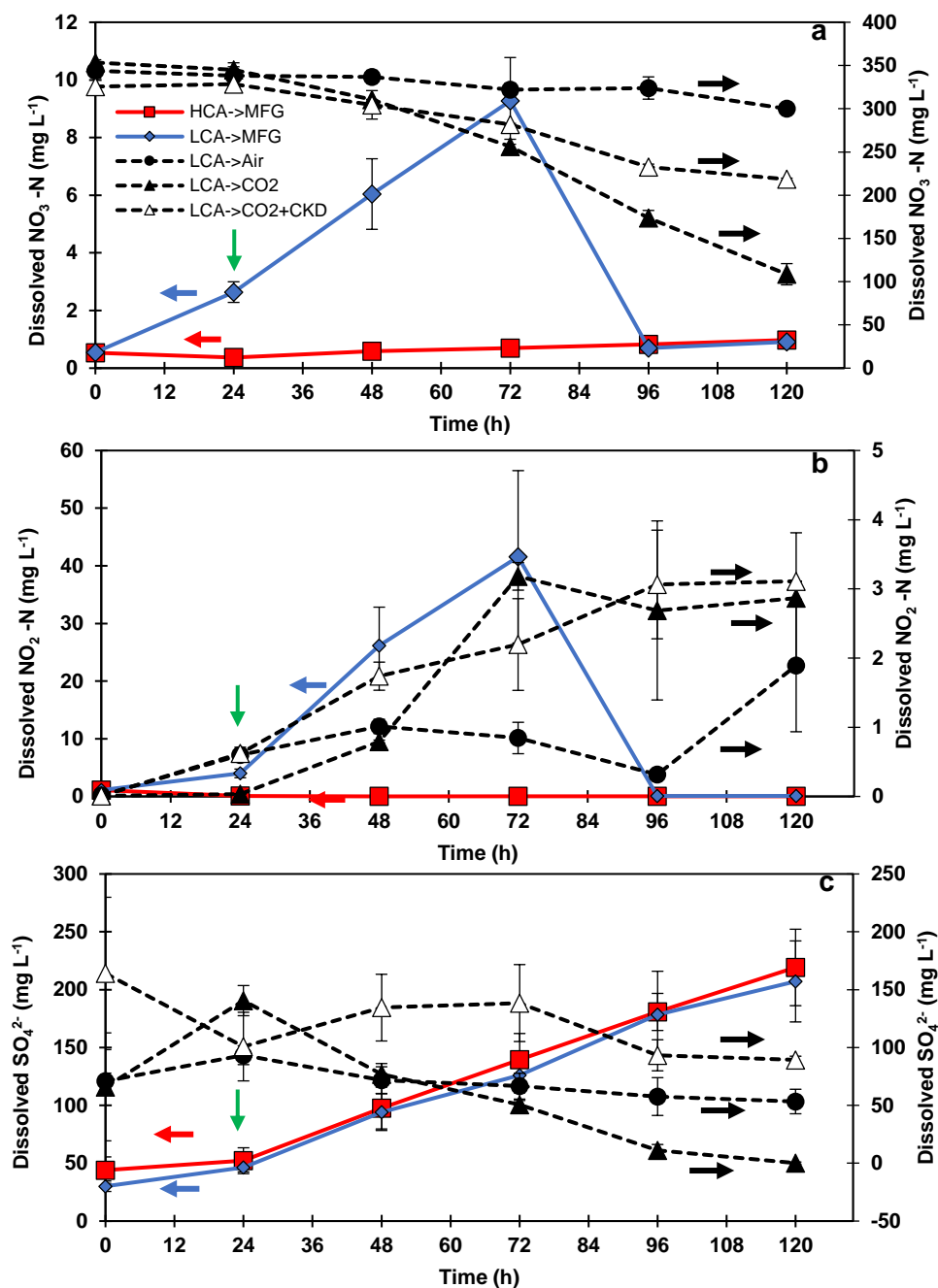


Figure 6. Sulfate (a), nitrate (b) and nitrite (c) in solution during culture of *D. abundans* strains HCA and LCA under MFG and controls with LCA strain under air, CO₂ and CO₂+CKD in a 1 L column photobioreactor with continuous flow (0.05 vvm), 24 °C, 80-90 μmol PAR-photons m⁻²s⁻¹ and 24 h light.

HCA: high CO₂ acclimated. LCA: low CO₂ acclimated. MFG: model flue gas. CKD: Cement kiln dust. MFG composition in dry air was (v/v): 25% CO₂, 700 ppm NO and 100 ppm SO₂. 150 ppm w/v CKD were added every 24 h for MFG and CO₂+CKD runs. CO₂ condition represents 25% CO₂. Values represent average ± SD (n=3-6). Green arrow indicates addition of total NO_x and SO_x after 24 h acclimation period at 40% concentration. 100% of dO₂ is equal to atmospheric O₂ (21%). Time 0 h corresponds to values after 4 h of aeration before culture inoculation.

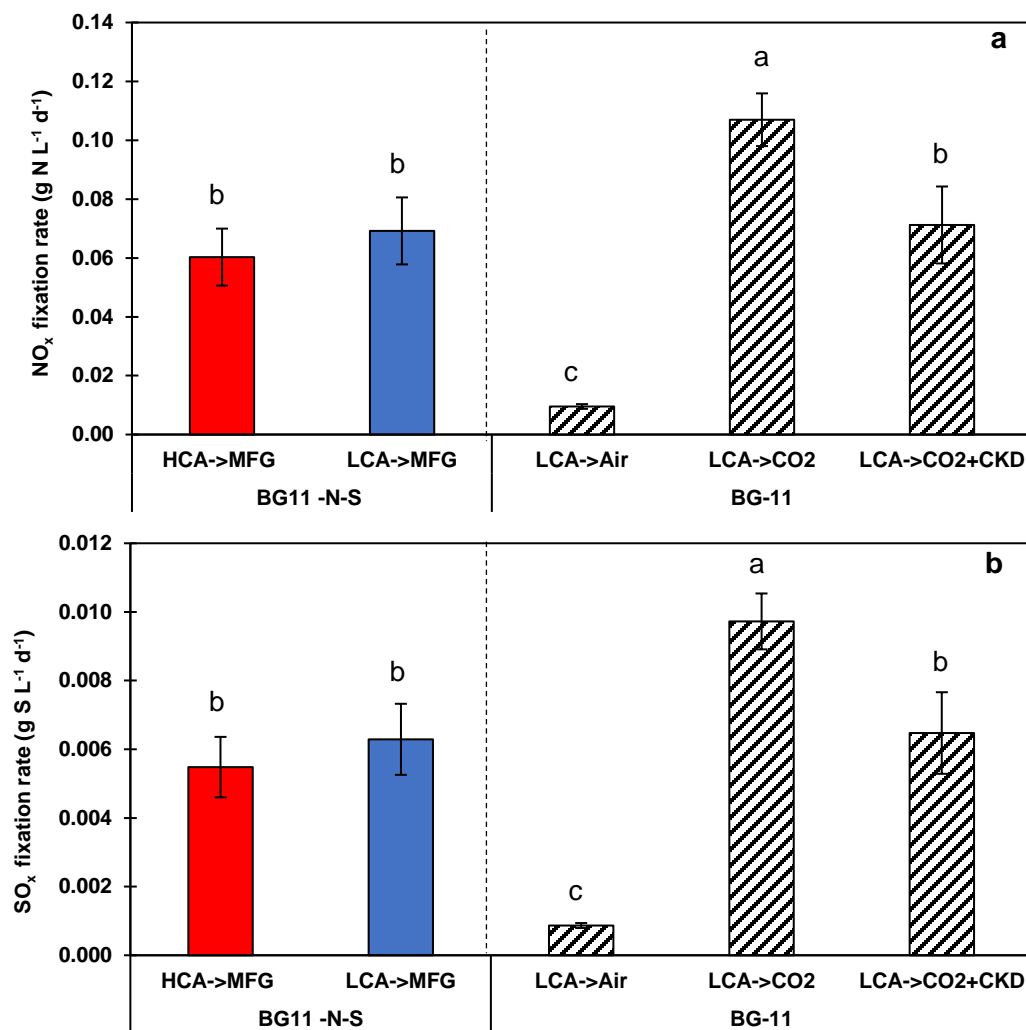


Figure 7. NO_x (a) and SO_x (b) utilization efficiencies of *D. abundans* strains HCA and LCA under MFG and controls with LCA strain under air, CO₂ and CO₂+CKD in a 1 L column photobioreactor with continuous flow (0.05 vvm), 24 °C, 80-90 μmol PAR-photons m⁻²s⁻¹ and 24 h light.

HCA: high CO₂ acclimated. LCA: low CO₂ acclimated. MFG: model flue gas. CKD: Cement kiln dust. MFG composition in dry air was (v/v): 25% CO₂, 700 ppm NO and 100 ppm SO₂. 150 ppm w/v CKD were added every 24 h for MFG and CO₂+CKD runs. CO₂ condition represents 25% CO₂. Values represent average ± SD (n=3-6). Means not connected by the same letter within each medium are significantly different (Tukey' HSD test, α=0.05, n=3-6).

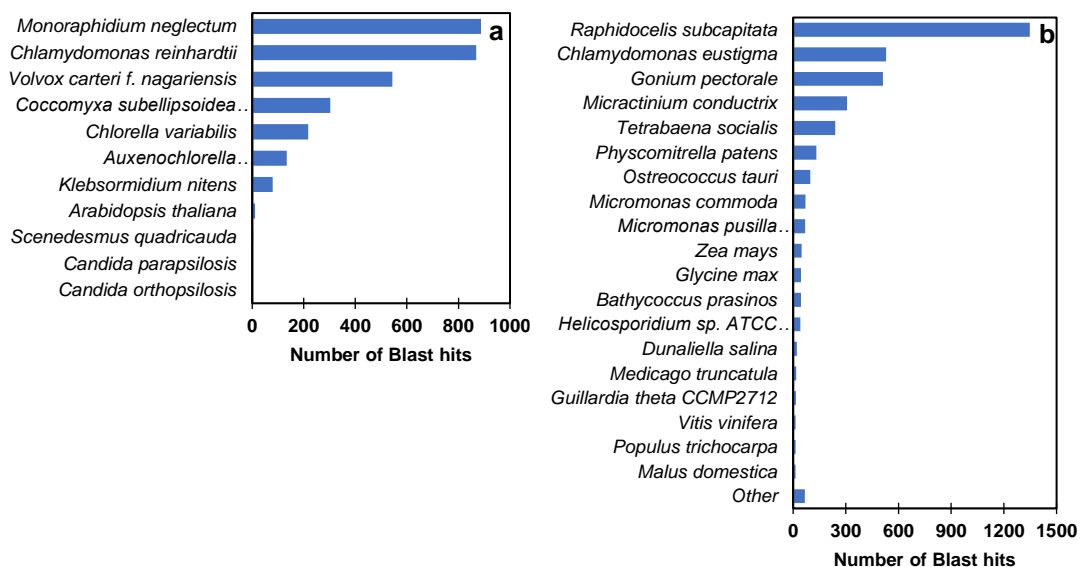


Figure 8. BLAST results of the assembled transcriptome using two databases created with the BLAST top-hit species reported for two chlorophyte microalgae, *Scenedesmus acutus* (Sirikhachornkit *et al.*, 2018) and *Dunaliella tertiolecta* (Shin *et al.*, 2015, Rismani-Yazdi *et al.*, 2011). a) Database with BLAST top-hit species for *S. acutus* plus *S. quadricauda* and *A. thaliana*, b) Database with BLAST top-hit species for *D. tertiolecta* plus other algae, bacteria and plants.

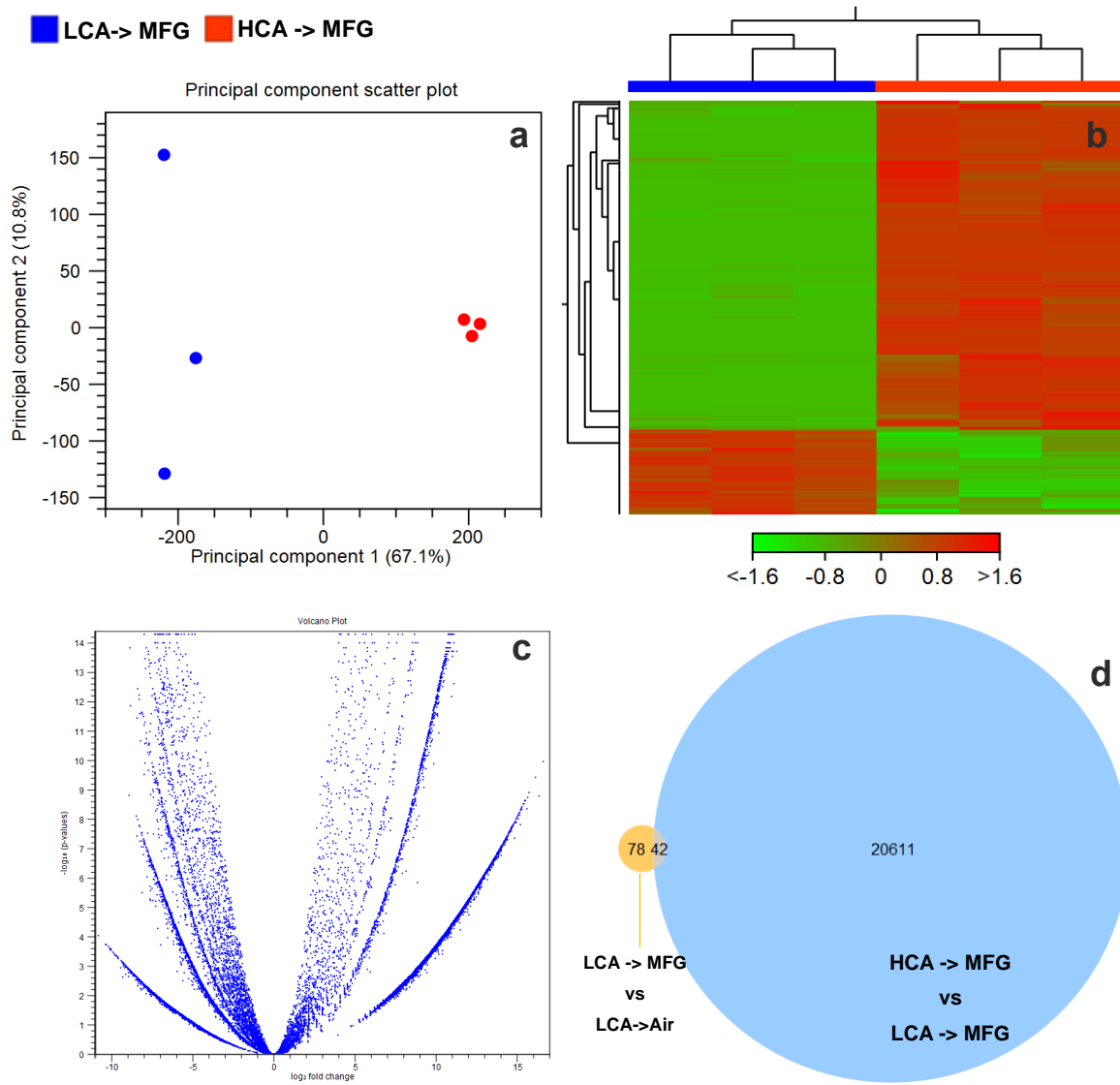


Figure 9. Transcriptome analysis of *D. abundans* strains HCA and LCA grown under MFG (n=3). a) Principal component analysis, b) Heatmap of DEGs (adjusted $p.value < 0.01$, $|\log_2 FC| > 2$) gradient color represents change in contig expression (red: up-regulated, green: down-regulated), c) Volcano plot of \log_2 fold change against $-\log_{10}$ (adjusted $p.values$) and d) Venn Diagram of DEGs shared between HCA->MFG vs LCA->MFG (light blue circle) and LCA->MFG vs LCA->air (yellow circle).

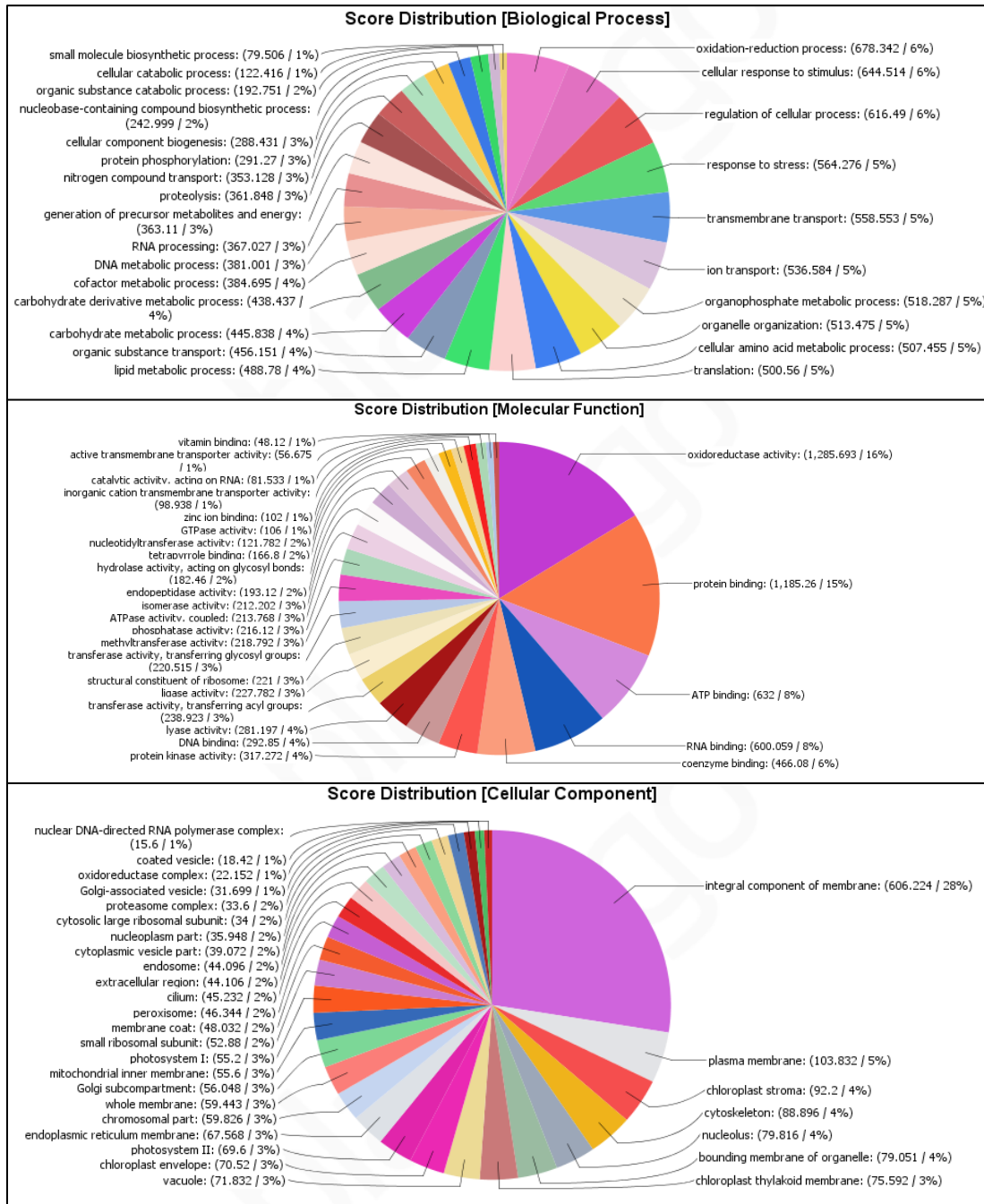


Figure 10. Multilevel pie charts of GO annotation enrichment of DEGs (adjusted p -value < 0.01, $|\log_2 FC| > 2$) found in *D. abundans* strain HCA against LCA grown under MFG (n=3). a) biological process, b) molecular function and c) cellular component.

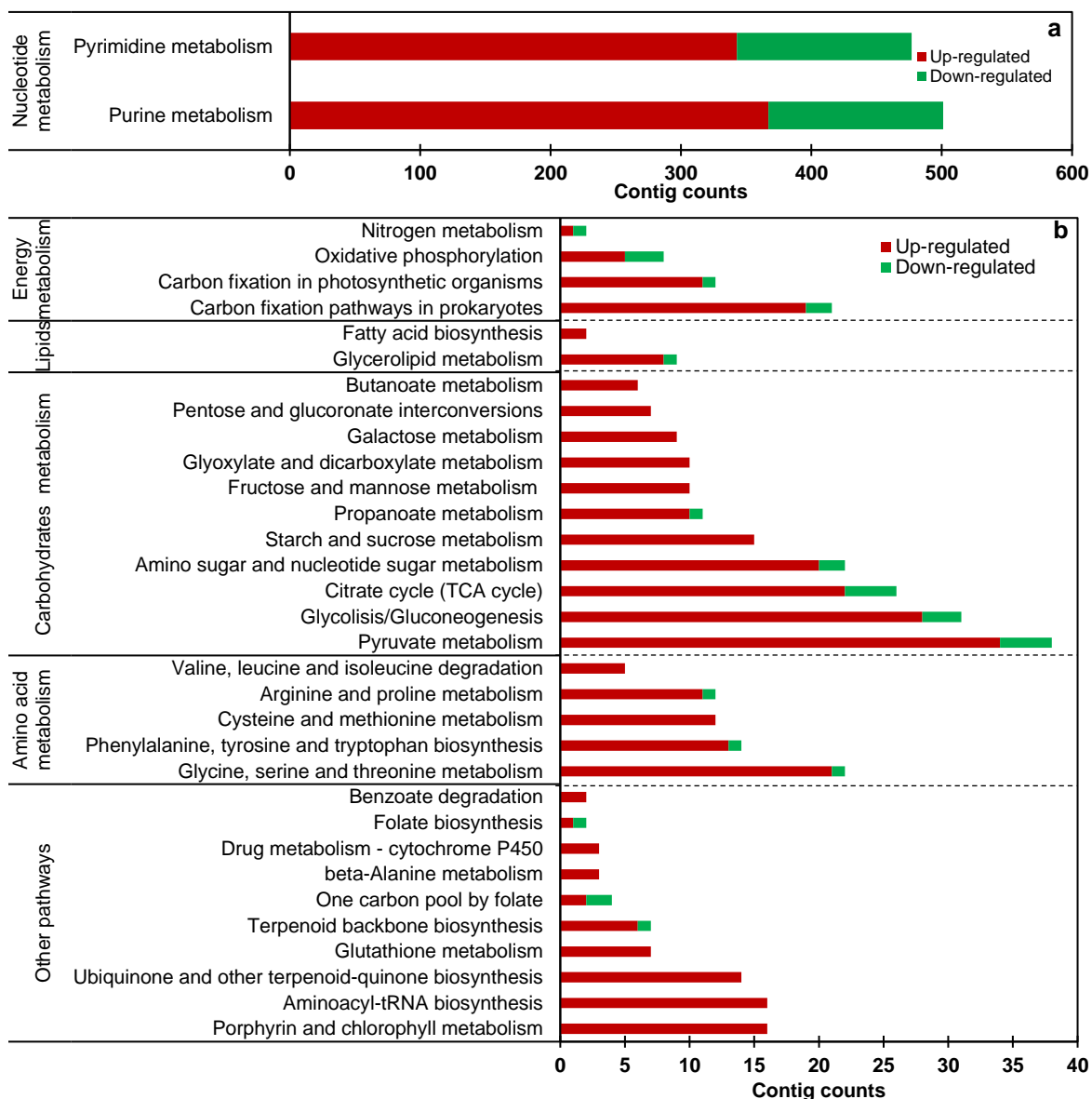
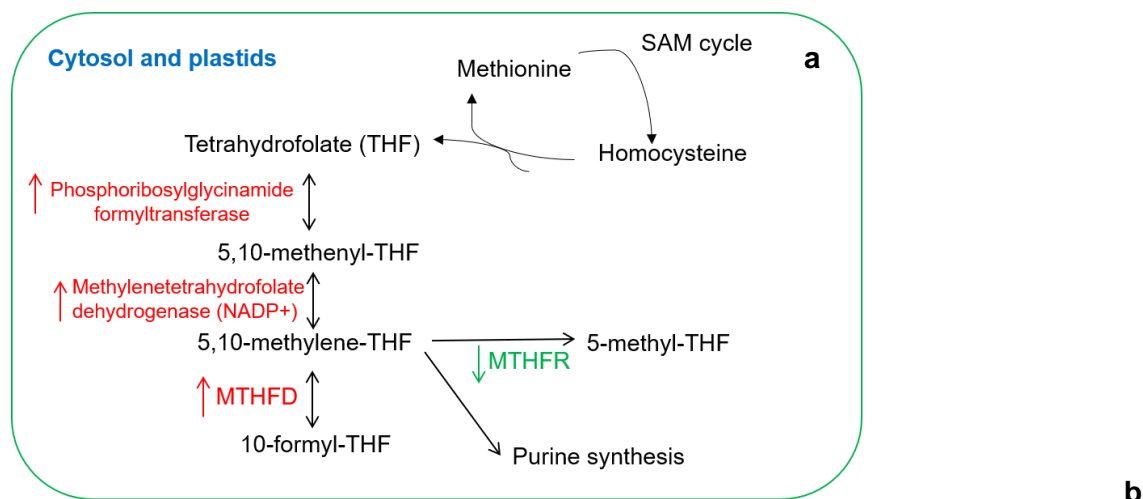


Figure 11. KEGG categories and subcategories of DEGs (adjusted $p.value < 0.01$, $|\log_2FC| > 2$) found in *D. abundans* strain HCA against LCA grown under MFG ($n=3$). Only KEGG categories with contig count ≥ 2 are shown. a) Nucleotide metabolism and b) Energy, lipid, carbohydrate, amino acid metabolisms, and other pathways. Up and down-regulated genes are represented with red and green colors, respectively.



Enzyme		Contig ID	Log ₂ FC	Adjusted p.value
Name	KEGG ID			
Phosphoribosylglycinamide formyltransferase	2.1.2.2	30909	7.26	7.9E-03
Methylenetetrahydrofolate dehydrogenase (NADP+)	1.5.1.5	42969	4.40	0.0E+00
Aminomethyltransferase (MTHFD)	2.1.2.10	3519	12.91	9.0E-07
Methylenetetrahydrofolate reductase (NADPH) (MTHFR)	1.5.1.20	4738	-3.91	1.4E-07

Figure 12. One carbon pool by folate metabolism. a) Pathways showing up and down-regulated enzyme contigs in HCA compared with LCA, red and green arrows indicate up- and down-regulation, respectively, and b) contig ID, log₂FC and adjusted *p*.values for enzyme contigs.

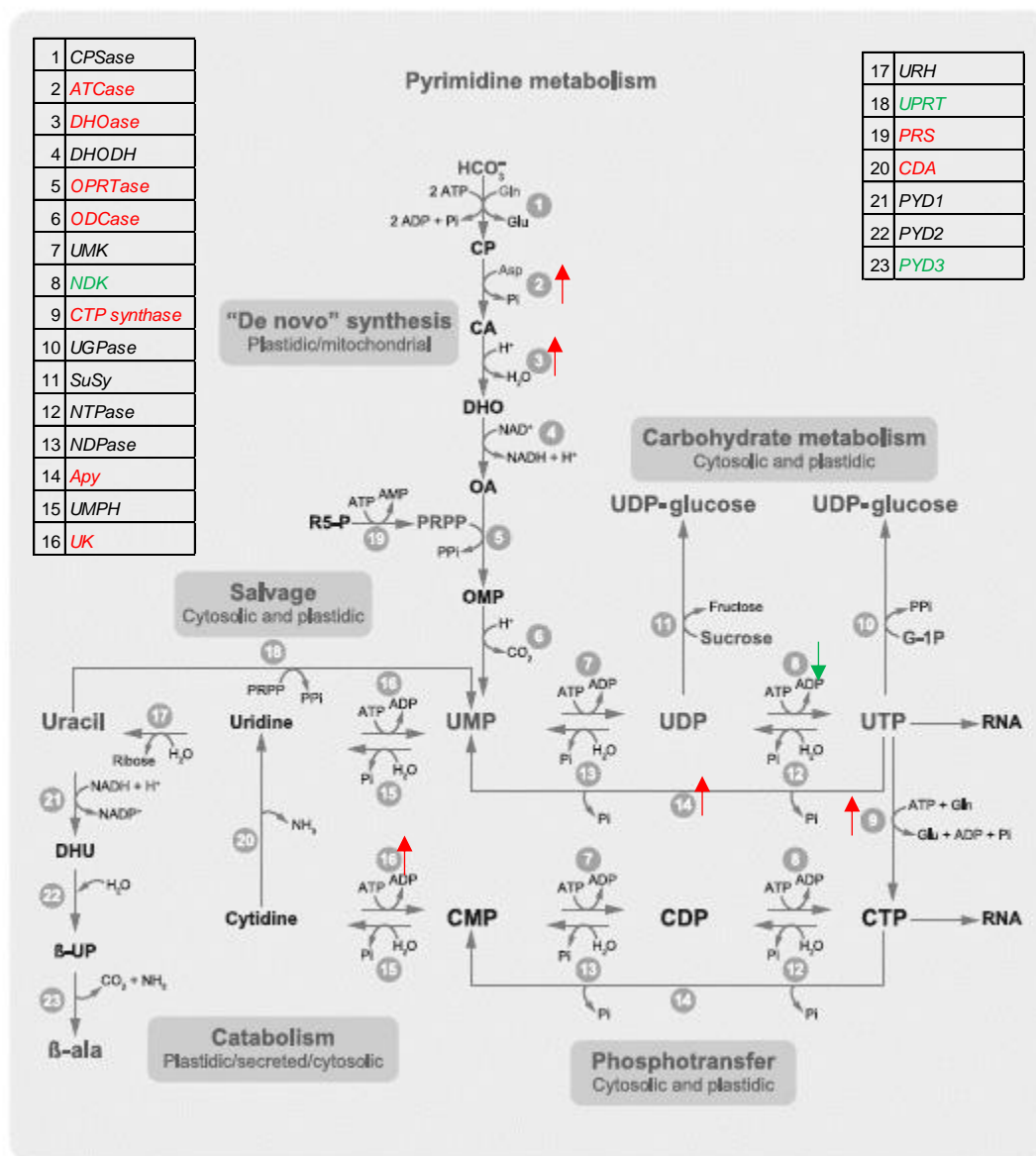


Figure 13. Pyrimidine metabolism described in plants. Red color indicates up-regulated and green down-regulated contigs in HCA strain compared with LCA strain under MFG (Figure adapted from Zrenner *et al.*, 2006). Numbers correspond to enzymes in the list.

24	<i>Atase</i>
25	<i>GARS</i>
26	<i>GART</i>
27	<i>FGAMS</i>
28	<i>AIRS</i>
29	<i>AIRC</i>
30	<i>SAICAR</i>
31	<i>ASL</i>
32	<i>ATIC</i>
33	<i>ASS</i>
34	<i>AMK</i>
36	<i>AMPD</i>
37	<i>IMPDH</i>
38	<i>GMPS</i>
39	<i>Guanosine deaminase</i>
40	<i>Ade Pase</i>
41	<i>Ado Nase</i>
42	<i>Ado Kinase</i>
43	<i>NPT</i>
44	<i>APT</i>
45	<i>PNPase</i>
46	<i>Inok</i>
47	<i>HGRT</i>
52	<i>NMPase</i>
53	<i>Ino Nase</i>
54	<i>XDH</i>
55	<i>GuaD</i>
56	<i>Urease</i>
57	<i>ALNase</i>
58	<i>ALNase</i>
59	<i>Urease</i>
60	<i>Ureidoglycolate lyase</i>
61	<i>Allantoin deaminase</i>
	<i>Ureidoglycine</i>
62	<i>amidothylase</i>
	<i>Ureidoglycolate</i>
63	<i>hydrolase</i>

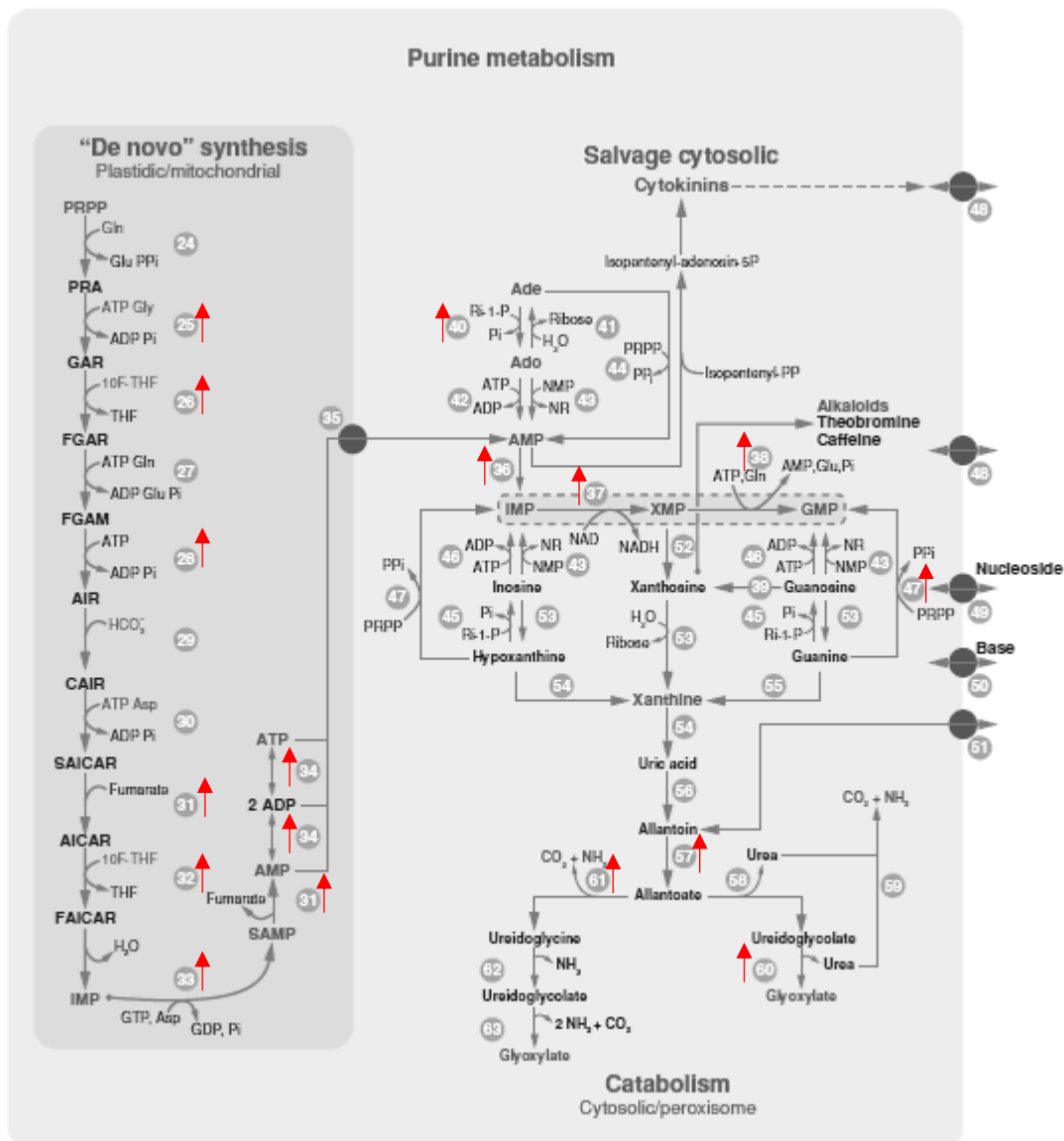


Figure 14. Purine metabolism described in plants. Red color indicates up-regulated contigs in HCA strain compared with LCA strain under MFG (Figure adapted from Zrenner *et al.*, 2006). Numbers correspond to enzymes in the list.

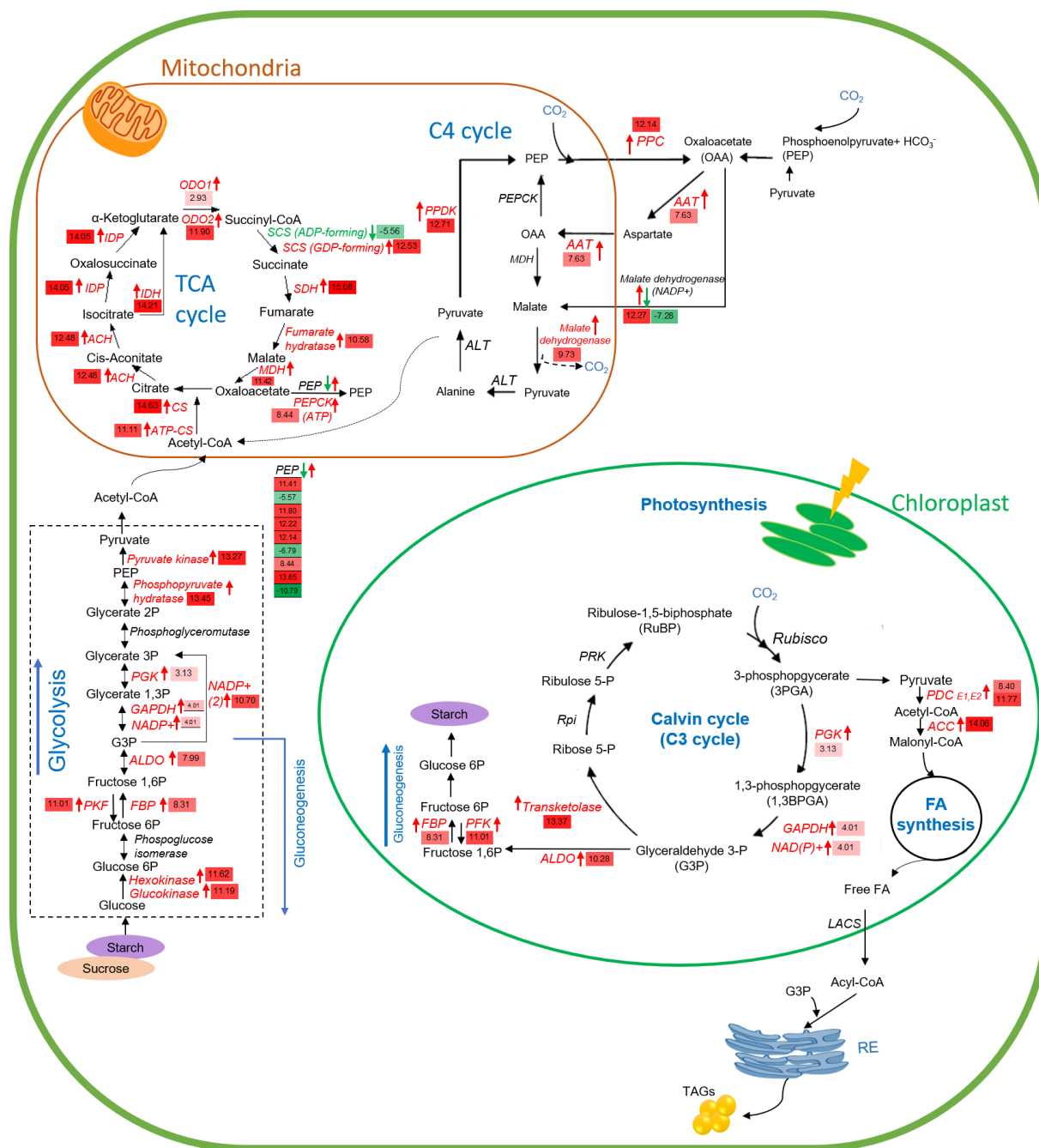


Figure 15. Proposed diagram of pathways involved in central carbon metabolism based on the transcriptome of *D. abundans* grown under model flue gas after nine years of acclimation under 50% CO₂ and air (HCA and LCA strains). Red and green arrows indicate up and down-regulation of enzyme contigs, respectively.

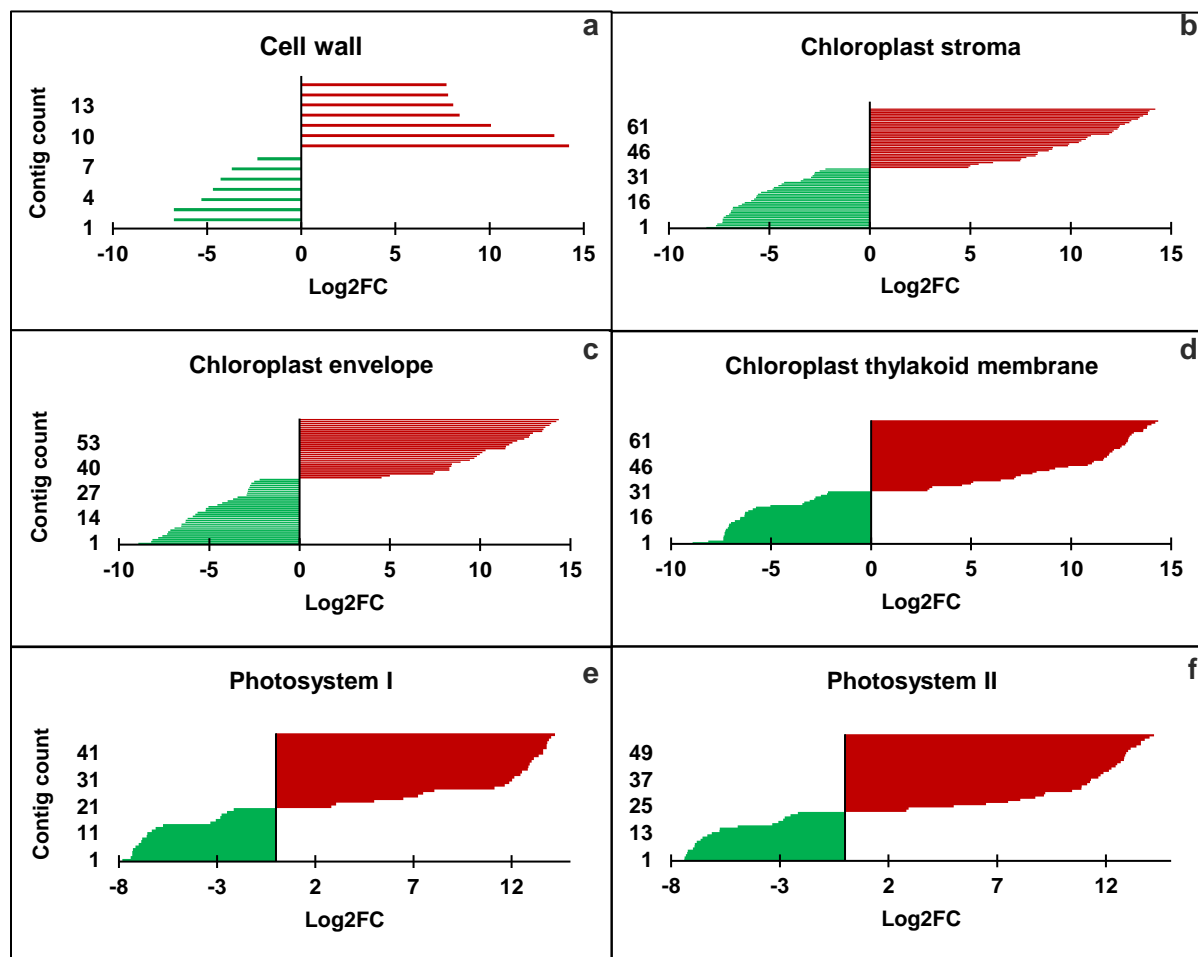


Figure 16. Contigs annotated as cell component GO terms of cell wall, chloroplast and photosystems. Log₂FC distribution of HCA vs LCA of cell components from a) cell wall, b-d) chloroplast parts and e-f) photosystems.

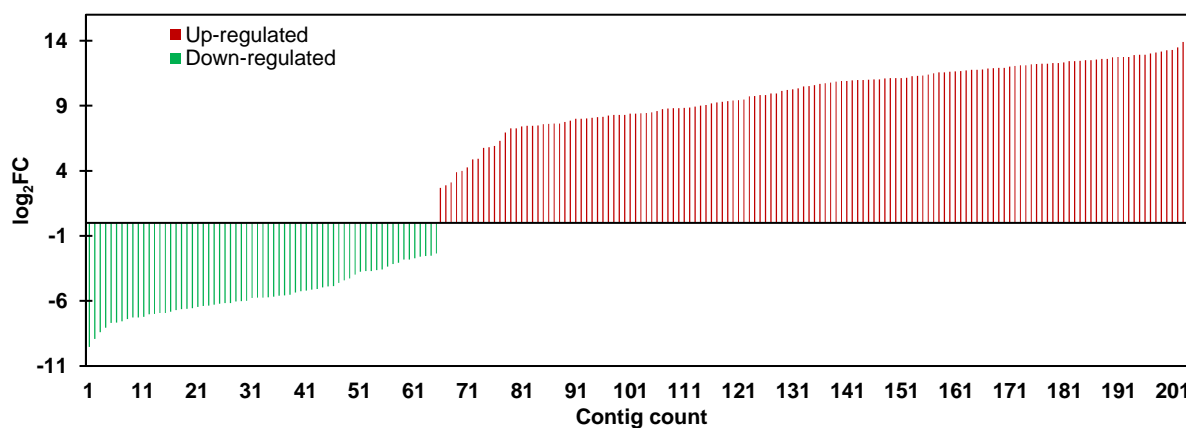


Figure 17. Log₂FC distribution of HCA vs LCA of contigs annotated as cell nitrogen compound transport GO terms.

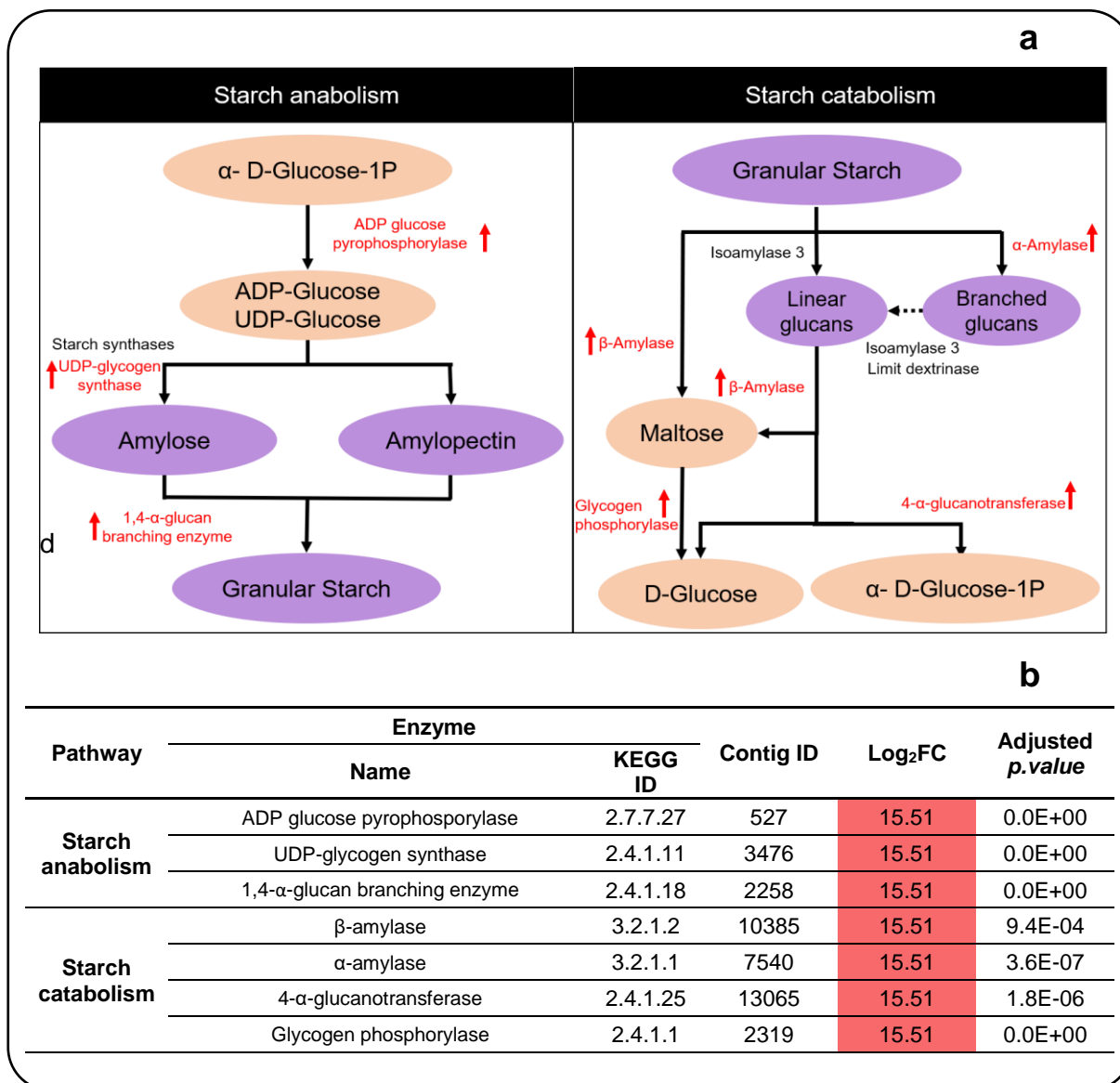


Figure 18. Starch metabolism. a) Starch anabolism and catabolism showing up and down-regulated enzyme contigs in HCA compared with LCA, red arrow indicates up-regulation, and b) contig ID, log₂FC and adjusted *p*.values for enzyme contigs.

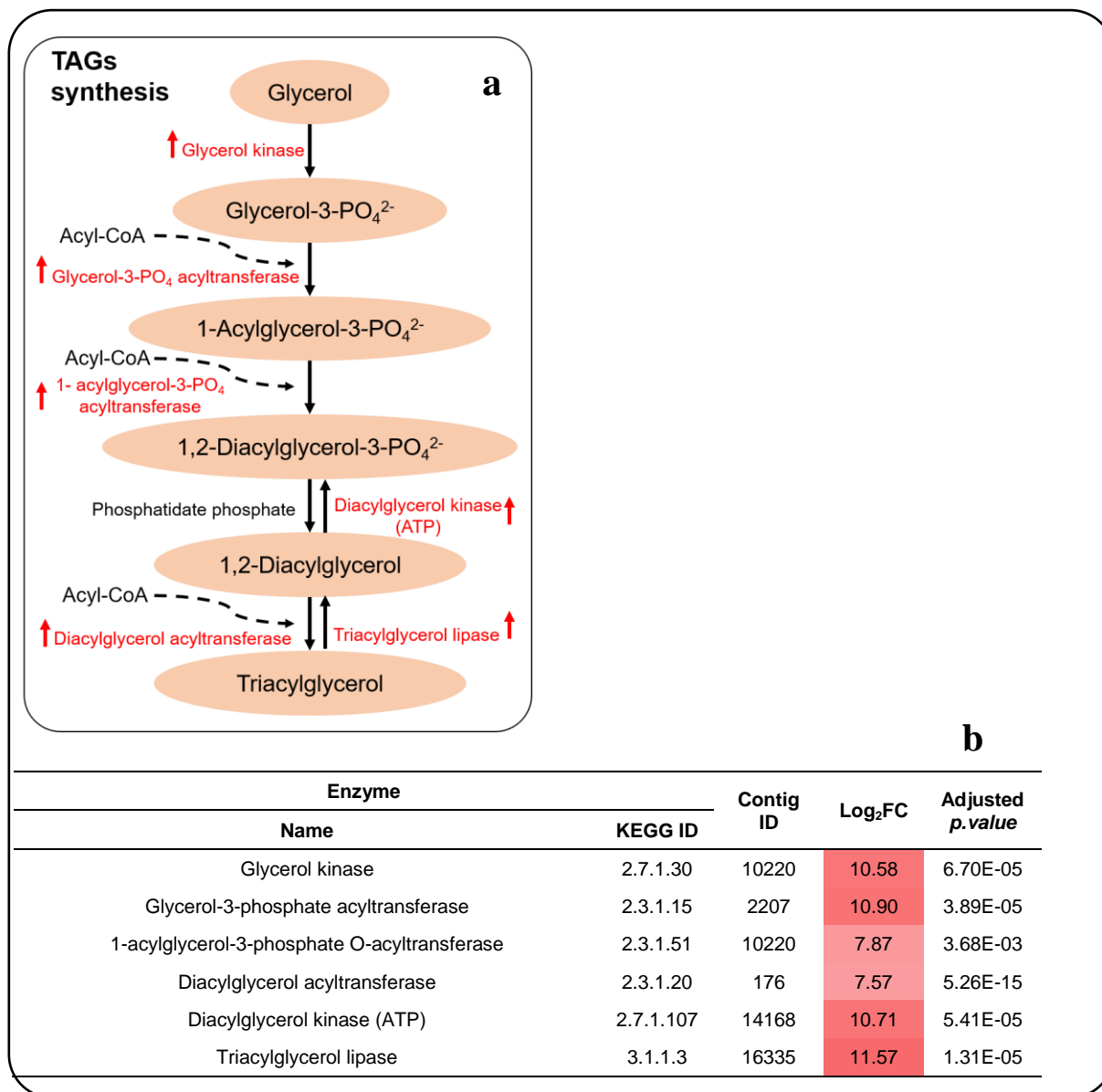


Figure 19. Final pathway steps of TAGs biosynthesis. a) TAGs synthesis showing up and down-regulated enzyme contigs in HCA compared with LCA, red arrow indicates up-regulation, and b) contig ID, log₂FC and adjusted *p*.values for enzyme contigs.

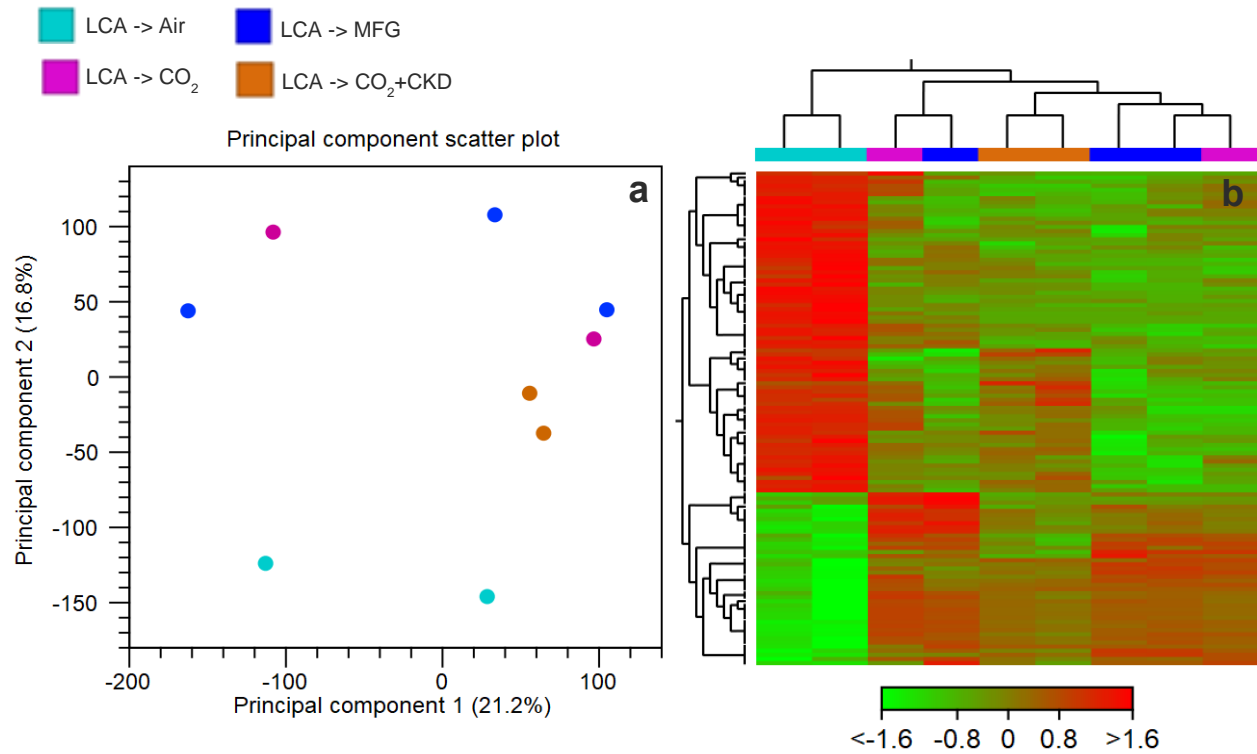


Figure 20. Transcriptome analysis of *D. abundans* controls with LCA strain under air, CO₂ and CO₂+CKD (n=2-3). a) Principal component analysis and b) heatmap of DEGs (adjusted *p.value*<0.01, $|\log_2 FC|>2$), gradient color represents change in contigs expression (red: up-regulated, green: down-regulated).

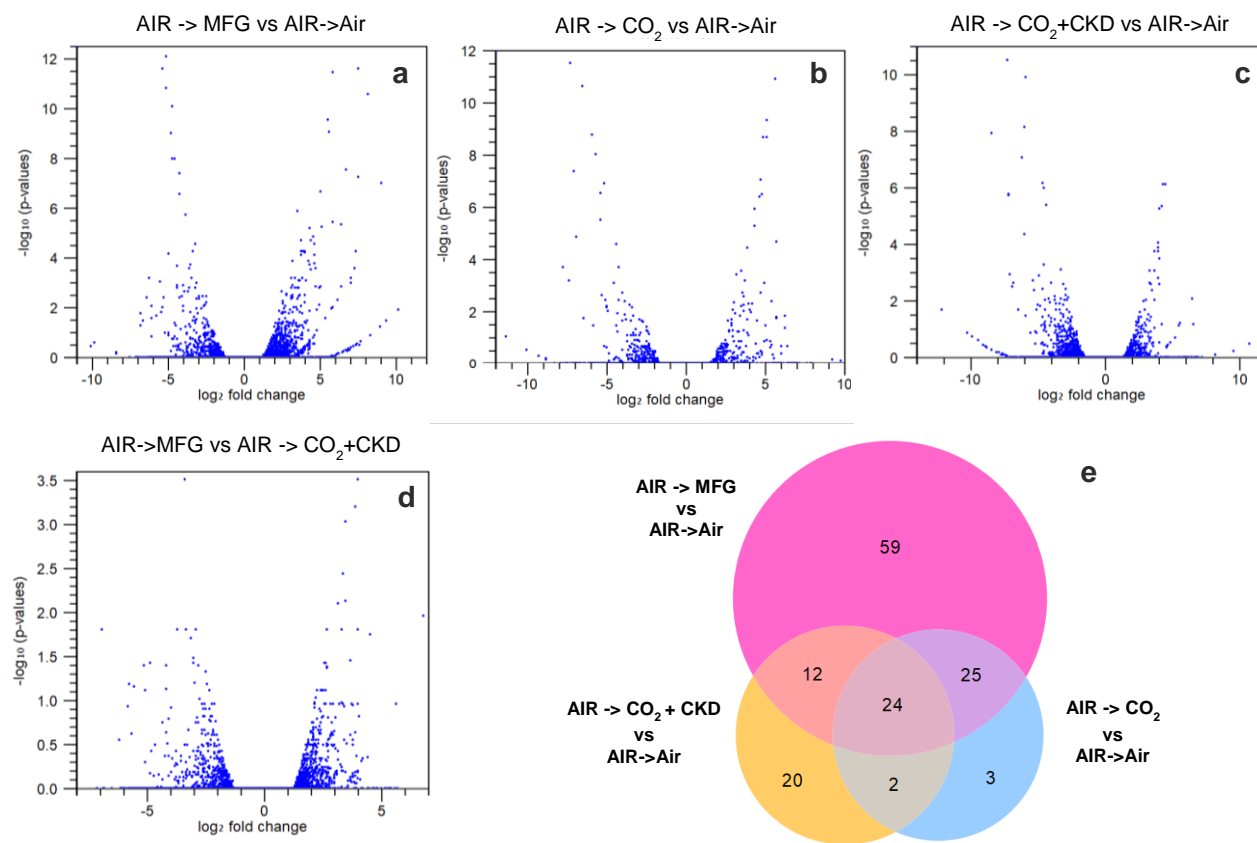


Figure 21. Volcano plot of \log_2 FC against the $-\log_{10}(\text{adjusted } p\text{-values})$ of the transcriptome analysis of *D. abundans* controls with LCA strain under air, CO₂ and CO₂+CKD. a) LCA->MFG vs LCA->air, b) LCA->MFG vs LCA ->CO₂ +CKD, c) LCA ->CO₂ vs LCA ->air, d) LCA ->CO₂+CKD vs LCA ->air and e) Venn Diagram of DEGs shared among LCA ->MFG vs AIR->air (pink circle), LCA ->CO₂ vs LCA ->air (blue circle), and LCA ->CO₂+CKD vs LCA ->air (yellow circle).

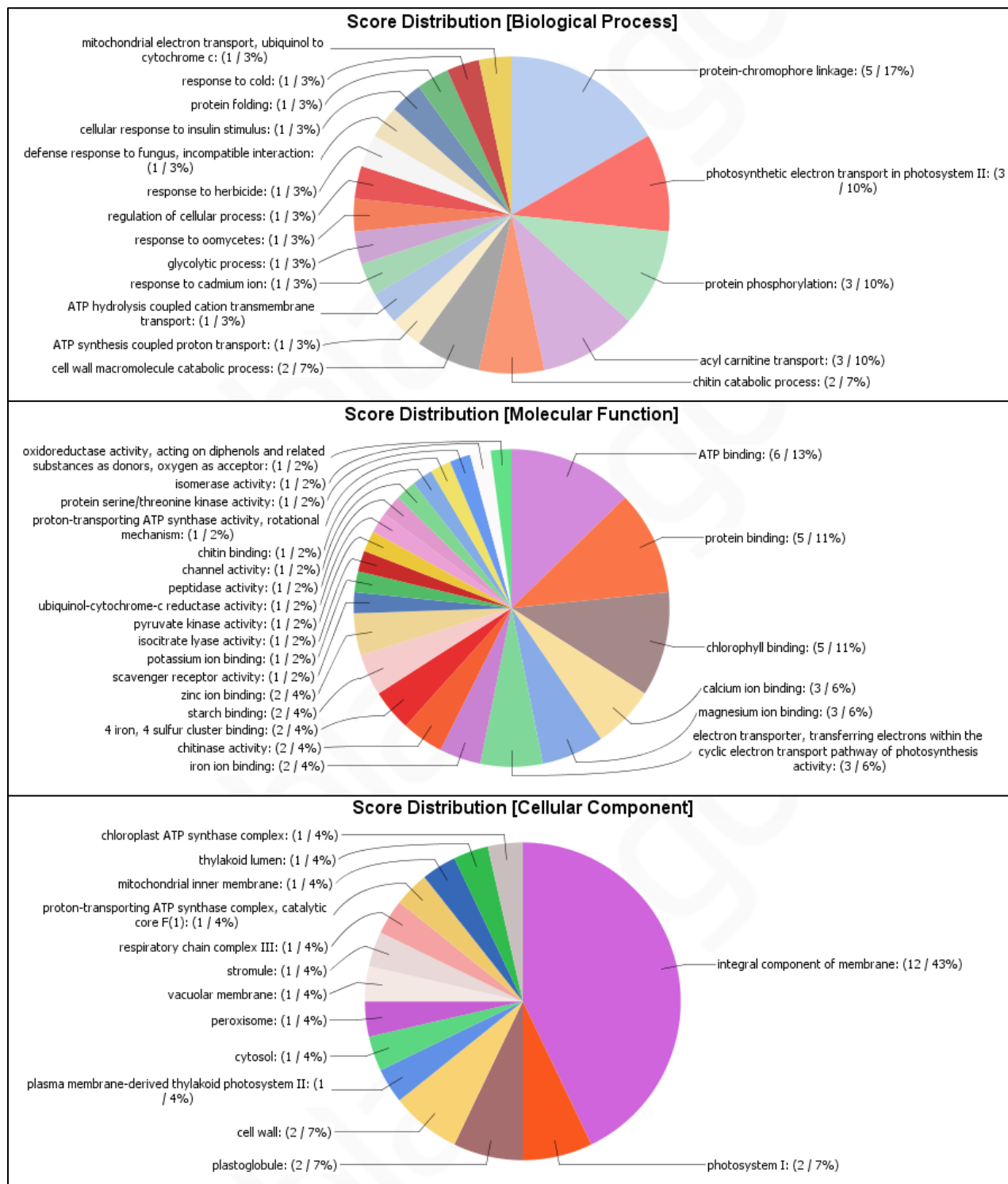


Figure 22. Multilevel pie charts of the GO annotation enrichment of DEGs (adjusted $p.value < 0.01$, $|\log_2 FC| > 2$) found in *D. abundans* control with strain LCA grown under MFG compared with an air atmosphere (n=3). a) biological process, b) molecular function and c) cellular component.

Chapter 5

Study 2: Biomass composition and lipidome analysis of the microalga *Desmodesmus abundans* under a continuous flow of model cement flue gas in a photobioreactor

Chapter 5

5. Study 2: Biomass composition and lipidome analysis of the microalga *Desmodesmus abundans* under a continuous flow of model cement flue gas in a photobioreactor

Abstract

Microalgae represent a potential strategy for flue gas mitigation as they capture CO₂ at high rates. Flue gases can also supply certain nutrients and, as a result, it can be valorized through biomass conversion into value-added compounds. The objective of this study was to characterize the biomass composition and lipidome, as well as morphological and structural changes of *Desmodesmus abundans* under an optimized supply scheme of continuous flow of cement model flue gas, using BG-11-N-S, in photobioreactor with the strain adapted for nine years to 50% CO₂ and air atmospheres. Controls with the LCA strain were also evaluated in air, CO₂ and CO₂+cement kiln dust (CKD). Cell structure analysis by SEM and TEM showed that most cells of both strains under MFG were unicellular contrary to the typical morphology of *Desmodesmus*; under air, some cells still preserved a grouping morphology. Cell size of strains under MFG was similar (17-37 μm²), while under air cells were significantly smaller (7-13 μm²). Both strains under MFG possessed high content of starch granules, a disorganized chloroplast and several lipid bodies, while a thicker cell wall was observed in strain HCA. Biomass composition at the end of the run (day 5) showed no differences in proximate analysis between strains under MFG. A 1.8 to 2-fold higher protein content in strain LCA was found in complete medium (BG-11) than under MFG (BG-11-N-S). Under MFG, the LCA strain presented the highest starch content (47.2 ± 22.3 % d.w), followed by strain HCA (23.1 ± 4.5 % d.w). On the contrary, strain HCA showed a higher content of pigments compared to the LCA strain, but the highest values were found in the control with only CO₂. Lipidome analysis resulted in 663 detected features. Between strains under MFG no many differences were found by day 5, most clear differences were observed at day 4, when both strains were in exponential growth. Particularly, 12 glycerolipids (GL) and 18 glycerophospholipids (GP) increased, and 27 GL and 3 GP decreased in strain HCA compared to the LCA strain. Still, most differences were found when the LCA strain under MFG was compared with CO₂+CKD (incomplete vs complete culture medium) that showed changes in GL (42 increased and 27 decreased) and GP (58 increased and 42 decreased), principally attributed to low N in MFG. Results showed that morphological changes appeared to be induced principally by the high CO₂ condition at the moment of growth, with no significant differences between strains, except for a thicker cell wall in the HCA strain. Overall, both strains presented a high content of starch that represents a high value compound under MFG. Further studies under flue gas could include continuous cultures with higher periods than 5 days to confirm

differences between strains HCA and LCA. Also, target metabolic of lipids that showed significant changes to a better understood of their role and potential as byproducts

Key words: Microalgae, *Desmodesmus*, flue gas, biomass composition, lipidome, morphology

5.1 Introduction

Atmospheric CO₂ has increased by 145% of the pre-industry (1750) age and it is considered the major greenhouse gas (GHG). Combustion of fossil fuels for energy generation and the cement industry are the major contributors worldwide (WBCSD, 2012; Shahzad, 2015, WMO and GAW, 2017). Therefore, there is urgency to design and implement mitigation systems and renewable energy alternatives. Microalgae possess the capacity to directly use CO₂ from industrial combustion gases with high CO₂ fixation rates, 12 times higher than terrestrial crops (Cuellar-Bermudez *et al.*, 2014; Fan *et al.*, 2015; Lara *et al.*, 2016). Therefore, these microorganisms represent an attractive strategy for mitigation systems. In addition, microalgae have been shown to use NO_x and SO_x as a nutrient source when these gases in solution oxidized to nitrite/nitrate and sulfate (Van Eynde *et al.*, 2016).

Microalga biomass present high content of value-added compounds such as pigments, proteins, carotenoids, triglycerides, fatty acids, and carbohydrates, among others (Cheban *et al.*, 2015; Duong *et al.*, 2015; Ghosh *et al.*, 2016; Sun *et al.*, 2018). Biomass composition vary among species and growth conditions. Lipid content can represent from 2 to 75% of dry weight (Ohse *et al.*, 2014; Duong *et al.*, 2015; Yao *et al.*, 2015), where Neutral lipids, mainly found as triacylglycerol (TAG), are accumulated under certain condition in a 25-50% (Chen *et al.*, 2011). Protein content vary from 10 to 45%, while carbohydrates from 25 to 75% has been reported for some species (Duong *et al.*, 2015; Yao *et al.*, 2015 Guo *et al.*, 2017).

Therefore, to stablish an economically viable and sustainable biomitigation system, flue gas from industries can be used as a nutrient source for microalgae culture, and the biomass generated used for byproduct obtaining. One of the major interests in microalga biomass is based in their use for biodiesel from lipid and bioethanol from starch (Bertozzini *et al.*, 2011; Sun *et al.*, 2018). CO₂ generated during combustion is equal or lesser than the captured by microalgae (Perrineau *et al.*, 2014) and the average yield of biofuel can be from 10 to 20 times higher than the yield obtained from vegetables oils or oleaginous seeds (Ghosh *et al.*, 2016).

Some advantages of microalga use over other biological systems are the rapid growth rate, capacity to grow in waste water and other low-cost culture media, high productivity reaching values up to 75 tons of biomass per hectare per year in open bioreactors and that they are cultivated in non-arable lands, therefore this process do not compete with food production (González-Lopez *et al.*, 2011; Bertozzini *et al.*, 2011; Oshe *et al.*, 2014; Duong *et al.*, 2015). Also, once the lipid has been extracted byproducts like protein, pigments and other compounds can be obtained (Garibay-Hernandez *et al.*, 2009).

The microorganism in study, *Desmodesmus abundans* (strain RSM, UTEX no.2976), is an environmental microalga isolated in 2008 by our group from a river in Monterrey, Nuevo León México (Lara-Gil *et al.*, 2014). The strain has been maintained under high CO₂ concentrations, 25 and 50% CO₂, and air for nine years. Lara-Gil *et al.* (2014 and 2018) demonstrated that *D. abundans* can tolerate, grow and used components from cement flue gas as nutrient sources by a supply scheme of 24 cycles of flue gas. In the present study an optimize supply scheme of continuous flow of cement flue gas in a 1 L column photobioreactor was used, and in order to found value-added compounds, microalgal biomass composition and lipidome was analyzed, as well as morphological and structural changes, *Desmodesmus abundans* strain adapted for nine years to 50% CO₂ and air atmospheres were used.

5.2 Materials and methods

5.2.1 Microalga and culture conditions

Desmodesmus abundans strain RSM (UTEX 2976) was isolated from an environmental sample collected in 2008 by our research group from a freshwater river (pH 7.4) in the city of Monterrey, Nuevo Leon, Mexico. The strain was isolated after sample enrichment under an atmosphere of 25% CO₂ (Lara-Gil *et al.*, 2014) and maintained for around nine years under atmospheres of air (0.04% CO₂) and 50% CO₂ in 125 mL flasks containing 20 mL of BG-11 medium, pH 7.4 (UTEX 2009). Cultures were maintained every 10 d in batch and the pH was not controlled during growth. Enriched CO₂ atmospheres were obtained by using rubber stoppers and removing with a 60 mL syringe the corresponding volume of air from the headspace and adding the same volume of 99.9% (v/v) CO₂ (AOC Mexico, NL, Mexico). Cultures were incubated at 25 ± 2 °C, 60-70 μmol PAR photons m⁻² s⁻¹ of continuous light and 110 rpm agitation using an orbital shaker. For experimentation, *D. abundans* acclimated to atmospheres of 50% CO₂ and air were studied and referred to as strains HCA (high CO₂ acclimated) and LCA (low CO₂ acclimated), respectively.

5.2.2 Microalga growth under model cement flue gas

D. abundans was cultured in a 1 L customized column photobioreactor (6 cm diameter, 45 cm height) with 980 mL working volume at 25 ± 2 °C and continuous illumination. Temperature was controlled by a water jacket made of glass covering the column and illumination by four external fluorescent lamps (4000 K cool white, Philips) placed around the column, which provided 80-90 $\mu\text{mol PAR photons m}^{-2} \text{ s}^{-1}$ to the interior of the vessel. Gas was supplied to the reactor at a continuous flow of 49 mL min^{-1} (0.05 vvm) by a sparger stone at the bottom of the column and axis with metal meshes of 1 mm distributed each 5 cm and covering the entire diameter of the bioreactor were used for gas retention.

Simulated flue gas components represented exhaust gas from a modern cement plant with a desulfurization system; concentrations used approximate maximum reported values (wbscd, 2012; LRTAP and EEA, 2016). Hence, the model cement flue gas consisted of 250 000 ppm CO_2 , 700 ppm NO and 100 ppm SO_2 (in v/v). Independent mass flow meters were used to aerate each gas to a principal line. Cement kiln dust (CKD) was also considered as a component of the flue gas and was used as a strategy to control culture pH (Lara-Gil *et al.*, 2014 and 2016). CKD was collected from a local cement plant in Hidalgo (NL, Mexico) and sterilized by thinly spreading 150 mg into a polystyrene weighing dish and exposing it to UV light for 30 min under a laminar flow cabinet. CKD was delivered to the bioreactor daily by dissolving 150 mg in 11 mL of fresh culture media.

To evaluate the potential of the cement flue gas as a nutrient source of N and S, culture medium was prepared without nitrogen and sulfur (BG-11-N-S). Therefore, NaNO_3 and $\text{MgSO}_4 \cdot 6\text{H}_2\text{O}$ were replaced with NaCl and $\text{MgCl}_2 \cdot 6\text{H}_2\text{O}$, respectively, to provide the same Mg and Na concentration and preserve medium conductivity. Before inoculation in the photobioreactor, 580 mL BG-11-N-S with 150 mg of CKD were aerated with flue gas for 4 h to provide N and S, and avoid microalga starvation. During this period, flue gas composition was 35-40% NO and SO_2 concentration (i.e., 233 ppm NO and 40 ppm SO_2), and 25% CO_2 . After, 400 mL of medium containing the inoculum was added and, from this moment on, an acclimation period of 24 h was conducted under this flue gas condition. After the acclimation period, gas concentrations were set to the simulated cement flue gas (25% CO_2 , 700 ppm NO, 100 ppm SO_2) and 150 ppm w/v of CKD was added every 24 h. Initial biomass concentration in the bioreactor was normalized to $\text{Abs}_{750 \text{ nm}} 0.13 \pm 0.02$ ($0.4 \text{ g d.w. L}^{-1}$) of an active $\frac{3}{4}$ log phase culture. These were previously grown in 500 mL flasks containing 75 mL of BG-11 medium and 25 mL of inoculum ($\frac{3}{4}$ log phase)

for a final work volume of 100 mL, and 50% CO₂ and air (0.04% CO₂) atmosphere were supplied according to the strain (See section 3.2.1) used. Before normalization, the inoculum was harvest by centrifugation (5000 rpm, 15 min, 4°C) and the pellet washed with the experimental medium (BG-11-N-S) for MFG runs.

Experiments under MFG were conducted with the strains HCA and LCA to compare strains differential responses to MFG after nine years of enrichment (see Section 4.2.1). In addition, the LCA strain was used to analyze the effect of the main components of the model flue gas. Control runs in complete culture medium (BG-11) contemplated aeration with only air, 25% CO₂ and 25% CO₂ + CKD, in order to assess the effect of CO₂, CKD and source of N and S. To maintain experimental culture pH as in the aeration of the MFG, the initial pH of BG-11 medium was adjusted to 6.2 using a phosphate buffer (pH 6.2). All bioreactor runs were sampled every 24 h by removing 11 mL of the culture that were centrifuged (5000 rpm, 5 min, 4°C) to generate a pellet that was used to determine productivity. Biomass at end of run (5 d) was harvested, lyophilized and used to determine biomass composition (proximal analysis), starch, chlorophyll and carotene content; and for lipidome analysis. A fresh sample was recollected at 5 d for scanning electron microscopy (SEM) and transmission electronic microscopy (TEM).

5.2.3 Scanning electron microscopy (SEM) and transmission electron microscopy (TEM)

D. abundans strain morphology under different growth conditions (strain HCA in MFG, strain LCA in MFG and strain LCA in air) was analyzed at day 5 during the bioreactor run using Zeiss EVO MA25 SEM (Zeiss, Germany). For SEM and TEM analysis, a sample of 2 mL was centrifuged (2250 rpm, 10 min, 20 °C) and the pellet was washed with 300 µL of medium, fixed with 2.5 % w/v glutaraldehyde Grade I (Sigma-Aldrich, MO, USA) solution in 0.1 M phosphate buffer for 24 h (Matusiak-Mikulín *et al.*, 2007) and washed 3X with 300 µL of 0.1 M phosphate buffer, each with 3 min of incubation. For SEM, fixed cells were then washed 2X with 70% v/v ethanol (DEQ, México), placed in a SEM conductive double side carbon tape, dried in desiccator at least for 2 h and coated with gold for charge dissipation. Images were obtained using an accelerating voltage of 20 kV. For TEM, fixed cells were storage at 4°C and analyzed by the Cell Physiology Institute (UNAM, Ciudad de Mexico, Mexico). From TEM images, the cell size and wall cell thickness were analyzed using ImageJ 2.0 program.

5.2.4 Proximate analysis of microalgae biomass

Biomass was harvested at the final of the run (5 d) by centrifugation at 5000 rpm 5 min, 4°C and washed two time with medium. The pellet was stored at -80° C for at least 24 h, lyophilized for 48 h and stored at -80 °C until be used. Dry matter content was determined by difference weight after oven-drying at 100 ± 5 for 24 h. Determination of lipid content was performed using 0.5 g d.w. of biomass and was quantified gravimetrically after ethylic ether extraction using the Goldfish method and oven-drying for 24 (Medina, 2006). Defatted samples were used for crude fiber and ash gravimetric determinations, utilizing the official methods AOAX 962.09 and AOAC 923.03, respectively. Crude protein was analyzed by micro-Kjeldahl Official method AOAC 978.02 using 50 mg d.w. of biomass. Protein were characterized by solubility according to Osborne method (Osborne, 1895).

5.2.5 Starch content determination

Starch was determined using a modified amylase/amylglucosidase method of the Starch Assay kit STA20 (Sigma-Aldrich, MO, USA). For sample preparation, a tube containing 25 mg of lyophilized biomass was added 2 mL 80% v/v ethanol and the mixture was incubated at 85°C for 5 min. Followed, 20 beads were added and rupture was performed in the FastPrep®-24 Homogenizer (MP Biomedicals, CA, USA) at 6 m s^{-1} for 40 s. Then, 2 mL 80% v/v ethanol was added to the mix, centrifuged (1000 g for 10 min) and the supernatant discarded. The pellet was resuspended in 4 mL 80% v/v ethanol, mixed, centrifuged (1000 g for 10 min) and the supernatant discarded. Followed, 500 μL of DMSO and 50 μL 80% v/v ethanol was added, vortexed for 30 s and incubated in a water boiling bath for 5 min. For starch digestion, 750 μL water and 20 μL of α -Amylase were added, mixed, incubated in a boiling water for 5 min and cooled to room temperature. The volume was bring up to 2.5 mL with water and mixed. Then, to a 250 μL of this solution, 250 μL of Starch Assay Reagent was added, mixed and incubate at 60°C for 15 min with vortex each 2 min. Tubes were cooled at room temperature, 250 μL of the solution was diluted to 2.5 mL with water. Finally, Glucose assay performed as indicate the protocol using $\frac{1}{4}$ of volumes.

5.2.1 Pigment content determination

Chlorophyll *a* and *b*, and carotenes were determined by optical absorbance in a microplate reader Synergy HT (Bio Tek, Vermont, USA) using a modified protocol described by Pancha *et al.*, (2014). In a 2 mL tube, 1.0-1.5 mg of lyophilized biomass were weighted, then 2 mL 100% v/v methanol (BHD, PA, USA) were added and the solution was sonicated for 1 min and incubated

at 45° C for 24 h. After, 250 µL of the solution were placed in a microplate and read at 665 and 652 nm for chlorophyll a and b, respectively; and at 470 nm for carotene determination. All absorbances were corrected at 750 nm. Pigment content was calculated using the following equations (Lichtenthaler, 1987):

$$Chl\ a\ (\mu\text{g}\ \text{mg}^{-1}) = (16.72 (A_{665\text{nm}} - A_{750\text{nm}}) - 9.16 (A_{652\text{nm}} - A_{750\text{nm}})) * (Ve/(Pm*L))$$

$$Chl\ b\ (\mu\text{g}\ \text{mg}^{-1}) = (34.09 (A_{652\text{nm}} - A_{750\text{nm}}) - 15.28 (A_{665\text{nm}} - A_{750\text{nm}})) * (Ve/(Pm*L))$$

$$C\ (\mu\text{g}\ \text{mg}^{-1}) = ((1000 (A_{470\text{nm}} - A_{750\text{nm}}) - 1.63\ Chl_a - 104.9\ Chl_b)/221) * (Ve/(X*L))$$

Where,

Chl= Chlorophyll

C= Carotenes

Ve = Extract volume (mL)

X = Biomass sample (mg)

L = Light path of cuvette (cm)

5.2.2 Statistical analysis

One-Way Analysis of Variance (ANOVA) was performed to compare group means of the different set of data using Minitab® 18 (Minitab Inc., PA, USA). Differences among groups were assessed with Tukey's HSD test. An alpha of 0.05 was used for all tests.

5.2.3 Lipidome analysis

Lipid extraction

To extract lipids, 5 mg of lyophilized biomass were weighed in 15 mL polypropylene tubes, where 1.5 mL 100% methanol (BDH, PA, USA), 500 µL HPLC water and 10 glass beads (1 mm diameter) were added. Then, cell rupture was performed in the FastPrep®-24 Homogenizer (MP Biomedicals, CA, USA) at 6 m s⁻¹ for 40 s. The lysed cells were mixed in a vortex, sonicated for 1 min and left at room temperature for 1 min, this step was repeated five times. The content, without the beads, was transferred into a glass tube covered with aluminum, where 5 mL methyl tert-butyl ether (J.T.Baker, PA, USA) were added, and mixed with vortex, sonicated for 1 min and incubated at room temperature in darkness in orbital shaker at 250 rpm for 1 h. After, 1.25 mL HPLC water were added, vortex, sonicated for 1 min and incubated at room temperature in the shaker (250 rpm, 10 min). The mixture was centrifuged (500 g, 20 min) and the organic phase (upper) was recovered in a new tube. The aqueous phase was washed with 2 mL methyl tert-

butyl ether:methanol:water (20:6:7), the solution was prepared a day before and the upper phase was used, the organic phase was recovered and combined with the previous. Then, the organic phase was evaporated at 55 °C using a CentriVap Concentrator (LABCONCO, MO, USA) to generate the lipid extract, which was stored at -80 °C until analysis.

Chromatographic separation

The lipid extract was separated by HPLC (Series 1100; Agilent, CA, USA) coupled via ESI to a TOF MS Detector (G1969A; Agilent, CA, USA) system, using a Luna C18(2) column (150x2 mm, 3 µm; Phenomenex, CA, USA). The gradient elution program consisted in water:acetonitrile (4:1 v/v; phase A) and isopropanol:acetonitrile (9:1 v/v; phase B) as mobile phases, both modified with 10 mM ammonium acetate and 0.1% formic acid. The program for sample separation was set at 55 °C and the elution gradient had a constant flow of 0.2 mL min⁻¹. A linear gradient was generated with ramps from 40 to 43% B (6 min); changing immediately to 50% B and increasing linearly to 54% B until minute 36; then jumped to 70% B and increased to reach 99% B by minute 54. This condition was kept until minute 55, in this point column returned to the initial condition (40% B), where it equilibrated (10 min). ESI drying gas, nitrogen, was set to 13 L h⁻¹, at 350 °C, using a nebulizer pressure of 35 psig, with a capillary voltage of 4.5 kV to favor the fragmentation. The optical parameters were set to 250 V for the octupole radio frequency voltage (Oct RFV), 225 V for the fragmentor and 60 V for the skimmer.

Runs were performed to acquire mass spectra in positive mode and files were saved in profile mode with an m/z range from 150 to 1500. Readings were obtained at 0.94 cycles per second, with a total of 10,000 transients per scan. Samples were injected in a random manner and began with a set of 3 'dummy' runs, 3 QC equidistants where the same amount of a mix of all samples was injected.

Feature detection

Raw files were converted to CDF with Agilent's Translator Utility (Agilent, CA, USA) and processed with MZmine 2.28 platform (Pluskal *et al.*, 2010). Peak detection was performed using GridMass algorithm (Treviño *et al.*, 2015), where the parameters used were: minimum height of 30000 counts, m/z tolerance of 0.05, retention time (RT) window between 0.1 and 1 min, smoothing time of 0.1 min, intensity similarity ratio of 0.5 and smoothing m/z of 0.05. Isotopes were grouped using a m/z tolerance of 0.001 or 10 ppm, RT tolerance of 0.25, maximum charge of 2 and a monotopic shape was assumed. The feature alignment was done by utilizing the

RANSAC algorithm, using a m/z tolerance of 0.025 (50 ppm), a RT tolerance of 1 min before and 0.8 after RT correction, a minimum of 20% points matching the non-linear model below a threshold of 0.4 min. Peaks were filtered using 2 as minimum of peaks in a row. Gap filling was performed using a same RT and gap range m/z filler algorithm with a m/z tolerance of 0.025 (50 ppm). Further analysis were performed in R platform (Team RC R, 2013).

Assignment of identity

An algorithm in R was created to automatize identity assignment based on the Lipid MAPS® database (Fahy *et al.*, 2009). Tolerance of 0.05 for m/z was utilized for researching and molecular formula, name and Lipid Maps® classification were retrieved. Assignations were cleaned by comparing theoretical isotopic pattern of the molecular formula with the intensities. Because a single feature returned more than one assignation, with all possible identities belonging to the same category, the category was fixed to only one category assignation. Also, for those which only one class was retrieved, the class was assigned too.

Statistical analysis

All statistical procedures were performed using R platform. Areas were log-transformed and quantile-normalized. Principal component analysis was performed using ggbiplot package (Wickham, 2016). t-test among independent groups was performed and *p.value* were corrected by false discovery rate (FDR) using Benjamini and Hochberg's method (Benjamini and Hochberg, 1995), where *p-values* <0.05 were considered a significant. Then, using only the significant features cloud plots were created by plotting the size and transparency in function of log₂FC and *p.value*, respectively.

5.3 Results

5.3.1 Cell morphology and structure

Cells of *D. abundans* strains were characterized by SEM and TEM when grown under MFG and an air atmosphere (Fig. 23-24). Most cells under MFG and air presented an unicellular circular morphology, contrary to typical *Desmodesmus* genus morphology that present linearly ordered groupings of 2-8 no. ellipsoidal cells with spines in the outer cells. Under optical microscopy and for the air condition only, some cells still preserved this grouping morphology (data not shown). Under MFG, using SEM and TEM information, strain HCA and LCA showed no significant

differences in cell diameter or area (Tukey' HSD test, $\alpha=0.05$) (Fig. 24, Table 10). However, when the LCA strain grew in an air atmosphere a 1.7- and 2.7-fold reduction in cell diameter and area was observed, respectively (Tukey' HSD test, $\alpha=0.05$) (Fig. 24e-f, Table 10). The majority of the air control grown cells presented an area of 7-13 compared to 17-37 μm^2 under MFG.

TEM analysis of the strains under MFG showed a great quantity of starch grains, and some lipid bodies and plastoglobuli (Fig. 24a-f). Also, a disorganized chloroplast was observed in this condition because the high amount of storage structures that presented these cultures. In particular, HCA CO_2 showed a large unidentified spherical organelle (Fig. 24b,c) and a significantly 1.6-fold thicker cell wall than the LCA strain under MFG (Tukey' HSD test, $\alpha=0.05$) (Fig. 24c,f; Table 10). Moreover, the LCA strain showed a particular large vacuole (Fig. 24d-f) that was not observed in the HCA strain. In the air condition, LCA strain showed larger vacuoles containing polyphosphate granules and organized chloroplasts, pyrenoid and mitochondrias located near the chloroplast periphery (Fig. 24g-i). No statistical difference in cell wall thickness between LCA strain grown under MFG and air was observed (Tukey' HSD test, $\alpha=0.05$) (Table 10). However, average values were 68% higher under MFG.

5.3.2 Biomass composition

As a first approach to characterize the biomass of the strains under the different growth conditions a proximate analysis was performed (Table 11). No significant differences were found between strains under MFG (Tukey' HSD test and t-test, $\alpha=0.05$). These cultures presented around 21% (w/w) protein, 3-4% (w/w) crude fat (ether extract), 10-11% (w/w) crude fiber, 6% ash and the rest corresponded to the N-free extract, basically carbohydrates (59% w/w). It is important to mention that crude fat represents the lipid fraction with affinity to ethylic ether. Biomass of the controls grown under air, CO_2 and CO_2 +CKD with complete culture medium possessed 1.8 to 2-fold more protein than the same strain under MFG. Crude fat (ether extract) was significantly lower (Tukey' HSD test and t-test, $\alpha=0.05$) by 97, 95 and 30 % in air, CO_2 and CO_2 +CKD, respectively.

Protein characterization of both strains under MFG showed that albumins represented the highest fraction of total protein (15 and 19 % for strain HCA and LCA, respectively) followed by glutelins and globulins (8-9 %); while prolamins (4 %) were the lowest (Fig. 25). A high proportion of residues were also found (40-43 %), these correspond to proteins that are not soluble in neither water, salt, ethanol and isopropanol.

5.3.3 Starch content

Starch content of *D. abundans* under MFG was 23.1 ± 4.5 and 47.2 ± 22.3 % d.w. for HCA and LCA, respectively. (Fig. 26). LCA strain in MFG showed significantly higher content of starch by 5.3 to 10.7-fold than under gas supply of air, CO₂ and CO₂+CKD. Among control runs no significant differences were found with 4.4 ± 1.1 , 6.9 ± 0.4 and 8.8 ± 1.23 % for air, CO₂ and CO₂+CKD, respectively.

5.3.4 Chlorophyll and carotenoid content

Chlorophyll a (*Chl a*) and b (*Chl b*), and carotenoid content of the microalga strains under the different growth conditions are shown in Figure 27. Strain HCA under MFG possessed 7.7 ± 0.5 $\mu\text{g mg}^{-1}$ *Chl a*, 2.5 ± 0.2 $\mu\text{g mg}^{-1}$ *Chl b* and 2.8 ± 0.2 $\mu\text{g mg}^{-1}$ carotenoids, being *Chl a* 2.5 to 3-fold higher than the other pigments. Under the same growth condition, the LCA strain showed significantly lower pigment content (Tukey' HSD test, $\alpha=0.05$), 35 %, 44 % and 32 % lower *Chl a*, *Chl b* and carotenoids, respectively. Control runs of the LCA strain in an air atmosphere did not showed differences in pigment content to MFG (Tukey' HSD test, $\alpha=0.05$). However, under CO₂, pigment content increased substantially by 2.1-fold *Chl a* and *Chl b*, and 1.7-fold carotenoids. The same behavior was observed under CO₂+CKD but with a smaller increase compared to CO₂ only. No significant differences were found in *Chl a/Chl b* ratio among strains or culture conditions (Table 12). Similarly, the carotenoids/*Chl a+b* ratio for both strains under MFG was similar but the control strain LCA under an air atmosphere presented a significantly higher ratio, while CO₂ and CO₂+CKD showed the lowest values (Tukey' HSD test, $\alpha=0.05$).

5.3.5 Lipidome changes of *D. abundans* under model cement flue gas

Lipidome profiles were determined for the microalga strains under the different growth conditions. The HCA strain under MFG showed a significantly lower lipidic extract content (9 ± 1 % d.w.) than the LCA strain under the same atmosphere (19 ± 1 % d.w.) (Tukey' HSD test, $\alpha=0.05$) (Fig. 28a). No differences were found among the LCA strain grown in MFG and the other control conditions (Tukey' HSD test, $\alpha=0.05$), which presented lipidic contents of 18-21 % d.w. However, principal component analysis of all detected peaks showed that MFG experiments clustered together apart from the control groups by component 1, which explained 41% of data variability (Fig. 28b). Principal component 2, separated strains in MFG and air from CO₂ and CO₂+CKD runs, explaining 16.9 % of the variability. These results are reflected in the scatter plots, where high dispersion of data sets was observed in MFG experiments against the controls (Fig. 28c). Furthermore, among

the controls, comparisons between air vs CO₂ and air vs CO₂+CKD also presented high dispersion, while CO₂ vs CO₂+CKD correlated to a higher degree.

HPLC-MS lipidome analysis resulted in a total of 663 peaks after feature alignment and gap filling using MZmine software, then identities were assigned in Lipid Maps® database, resulting in 480 peaks with identity. From these molecules, 49 fatty acyls (FA), 211 glycerophospholipids (GP), 163 glycerolipids (GL), 34 sterol lipids (ST), 21 polyketides, 52 sphingolipids (SP) and 2 prenol lipids (PL) were identified (Fig. 29).

Differential lipidome analysis between strains HCA and LCA under MFG showed 21 features with differential changes (*t-test*, *p.value*<0.05), where the most changes occurred in the lipid categories of glycerolipids (GL) (7 of 163 identified) and glycerophospholipids (GP) (9 of 211 identified) (Fig. 30). The tendency of these features in the HCA strain was 5 GL and 4 GP decreased and 2 GL and 5 GP increased (Fig. 30). Most of these lipids presented a fold change lesser than 3-|log₂FC| (Fig. 31a). Additionally, one SL, one sphingolipid and two polyketides presented higher intensities in the HCA strain.

Furthermore, lipidome analysis of the strains under MFG was also conducted at day 4 of culture to evaluate the effect of growth phase. At day 4, both strains were in exponential phase contrary to day 5 where HCA was entering the stationary phase (Fig. 4). At this moment, more differences in lipidome were found, 12 GL and 18 GP increased, and 27 GL and 3 GP decreased in HCA strain compared to the LCA strain (Fig. 32).

The LCA strain was further evaluated in the other control growth conditions, comparing MFG with an air atmosphere resulted in an increased of differential changes; mainly, GL and GP with 27 and 40 molecules, respectively (*t-test*, *p.value*<0.05) (Fig. 30). The most affected GL classes were glycerophosphates and glycerophosphocolines/ethanolamines (Fig. 30-31). Log₂FC for GL were between 2.0 and 5.0 with the majority being TAGs, except for three DAGs (Fig. 31b); and GP exhibited 1.6 to 4.2 log₂FC. In addition, some SP (2 to 5 log₂FC) and ST (4 to 5.5 log₂FC) also increased under MFG. Air supply of only CO₂ and CO₂+CKD were also compared to an air atmosphere to evaluate the effect of these components individually; however, less than 4 % of the 663 detected features corresponded to significant changes in these conditions (Fig. 30). The lipids categories with the most notable changes were found in the CO₂+CKD condition where GL

showed 5 features decreasing and 8 increasing (3 to 1 \log_2FC), and 8 GP decreasing (-4 to -1.5 \log_2FC).

To evaluate the effect of the source of N and S, LCA strain under MFG (in incomplete culture medium, BG-11-N-S) was compared to LCA strain under CO₂+CKD (in complete culture medium, BG-11) (Fig. 30, 31). A total of 236 features with significant changes were obtained in most lipid categories (*t-test*, *p.value*<0.05). These corresponded to 69 GL, 100 GP, 19 ST and 15 SP, of which notable changes are shown in the cloud plot (Fig. 31c). The most drastic changes when grown in BG-11-N-S were observed in GL (42 increase and 27 decrease) and GP (58 increase and 42 decrease) with \log_2FC up to 8 (largest circles). Of the GP molecules, major changes were found in glycerophosphates with 27 features decreasing and only 1 feature increasing and in glycerophosphocolines/ethanolamines with 18 assignments increasing and 5 decreasing (Fig. 33). The majority of ST (17 assignments) and SP (11 assignments) with significant changes presented higher intensities in MFG than air.

Characterization of these molecules by number of carbon atoms and unsaturations is presented in Figures 34 and 35. All GP with significant changes had 15 to 52 carbon atoms and 0 to 9 unsaturations (Fig. 34a-c). Especially, GP from the comparison of the LCA strain under MFG vs CO₂+CKD showed a higher frequency of molecules with 40-44 carbons and 0-1 unsaturations. For TAGs, number of carbon atoms was 44 to 60, of these 54, 56, and 58 C were more frequent (Fig. 35a); and unsaturation numbers presented a range of 0 to 9 (Fig. 30b). DAGs presented 31 to 45 carbon atoms, and from 0 to 9 unsaturations (Fig. 35c-d).

5.4 Discussion

5.4.1 Morphological and structural changes

Cell morphology of the *Desmodesmus* genus is characterized by 2-8 linearly ordered cells with ellipsoidal shape and spines (El Semary, 2011; Hegewald and Braband, 2017; Ozturk *et al.*, 2018), these characteristics were originally shown by the microalga in this study. However, after laboratory culturing, individual circular cells without spines have been observed. When *D. abundans* strains were grown in the photobioreactor and aerated with MFG and air this morphology was also observed (Fig. 23). However, the strain LCA under an air atmosphere presented some grouping of cells with ellipsoidal shape (data not shown). Similarly, Pancha *et al.* (2014) observed morphological changes in *Scenedemus sp.*, a phylogenetically close microalga, when cultured under different N concentrations, and explained that diverse growth conditions

(photoperiod, pH, nutrients and other parameters) can trigger morphological changes from unicell to coenobia. This phenotypic plasticity has also been reported for the genus *Desmodesmus* under different N sources (ammonia or nitrate) or induced by plant hormones (Malerba *et al.* 2016; Chung *et al.* 2018).

Cell size differences as a function of cell diameter and area between strains under MFG showed no differences, but significant smaller cells were observed under an air atmosphere for the LCA strain (Fig. 23, Table 10). An increase in cell size seems to be correlated with the MFG atmosphere that resulted in a high quantity of starch grains and several lipid bodies observed in the TEM micrographs (Fig. 24). Furthermore, under MFG the HCA strain showed a large unidentified spherical organelle, while the LCA strain presented clear vacuoles. Matusiak-Mikulin *et al.* (2007) reported that a small number of vacuoles with low amounts of polyphosphates is a characteristic of high cell metabolic activity. This structure was also identified in the LCA strain under an air atmosphere, where larger vacuoles containing polyphosphate granules were observed. Also, in air this strain showed organized chloroplasts, pyrenoid and mitochondrias located near the chloroplast periphery (Fig. 24g-i). Absence of lipids and starch grains in the air condition could be caused by a low photosynthetic activity of the strain caused by limited CO₂. This is also reported when an organized chloroplast is observed as *Desmodesmus* has been shown to consume energy from lipids under respiratory, glycolytic and photosynthetic conditions, where the demand for carbon skeletons and energy is high, allowing cell growth (Matusiak-Mikulin *et al.*, 2007).

A significant thicker cell wall was exhibited by the strain HCA under MFG. This seems to be caused by previous acclimation of the strain to high CO₂, several studies have found a higher content of cell wall components in microalgae under high CO₂ (Westerhoff *et al.*, 2013; Cheng *et al.*, 2014; Solovchenko *et al.*, 2015). Previously, it has been found that the principal contributor to cell wall thickness in *Desmodesmus sp.* is the polysaccharide layer that thickens because it works like a sink for excessive content of photosynthates (Solovchenko *et al.*, 2015). Likewise, diverse species of *Chlorella* showed an increase in cell wall thickness under high CO₂, where uronic acid accumulated (Cheng *et al.*, 2014).

5.4.2 Biomass composition

Microalga biomass is rich in value-added compounds such as protein, lipids, carbohydrates, pigments and polymers, among others (Oshe *et al.*, 2014; Cheban *et al.*, 2015; Gosh *et al.*, 2016;

Guo *et al.*, 2017). Considering microalga capability to grow and use waste components from exhaust gases as a nutrient source, their conversion into valuable byproducts is of interest (Cuellar-Bermudez *et al.*, 2015; Lara-Gil *et al.*, 2016). In this study, as a first approach to characterize the generated biomass under model flue gas, proximate analysis in the different culture conditions were performed. *D. abundans* strains HCA and LCA did not show significant differences in their biomass composition under MFG and possessed around 21 % (w/w) protein, 3-4 % (w/w) crude fat (ether extract), 10-11 % (w/w) crude fiber, 6 % (w/w) ash and 59 % (w/w) carbohydrates (N-free extract) (Table 11). Controls with the LCA strain grown in air, CO₂ and CO₂+CKD with complete culture medium exhibited 1.8 to 2-fold more protein than the LCA strain under MFG, while crude fat (ether extract) was lower. It has been reported that microalga growth and biomass composition vary under different culture conditions, as a result of changes in metabolic pathways in response to factors like nutrient limitations and high or low CO₂ (Sun *et al.*, 2018).

Because nitrogen is an essential element for protein biosynthesis (Valenzuela *et al.*, 2012; Giordano and Raven, 2014), lower protein content in the MFG condition could be caused by limited N supply, since N in this growth condition was only provided by the bubbled flue gas. Analysis of dissolved NO_x under abiotic conditions showed that MFG supplied 60% less N than the culture medium at the end of run (Appendix A, Fig. A.1). Similarly, Lara *et al.* (2016) observed for the microalga in this study a reduction of 28% in protein content when it was grown in 24 cycles of flue gas using BG-11-N-S compared with flue gas in complete BG-11. As a consequence of N limitation, microalgae tend to accumulate storage compounds (Min *et al.*, 2016; Huang *et al.*, 2017; Sun *et al.*, 2018), which was reflected in this study as an increase in crude fat (ether extract) with 3.2-3.7% d.w and starch with 23.1-47.2 % d.w under MFG with (Table 9, Fig. 22). Pancha *et al.* (2014) observed for *Scenedesmus sp.* that with less nitrate in the medium, carbohydrate and lipid content increased, while protein content decreased. The protein content for different species of *Desmodemus/Scenedesmus* has been reported in a range of 20-45% (Duong *et al.*, 2015; Guo *et al.*, 2017). In concordance with this, *D. abundans* under MFG presented around 21% (w/w) protein for strain HCA and LCA, whereas controls in air, CO₂ and CO₂+CK was a 38.3-43.7 % (w/w) of protein (Table 11).

Biomass from the LCA strain controls presented differences in crude fat (ether extract) among them (Table 11), where the condition CO₂+CKD had 12 times more lipids than the CO₂. Since only CKD varied between these treatments, it can be suggested that the increase in lipid content is caused by CKD. It is important to mention that the crude fat quantified here is the fraction with

affinity for ethylic ether that is a relatively non-polar solvent, therefore, extracted lipids are principally triacylglycerols, sterols, tocopherols and others, while polar lipids such as glycolipids and phospholipids are poorly extract (Shahidi, 2003).

Protein fractions are classified according to their solubility mainly in four classes, albumins in water, globulin in weak ionic solutions, glutelins in weak acid or basic solutions; and prolamines in 70 % ethanol (Maehre *et al.*, 2018). The analysis of protein fractions in *D. abundans* strain HCA and LCA under MFG showed from the total protein a 14.8-19 % albumins, 8-9 % glutelins, 8-9 % globulins, 4 % prolamins and 40-43 % as insoluble fraction (Fig. 25). Similar proportion of protein fractions were found for *Scenedesmus obliquus* and *Chlorella kessleri* when NaNO_3 was used as nitrogen sources, with 41 % albumin, 26-27 % globulin, 13-14 % prolamins, 7-8 % glutelin and 10-11% insoluble (El-Sheekh *et al.*, 2015). Moreover the insoluble fraction in the present study was much higher in MFG, with a notable decrease in albumins. Glutelins and prolamines are related with storage proteins whose biological function in cereals is to provide nitrogen and amino acids, while albumins and globulins include metabolic, structural and regulatory proteins (Gaur *et al.*, 2010; Koehler and Wieser *et al.*, 2013; Katsube-Tanaka *et al.*, 2016). However, no information about the function of these protein fractions in microalgae is known.

Starch content was also determined for *D. abundans* strains under the different growth conditions. The LCA strain under MFG exhibited higher amounts of starch, this was also visualized in TEM micrographs. Despite the cell growth for LCA strain was lower in MFG condition compared with control $\text{CO}_2 + \text{CKD}$, which differs only in N and S source, there was no differences in biomass productivity with around $0.3 \text{ g d.w. L}^{-1} \text{ d}^{-1}$. The same could be correlated with the high starch content, and hence the larger cell size. The increase of starch content in microalgae is influenced by N availability, Min *et al.* (2016) observed an increase from 7-8 to 19 pg cell^{-1} when N was depleted. Probably associated to carbon skeletons from proteins that are redirected to the central carbon metabolism to generated pyruvate, which could be used to synthesize lipid or starch. The latter storage macromolecule could be preferred by microalga since energy required to guide *per* carbon molecule into starch is lower than to lipid (Sun *et al.*, 2018). A previous study of *Desmodesmus* grown under atmospheric CO_2 (0.04 %) and 20 % CO_2 did not show differences in starch content until day 9, where starch increased for air condition (Solovchenko *et al.*, 2015). Because the control runs with the LCA strain under air and CO_2 did not showed significant differences, it can be suggested that the high starch content in MFG was caused by limited N, and probably excess CO_2 related to this condition.

Pigment content analysis showed that strain HCA under MFG presented more pigments than strain LCA by 35% *Chl a*, 44% *Chl b* and 32% carotenoids (Fig. 27), probably evidencing superior adaptation capability with higher photosynthetic activity as result of nine years of acclimation to high CO₂, where other strategies are used to obtain N, such a scavenge NO_x from medium (Valenzuela *et al.*, 2012), this correlated with the lower dissolved NO_x in HCA strain culture. In accordance with a report by Pancha *et al.* (2014) where *Scenedesmus sp.* presented a reduction of 75.43% when nitrate was reduced from 247 to 0 mg L⁻¹, is suggested that content of pigments decreases as an indicator of stress. In concordance, under CO₂ with complete medium pigment content presented a substantial increased by 2.1 times *Chl a* and *Chl b*, and 1.7-fold carotenoids compared with LCA strain in MFG (BG-11-N-S). This is probably because chlorophyll is a N-rich molecule, then it is degraded under N limited conditions, this has been observed in *Scenedesmus acutus*, *Scenedesmus sp.* and *Phaeodactylum tricornutum* (Valenzuela *et al.*, 2012; Sirikhachornkit *et al.*, 2018). Carotenoid also has shown to decrease under limited nitrogen source (Kim *et al.*, 2013), like was observed in LCA strain in MFG compared with CO₂ and CO₂+CKD controls.

No significant differences were found in the ratio *Chl a/Chl b* among culture conditions (Table 12). Also, strains HCA and LCA under MFG presented a similar ratio of carotenoids/*Chl a+b*. Controls of the strain LCA under an air atmosphere showed a significantly higher carotenoids/*Chl a+b*, while CO₂ and CO₂+CKD exhibited the lowest values (Tukey' HSD test, $\alpha=0.05$). An increase in carotenoids/*Chl a+b* ratio has been observed for *Scenedesmus sp.* when nitrogen is limited, which indicated a decrease in light harvesting complex and PS II activity, moreover this balance in pigment content allows an efficient utilization of carbon and energy (Pancha *et al.*, 2014). It has been suggested that an increase in the carotenoids/*Chl a+b* ratio under nitrogen starvation function as a protective strategy against oxidative stress (Zhang *et al.*, 2013). From this, could be suggested that strain in MFG were under a higher stressed condition compared with CO₂ and CO₂+CKD controls since higher ratios of carotenoids/*Chl a+b* were obtained, mainly caused by limited N. The higher carotenoids/*Chl a+b* ratios in air control is probably because a lower photosynthetic rate (Yeh *et al.*, 2017) because the low CO₂.

5.4.1 Lipidome changes of *D. abundans* under model cement flue gas

Because the high content of lipids in microalgae and their commercial value, diverse studies have been dedicated efforts to characterize and increase the lipid content in microalgae. In the present study changes in the lipidome of *D. abundans* strain HCA and LCA grown as response to MFG

was analyzed. The lipidic extract obtained from samples, was lower for HCA strain and no difference in LCA strain under the different condition were found, which differs from the extraction with ethylic ether, this is because as was already mention ethylic ether has a higher affinity by non-polar lipids. The extract for lipidomic was realized using MTBE and methanol as solvents, which recovery almost all lipid classes (Matyash *et al.*, 2018). However, Shahidi (2003) explains that methods to extract crude fat can recover some other components that are soluble under determined conditions, like residual moisture, pigments, carotenes and other, then a method is not only specific to lipids and either can be ensured an efficiency of 100% of lipid extracted. The lipid content in microalgae can vary from 2 to 75% d.w. and depends of the specie and the culture condition (Li *et al.*, 2014; Ohse *et al.*, 2014; Yao *et al.*, 2015). Specifically, for *Scenedesmus* species 25-28 (García-cubero *et al.*, 2017; Patil and Kaliwal., 2017)

Differential lipidomes analysis between strains HCA and LCA under MFG showed only 21 features with differential changes. Of these 5 GL and 4 GP decreased and 2 GL and 5 GP increased (Fig. 30), with changes not higher than $3-|\log_2FC|$ (Fig. 31a). This general overview of the lipidome could suggest a similar lipid composition for both strains under MFG by the day 5, where HCA is entering to the stationary phase and LCA continues with an exponential growth. More differences were found when the lipidome was analyzed by the 4 d, where both cultures were in exponential growth. From these, 12 GL and 18 GP increased, and 27 GL and 3 GP decreased in HCA strain (Fig. 32). Lipidic composition in microalgae is affected by the growth condition, under optimal conditions fatty acids are synthetized and used to generate membrane lipids such as glycerophospholipids (Rismani-Yazdi *et al.*, 2011; Niu *et al.*, 2013; Yao *et al.*, 2015), while under stress condition glycerolipids are accumulated (Duong *et al.*, 2015; Sun *et al.*, 2016). The higher intensities for GL in LCA strain compared with HCA, suggests a higher stress in MFG which was reflected in a lower growth in the first days (24-96 h). Strain HCA achieved to grow at a higher rate in this period, evidencing a higher intensity in some GP than LCA strain.

The comparison of the LCA strain in MFG vs in air atmosphere showed that all lipids with differential changes increased. Most of these lipids were GL and GP with 27 and 40 molecules, respectively, and some ST (4) and SP (7) increasing (Fig. 30). This data can be associated with the higher growth in MFG because a higher carbon flux (Sun *et al.*, 2016) since GP, ST and SP are related with structural and functional components (Yao *et al.*, 2015). Moreover, a clear effect of the N and S sources was observed since when CO₂ and CO₂+CKD, experiments with complete BG-11, were also compared to an air atmosphere presented less than 4% of the 663 detected features with significant changes (Fig. 30). The most notable changes were found in the

CO₂+CKD condition with only 5 GL decreasing and 8 increasing (3 to 1-|log₂FC|), and 8 GP decreasing (-4 to -1.5-log₂FC).

A further comparison between LCA in MFG and CO₂+CKD, which differs principally in N and S sources, was performed, resulting in 236 features with significant changes. These changes in incomplete medium with NO and SO₂ from flue gas as nutrients source, were more evident in the 42 GL and 58 GP increasing and 27 GL and 42 GP decreasing (Fig. 31c). The accumulation of TAGs under delimited N has been reported before for several microalgae (Ito *et al.*, 2013; Kim *et al.*, 2013; Matich *et al.*, 2018). The glycerophospholipid classes with more molecules changing were glycerophosphates with 27 features decreasing and glycerophosphocolines/ethanolamines with 18 assignments increasing and 5 decreasing. Matich *et al.* (2018) observed an important effect in glycerophospholipids when the green microalga *Ettlia oleoabundans* was grown under N starvation, in lipids such as phosphatidic acids (PAs), phosphatidylcholines (PCs), phosphatidylinositol (PIs) and phosphatidylglycerols (PGs). Because phospholipids are essential molecules in microalgae metabolism, a decrease in their biosynthesis could trigger a diminish in PAs and PGs, and then of other glycerophospholipids (Matich *et al.*, 2018). In the present study was observed a decrease in several GP in MGF condition, however these were not depleted, which could be because there is a low nitrogen concentration, no eliminated, but also a high CO₂. Some molecules such as glycerophosphocolines/ethanolamines, glycerophosphoglycerols and glycerophosphoinositol demonstrated an increase under this condition. These lipids have diverse functions, and not only like structural component of the membrane. PC acts like acyl donor to TAGs synthesis (Kim *et al.*, 2013), the increase of these molecules in MFG can be correlated with an augmentation of TAGs. PI is related with cell signaling, has been reported that increase under osmotic, drought and salt stress (Kim *et al.*, 2013). PGs are the only GP found in significant quantities in thylakoid membranes, where increase the fluidity of the membrane and then in the improvement of electron transport rate and photosynthetic efficiency (Lu *et al.*, 2013)

Glycerolipids and glycerophospholipids were characterization by number of carbons and unsaturations. All GP with significantly changes had 15-52 carbons and 0-9 unsaturations. Especially, GP from the comparison of the LCA strain under MFG vs CO₂+CKD showed a higher frequency of molecules with 40-44 carbons and were saturated or monounsaturated. An increase in carbon length chain increment the thickness and rigidity of the bilayer since interaction between acyl chains increase, however it could depend in GP class, where variations in PG and PI appear to cause an increase of the membrane fluidity and PC, PE and PA the opposite (Lu *et al.*, 2013). Higher number of unsaturations in GP increase the spatial configuration among molecules,

affecting the membrane fluidity, this allows to the cells adapt to several conditions. Also, a decrease in unsaturation in PG could cause down-regulation of photosystem I (Lu *et al.*, 2013). TAGs presented a total of 44 to 60 carbons, of these 54, 56, and 58 C were show a higher frequency, and the unsaturation number was from 0 to 9. DAGs presented from 31 to 45 carbons, and from 0 to 9 saturations. Kim *et al.* (2013) mention that an improvement in the photosynthetic activity requires a higher membrane fluidity and this could be reflected in an increase in glycerolipid species with desaturated fatty acyl chains. Under nitrogen starvation has been observed a decreased in saturated molecules and increase in unsaturated (3-4), as well as an increase in molecules with more carbons (58-60 C) (Yang *et al.*, 2014).

5.5 Conclusions

After nine years in a laboratory setting and under different atmospheres, microalga morphology differed from typical *Desmodesmus* genus cells. Strains presented phenotypic plasticity that seems to be influenced by high CO₂. However, it appears to be an immediate response to the new condition, as well as the presence of a larger circular unicellular morphology. Even though, strain HCA under MFG presented a significantly thicker cell wall than LCA that might represent an adaptation to prolonged exposure to high CO₂. Under MFG both strains presented less protein content and more crude fat (neutral lipids). Also, accumulated considerable amounts of starch up to 43 % d.w. in the LCA strain; resulting in a biomass with a high value byproduct. Accumulation of starch appears to be induced by the limited N in the incomplete culture condition (BG-11-N-S). High pigment content in strain HCA evidenced active photosynthetic activity, while a lower content in LCA might represent stress and degradation of pigments.

Lipidome analysis at the end of the experimental period (day 5) did not showed significant differences between strains under MFG. However, at day 4 during exponential growth for both strains differences in glycerolipids (GL) and glycerophospholipids (GP) were found. An increase in GP and a decrease in GL was observed in strain HCA that might evidence active growth and less lipid reserves. In the controls, lipid profile changes were found when the LCA strain under MFG (incomplete medium, BG-11-N-S) was compared with CO₂+CKD (complete medium, BG-11), mainly an increase in GL and GP that might be attributed to N limitation.

Tables and figures

Table 10. Cell diameter, area and cell wall thickness of *D. abundans* strains HCA and LCA under MFG and controls with LCA strain under air, CO₂ and CO₂+CKD in a 1 L column photobioreactor with continuous flow (0.05 vvm), 24 °C, 80-90 μmol PAR-photons m⁻²s⁻¹ and 24 h light.

Strain-> Gas supply	Cell diameter (μm)	Cell area (μm ²)	Cell wall thickness (nm)
HCA->MFG	6.4 ± 1.3 ^A	29.1 ± 10.1 ^A	203.8 ± 43.9 ^A
LCA->MFG	6.1 ± 1.1 ^A	27.0 ± 10.2 ^A	128.2 ± 18.9 ^B
LCA->Air	3.7 ± 0.7 ^B	10.0 ± 3.3 ^B	76.0 ± 11.7 ^B

MFG composition balanced with dry air (v/v) was 25% CO₂, 700 ppm NO and 100 ppm SO₂. 150 ppm of CKD was added each 24 h for MFG and CO₂+CKD runs. Values represent average ± SD for cell diameter and area (n=15-18) and cell wall thickness (n=4-12). Different letters within the same column indicate significantly differences (Tukey' HSD test, α=0.05, n=15-18).

Table 11. Biomass composition of *D. abundans* strains HCA and LCA under MFG and controls with LCA strain under air, CO₂ and CO₂+CKD in a 1 L column photobioreactor with continuous flow (0.05 vvm), 24 °C, 80-90 μmol PAR-photons m⁻²s⁻¹ and 24 h light.

Strain-> Gas supply	Crude protein (% w/w)	Crude fat (% w/w) ^a	Crude fiber (% w/w)	Ash (% w/w)	Carbohydrates (% w/w) ^b
HCA->MFG	21.3 ± 0.1 ^C	3.2 ± 0.2 ^A	10.9 ± 0.6 ^A	5.8 ± 0.2 ^A	58.7 ± 0.3 ^A
LCA->MFG	21.4 ± 0.5 ^C	3.7 ± 0.3 ^A	10.4 ± 0.4 ^A	5.6 ± 0.2 ^A	58.9 ± 0.4 ^A
LCA ->Air ^c	43.7	0.1	-	-	-
LCA ->CO ₂	42.8 ± 0.4 ^{AB}	0.2 ± 0.0 ^C	-	-	-
LCA->CO ₂ +CKD	38.3 ± 0.8 ^B	2.4 ± 0.1 ^B	-	-	-

MFG composition balanced with dry air (v/v) was 25% CO₂, 700 ppm NO and 100 ppm SO₂. 150 ppm of CKD was added each 24 h for MFG and CO₂+CKD runs. Values represent average ± SD (n=2-3). Different letters within the same column indicate significantly differences (Tukey' HSD test and t-test, α=0.05, n=2-3).

^aEther extract. ^bBy subtraction of the other components (N-free extract). ^cNot contemplated in statistical analysis (n=1).

Table 12. Ratio of chlorophyll *a* and *b* and ratio of total carotenoids and total chlorophyll *D. abundans* strains HCA and LCA under MFG and controls with LCA strain under air (0.04% CO₂), 25% CO₂ and 25% CO₂+CKD in a 1 L column photobioreactor with continuous flow (0.05 vvm), 24 °C, 80-90 μmol PAR-photons m⁻²s⁻¹ and 24 h light.

Strain-> Gas supply	Chl <i>a</i> /Chl <i>b</i>	Carotenoids/Chl <i>a+b</i>
HCA->MFG	3.15 ± 0.27 ^A	0.27 ± 0.01 ^B
LCA->MFG	3.66 ± 0.54 ^A	0.29 ± 0.01 ^{AB}
LCA ->Air	2.95 ± 0.08 ^A	0.31 ± 0.00 ^A
LCA ->CO ₂	3.55 ± 0.14 ^A	0.23 ± 0.01 ^C
LCA ->CO ₂ +CKD	3.11 ± 0.11 ^A	0.24 ± 0.01 ^C

MFG composition balanced with dry air (v/v) was 25% CO₂, 700 ppm NO and 100 ppm SO₂. 150 ppm of CKD was added each 24 h for MFG and CO₂+CKD runs. Values represent average ± SD (n=2-3). Different letters within the same column indicate significantly differences (Tukey' HSD test and t-test, α=0.05, n=2-3).

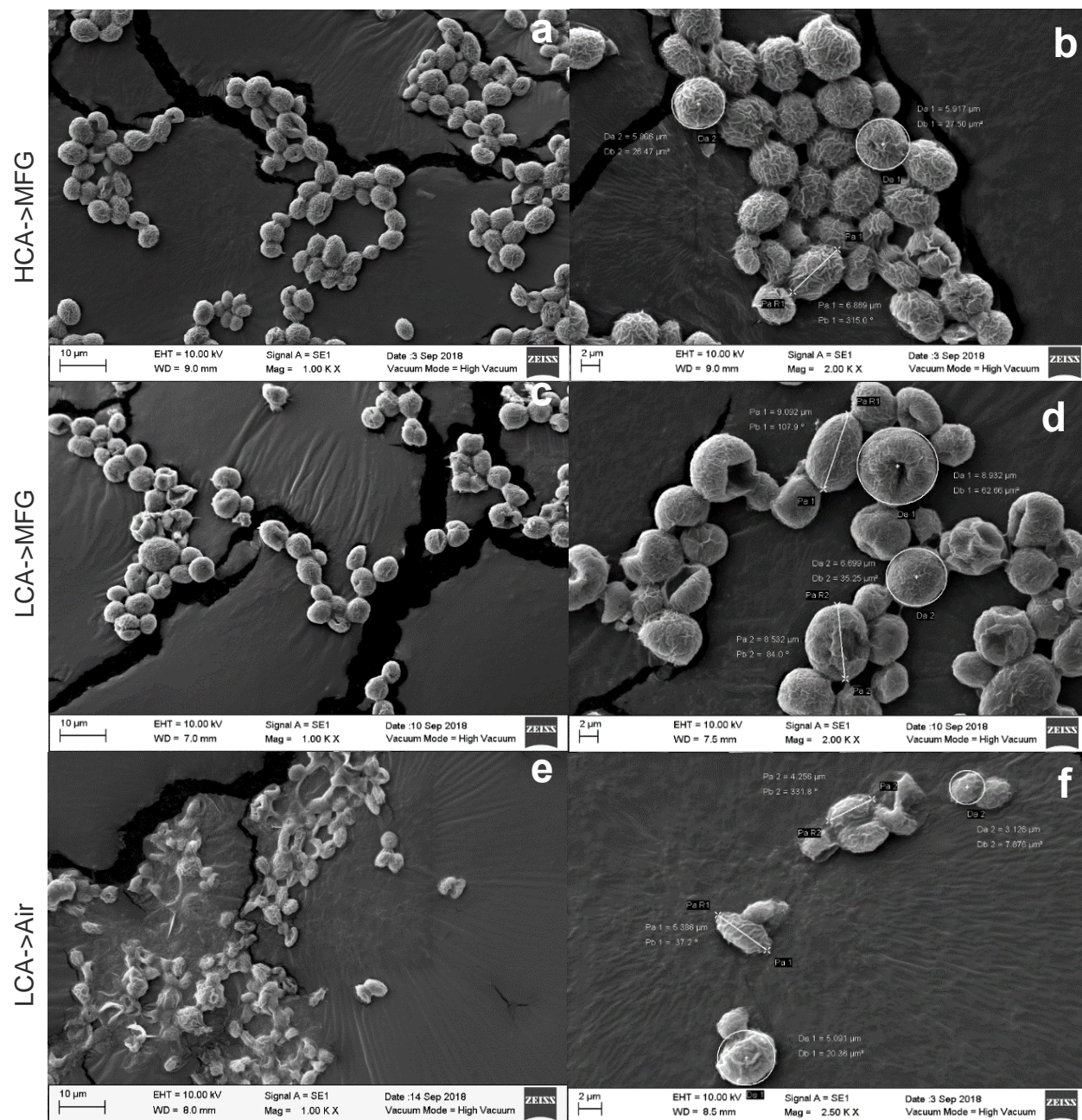


Figure 23. Scanning electron micrographs of *D. abundans* strains. (a-b) HCA strain grown under MFG, (c-d) LCA strain grown under MFG and (e-f) LCA strain grown under air. Magnitude: 1000X (a,c,e), 2000X (b,d) and 2500X (f).

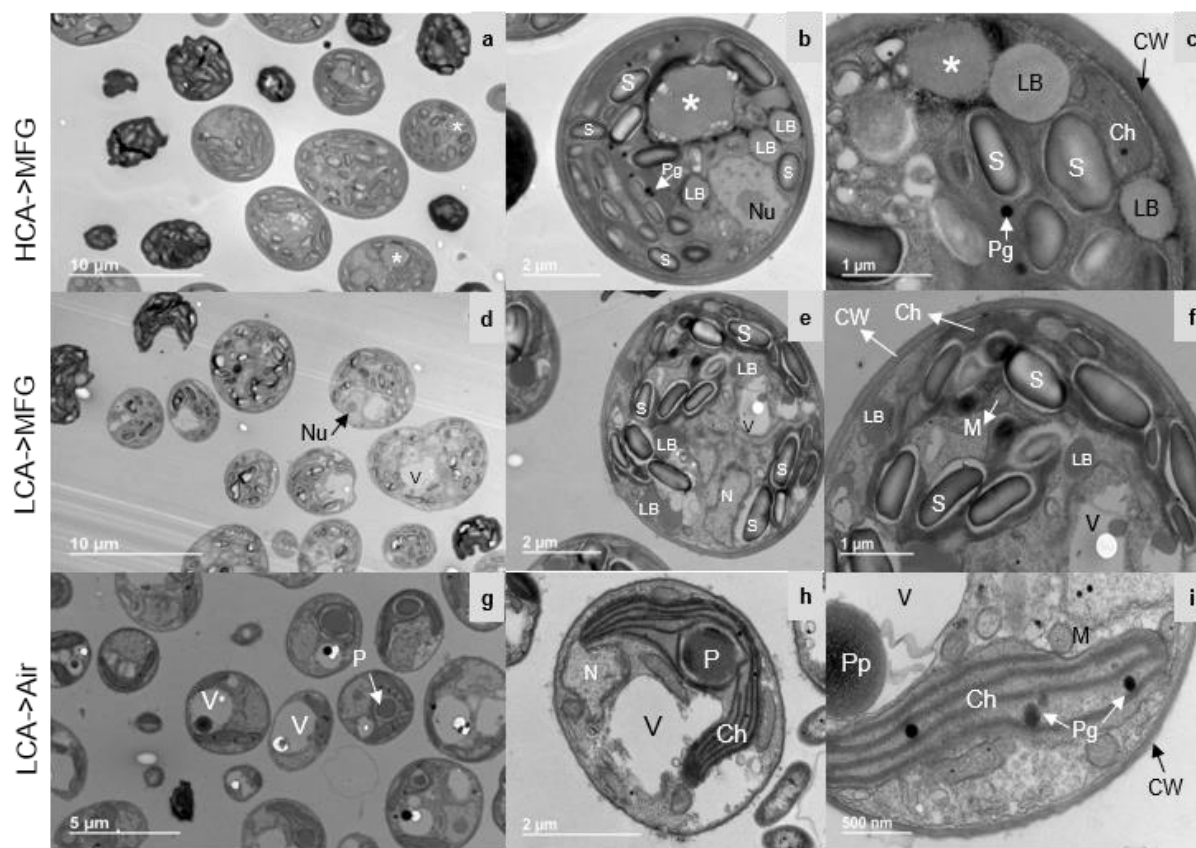


Figure 24. Transmission electron micrographs of *D. abundans* strains. (a-c) HCA strain grown under MFG, (d-f) LCA strain grown under MFG and (g-i) LCA strain grown under air. Ch, chloroplast; M: mitochondria; N: nucleus; Nu: nucleolus; V: vacuole; S: starch grain; LB: Lipid body; P: pyrenoid; Pg: plastoglobuli; Pp: polyphosphate granule; CW: cell wall; white asterisk: large spherical organelle.

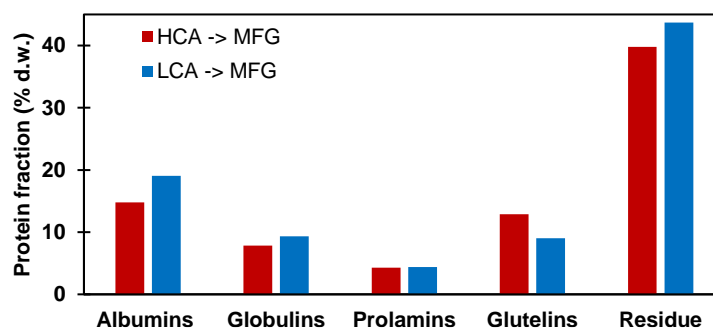


Figure 25. Protein fractions of *D. abundans* strains HCA and LCA under MFG determined by Osborne solubility method.

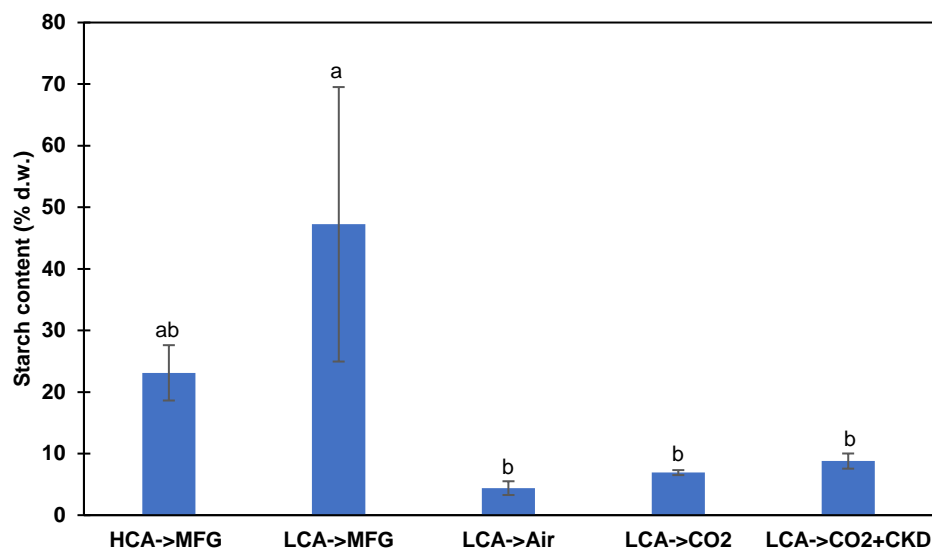


Figure 26. Starch content of *D. abundans* strains HCA and LCA under MFG and controls with LCA strain under air, CO₂ and CO₂+CKD in a 1 L column photobioreactor with continuous flow (0.05 vvm), 24 °C, 80-90 $\mu\text{mol PAR-photon s}^{-1}\text{m}^{-2}$ and 24 h light. Different letters indicate significantly differences (Tukey' HSD test, $\alpha=0.05$, $n=2-3$).

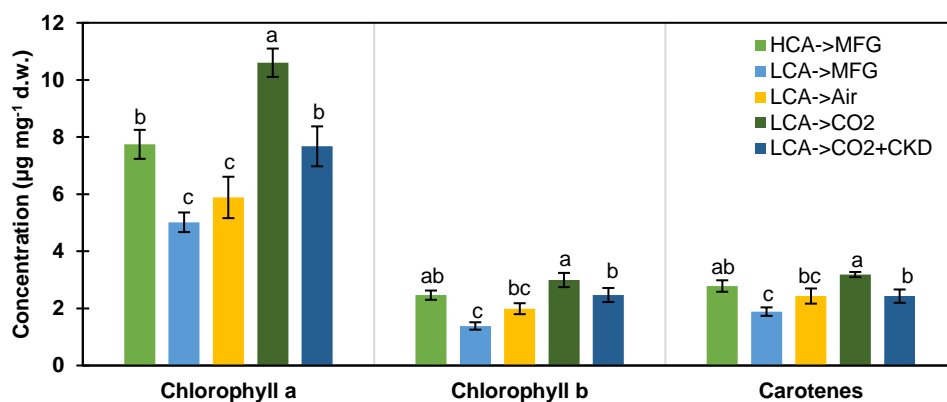


Figure 27. Chlorophyll a and b, and carotenoids content of *D. abundans* strains HCA and LCA under MFG and controls with LCA strain under air, CO₂ and CO₂+CKD in a 1 L column photobioreactor with continuous flow (0.05 vvm), 24 °C, 80-90 $\mu\text{mol PAR-photon s}^{-1}\text{m}^{-2}$ and 24 h light. Different letters within each pigment group indicate significantly differences (Tukey' HSD test, $\alpha=0.05$, $n=2-6$).

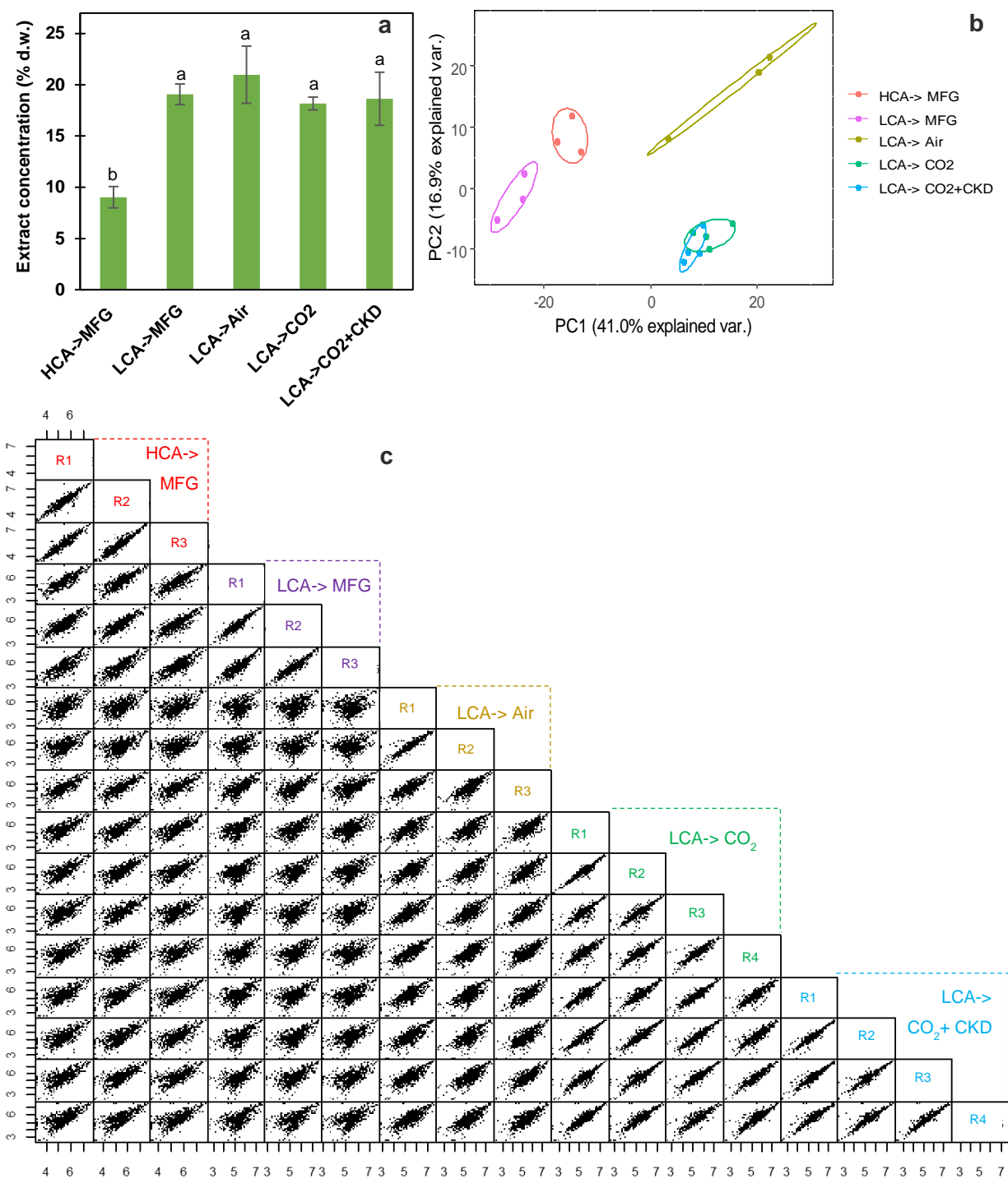


Figure 28. Untargeted of *D. abundans* strains HCA and LCA under MFG and controls with LCA strain under air, CO₂ and CO₂+CKD in a 1 L column photobioreactor with continuous flow (0.05 vvm), 24 °C, 80-90 μmol PAR-photons m⁻²s⁻¹ and 24 h light. a) Sample lipid extract content, b) principal component analysis of features detected in samples and c) scatter plots between sample comparisons. MFG composition balanced with dry air (v/v) was 25% CO₂, 700 ppm NO and 100 ppm SO₂. 150 ppm of CKD was added each 24 h for MFG and CO₂+CKD runs.

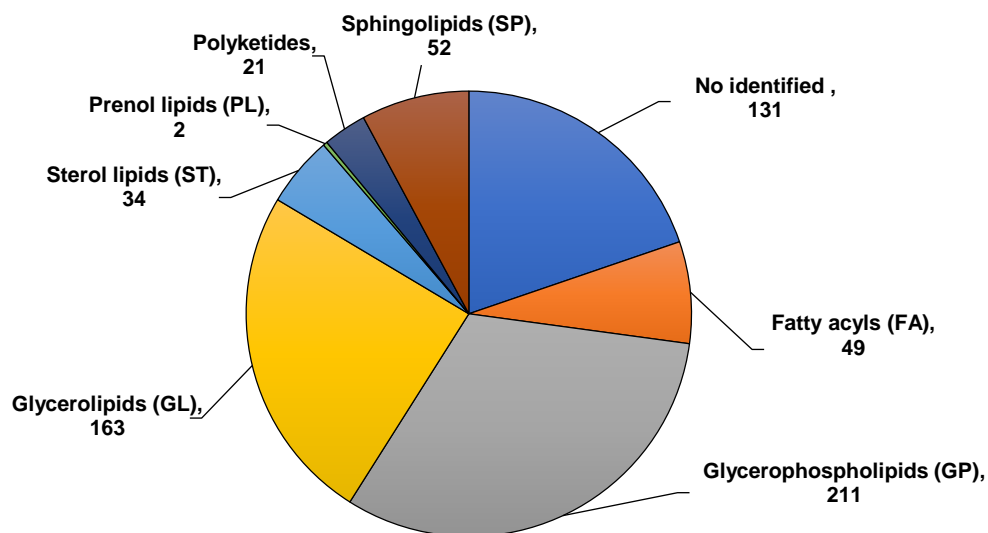


Figure 29. Total identified lipidic features and cured lipid category level assignment after alignment and gap filling of *D. abundans* strains HCA and LCA under MFG and controls with LCA strain under air, CO₂ and CO₂+CKD in a 1 L column photobioreactor with continuous flow (0.05 vvm), 24 °C, 80-90 μmol PAR-photons m⁻²s⁻¹ and 24 h light.

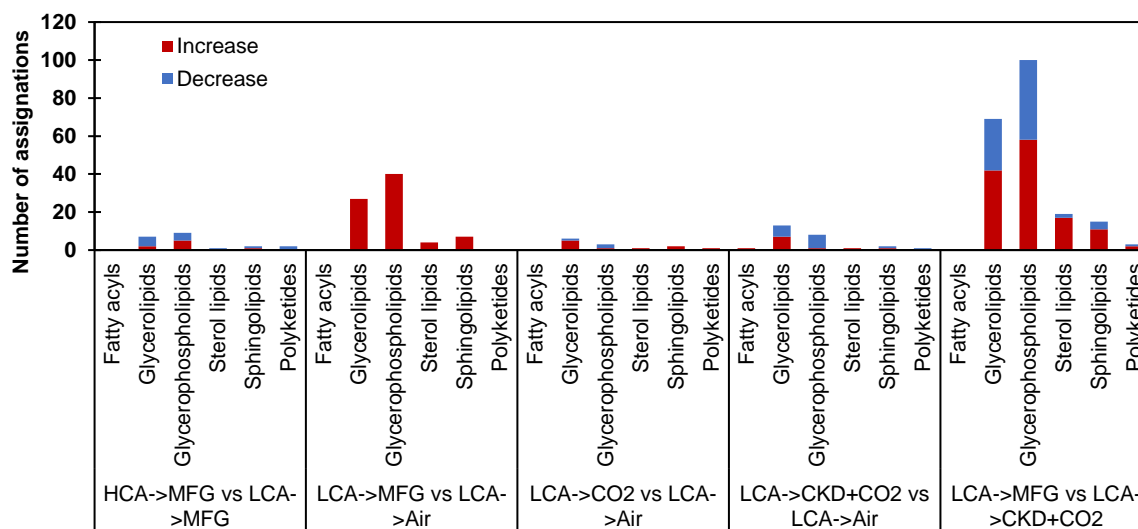


Figure 30. Differential lipidome analysis of *D. abundans* strains HCA and LCA under MFG and controls with LCA strain under air, CO₂ and CO₂+CKD in a 1 L column photobioreactor with continuous flow (0.05 vvm), 24 °C, 80-90 μmol PAR-photons m⁻²s⁻¹ and 24 h light (t-test, *adjusted p.value*<0.05, n=3-4). Number of significantly features increasing and decreasing per lipid category.

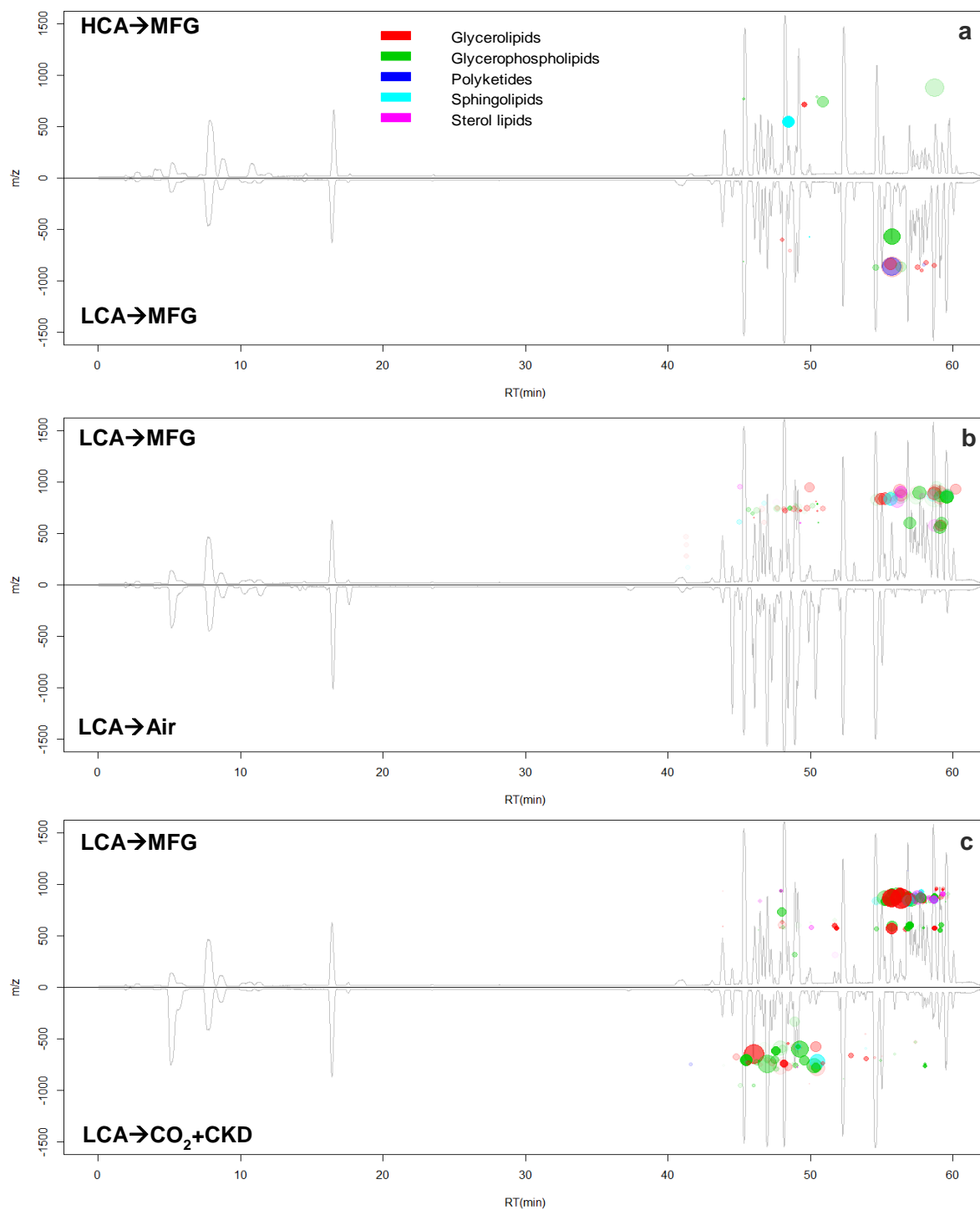


Figure 31. Cloud plots representing molecules with significant changes when comparing HCA-→MFG vs LCA-→MFG (b), LCA-→MFG vs LCA-→air (c) and LCA-→MFG vs LCA-→CO₂+CKD (d), dots placed in negative m/z represent lipids decreasing, bigger dots indicate higher $|\log_2FC|$ and transparency represents less significance.

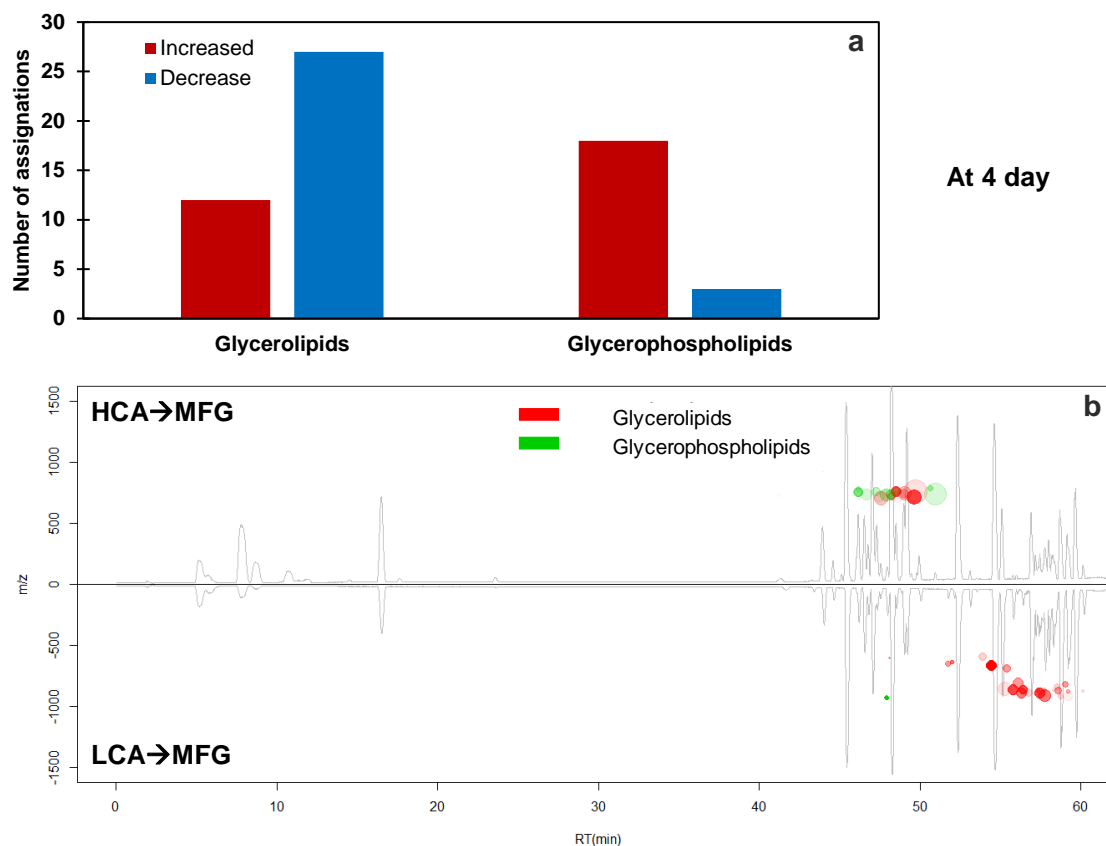


Figure 32. Glycerolipid and glycerophospholipid changes between strains HCA and LCA under MFG by the 4 day of growth in a 1 L column photobioreactor with continuous flow (0.05 vvm), 24 °C, 80-90 μmol PAR-photons $\text{m}^{-2}\text{s}^{-1}$ and 24 h light (t-test, *adjusted p.value* < 0.05, n=3-4). a) Number of significantly features increasing and decreasing. (b) Cloud plots representing molecules with significant changes, dots placed in negative m/z represent lipids decreasing, bigger dots indicate higher $|\log_2\text{FC}|$ and transparency represents less significance.

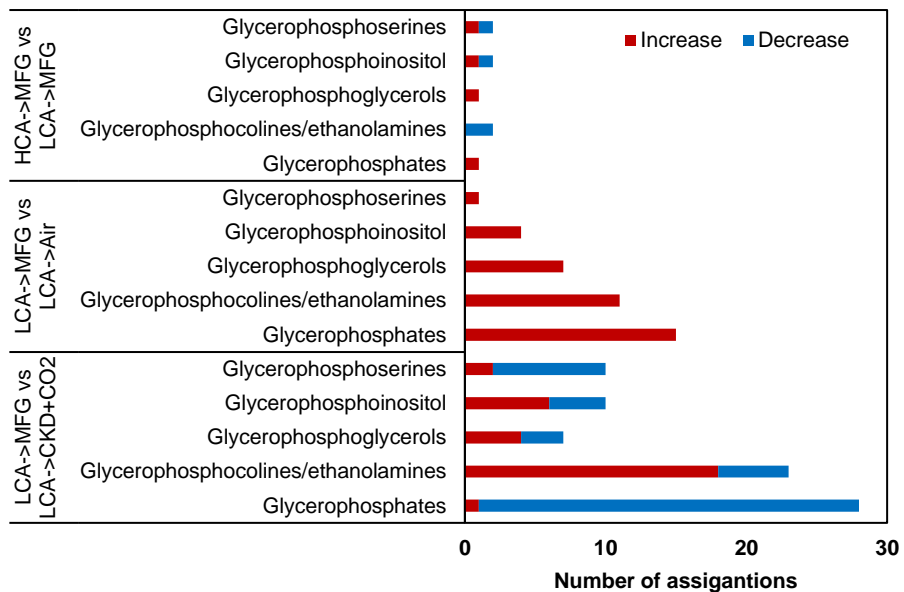


Figure 33. Glycerophospholipid class distributions of *D. abundans* strains HCA and LCA under MFG, and controls with LCA strain in MFG vs air, and MFG vs CO₂+CKD in a 1 L column photobioreactor with continuous flow (0.05 vvm), 24 °C, 80-90 μmol PAR-photons m⁻²s⁻¹ and 24 h light.

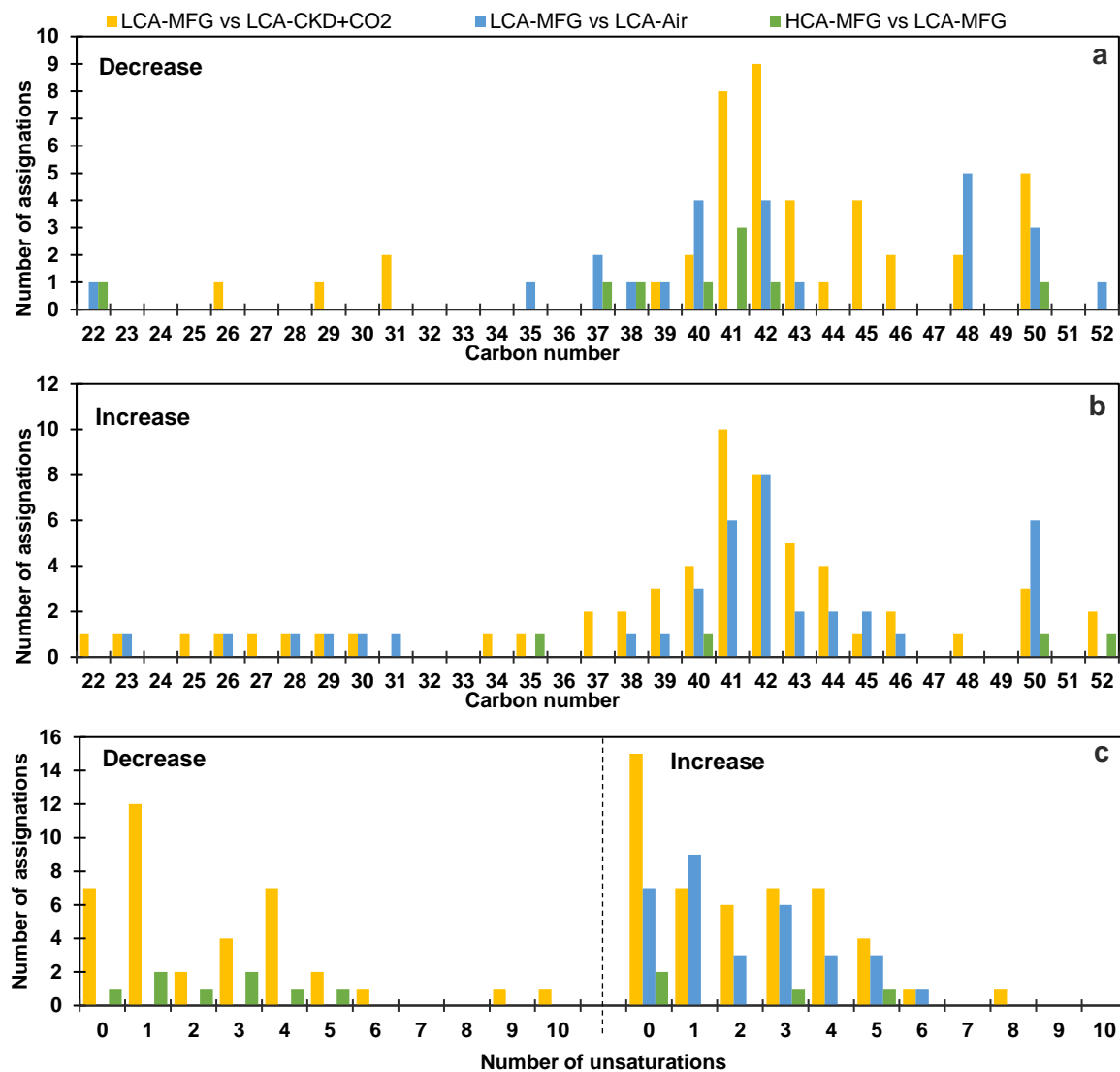


Figure 34. Characterization of glycerophospholipids by number of carbons (a-b) and unsaturations (c) significantly decreasing and increasing between experimental group comparison.

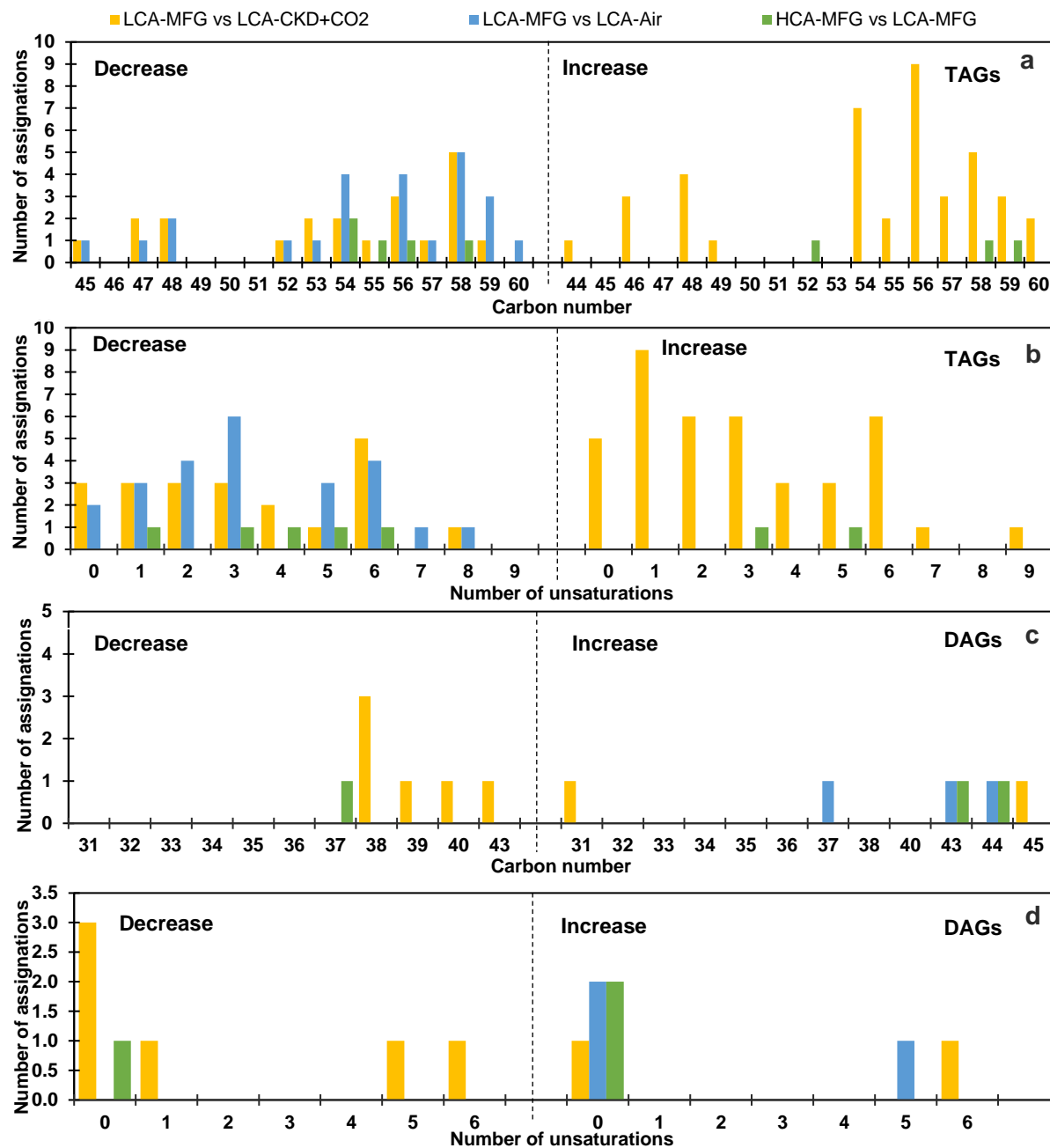


Figure 35. Characterization of glycerolipids TAG and DAG by number of carbons (a and c) and unsaturations (b and d) significantly decreasing (left) and increasing (right) between experimental group comparison.

Chapter 6

Conclusions

6. Conclusions

- *D. abundans* strains HCA and LCA tolerated, grew and used cement flue gas components (CO₂, NO_x and SO_x) as a nutrient source. Addition of CKD effectively controls system pH under model cement flue gas, representing a low-cost strategy to increase microalga tolerance.
- *de novo* transcriptome assembly revealed that *D. abundans* is more similar to the family Selenastraceae than Scenedesmaceae; however, this analysis was based on available data still poor in comparison with the high diversity of microalgae.
- Transcriptome changes in strain HCA compared with strain LCA under MFG were related with a probably higher flux of carbon that activated all central carbon metabolism pathways. In addition, TAG and starch catabolism and anabolism were both expressed and up-regulated.
- Characteristic features of adaptation or tolerance to high CO₂ might be related to: nitrogen transporters, active synthesis of essential macromolecules for growth (nucleotides and amino acids) and cellular components of cell wall and the photosynthetic apparatus. In particular, it appears, as nitrogen transporters between strains possess different substrate affinities or gene regulators as in the LCA strain dissolved N accumulated to day 4 but not in the HCA strain.
- DEGs related with photosynthesis in the LCA strain under MFG compared with air were down-regulated, while in the control with CO₂ were down-regulated (low FC), suggesting a stress condition for the LCA strain in air since this culture presented almost no growth (long adaptation phase).
- Differences between strains were not evident based on growth but transcriptome analysis revealed important differences at day 4. However, as both produced the same biomass at the end of the experimental period (5 days) could imply that either strain adapts to MFG eventually. Further studies to evaluate the LCA strain after more days of growth under MFG could evidence the same expression pattern of the strain HCA.

- After nine years in a laboratory setting and under different atmospheres, microalga morphology differed from typical *Desmodesmus* genus cells. Strains presented phenotypic plasticity that seems to be influenced by high CO₂. However, it appears to be an immediate response to the new condition, as well as the presence of a larger circular unicellular morphology.
- Strain HCA under MFG presented a significantly thicker cell wall than the LCA strain in the same growth condition that might represent an adaptation to prolonged exposure to high CO₂.
- Under MFG both strains presented less protein content and more crude fat (neutral lipids). Also, accumulated considerable amounts of starch up to 43 % d.w. in the LCA strain; resulting in a biomass with a high value byproduct. Accumulation of starch appears to be induced by the limited N in the incomplete culture condition (BG-11-N-S).
- High pigment content in strain HCA evidenced active photosynthetic activity, while a lower content in the LCA strain might represent stress and degradation of pigments.
- Lipidome analysis at the end of the experimental period did not showed significant differences between strains under MFG. However, at day 4 during exponential growth for both strains differences in glycerolipids (GL) and glycerophospholipids (GP) were found. An increase in GP and a decrease in GL were observed in the strain HCA that might evidence active growth and less lipid reserves.
- In the controls, lipid profile changes were found when the LCA strain under MFG (incomplete medium, BG-11-N-S) was compared with CO₂+CKD (complete medium, BG-11), mainly an increase in GL and GP that might be attributed to N limitation.

6.1 Further studies

- Growth under model flue gas using a continuous culture with a longer experimental period (more than 5 days) could validate differences between *D. abundans* strains.

- If further evidence confirms transcriptome strain similarity, a strategy to optimize CO₂ capture could be to work with LCA strain, since it possesses the same biomass productivity but a thinner cell wall and higher starch content that could be beneficial for byproduct harvesting.
- Sequencing the genome of the strains would help to clarify differences, including synonymous mutation rates. Also, analysis of epigenetic changes would give more information about the regulation of gene expressions between strains.
- Validation of the RNA-seq analysis by qPCR to confirm expression levels and further evaluate target genes involved in pathways of interest with high changes in expression.
- Metabolome and proteome analysis could help understand differences under the different control conditions since no many differences were observed at the transcriptome level but notable changes in biomass composition were observed.
- Target metabolic of lipids that showed significant changes under the different growth conditions would help understand their biological role and potential as byproducts.
- Characterize biomass amino acid and fatty acids profiles could help understand differences between strains, the effect of gas components (CO₂, NO_x and SO_x and CKD), and evaluate the potential of these macromolecules as byproducts of the mitigation system.

Appendix A

6.2 Theoretical dissolved gases

Calculations of theoretical dissolved CO₂, NO and SO₂ in the culture medium at 25 °C.

Gas	Concentration in MFG (ppm)	Solubility in water (g L ⁻¹)	Density (g L ⁻¹)	Solubility in water (% v/v)	Gas supply (L) ^a	Soluble (L)	Soluble (g)
CO ₂	250 000	1.50	1.84	81.22	88.20	71.63	131.95
NO	700	5.0E-05	1.25	0.00	0.25	9.9E-06	1.2E-05
SO ₂	100	94.00	2.28	4124.62	0.04	1.46	0.08

^aTotal amount of gas injected continuously for 5 d at 0.05 vvm.

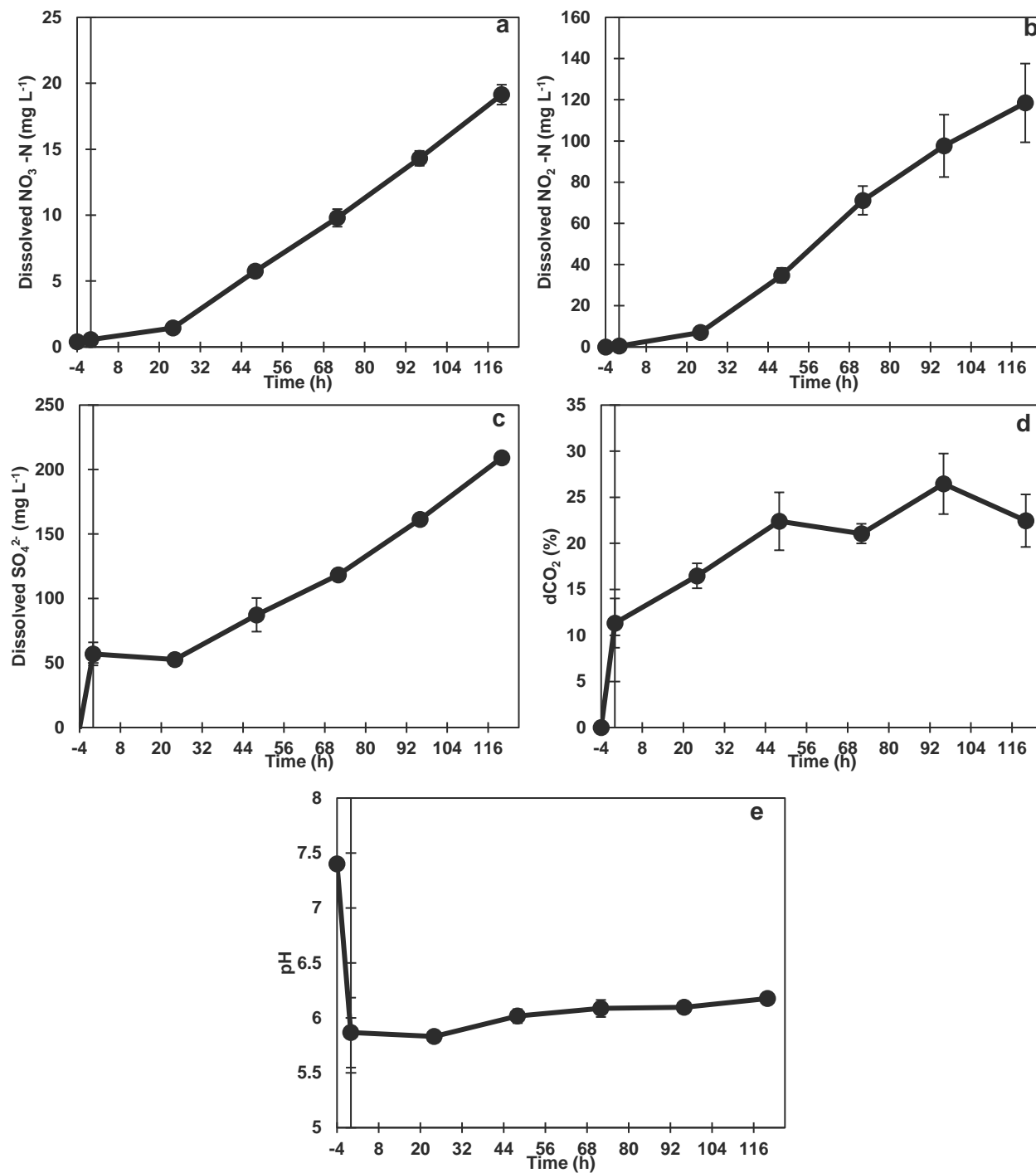


Figure A. 1. Dissolved sulfate (a), nitrate (b), nitrite (c) and dCO_2 in BG-11-N-S during aeration with model flue gas (MFG) for 5 d. MFG composition balanced with dry air (v/v) was 25% CO_2 , 700 ppm NO and 100 ppm SO_2 . 150 ppm of CKD was added each 24 h. Experiments were performed in 1 L column photobioreactor with a continuous flow rate of 0.05 vvm, 24°C.

Appendix B

6.3 RNA quality and quantification

Table A. 1. RNA quantification and quality parameters.

Strain -> Gas supply	Sample ID	Nanodrop quality indexes		Bioanalyzer		Qubit
		260/230 nm	260/280 nm	RIN	r 28s/18s	[ng/ μ L]
HCA->MFG	P25B1	1.71	2.03	7.4	1.5	640
	P23B1	1.73	2.18	7.9	1.4	262
	P23B2	2.12	2.2	7.6	1.5	334
LCA->MFG	P24B2	1.53	2	7.8	1.4	188
	P22B1	2.24	2.22	8.8	2	664
	P22B2	2.23	2.25	8.4	1.9	1190
LCA ->Air	P29B1	2.25	2.23	6.7	1.7	806
	P29B2	2.42	2.23	6.4	1.3	274
LCA -> CO ₂	P28B1	0.55	2.12	8.6	1.7	122
	P28B2	2.21	2.28	8.9	1.9	1440
LCA ->CKD+CO ₂	P30B1	2.13	2.25	7.5	1.7	668
	P30B2	1.84	2.15	8.1	1.6	640

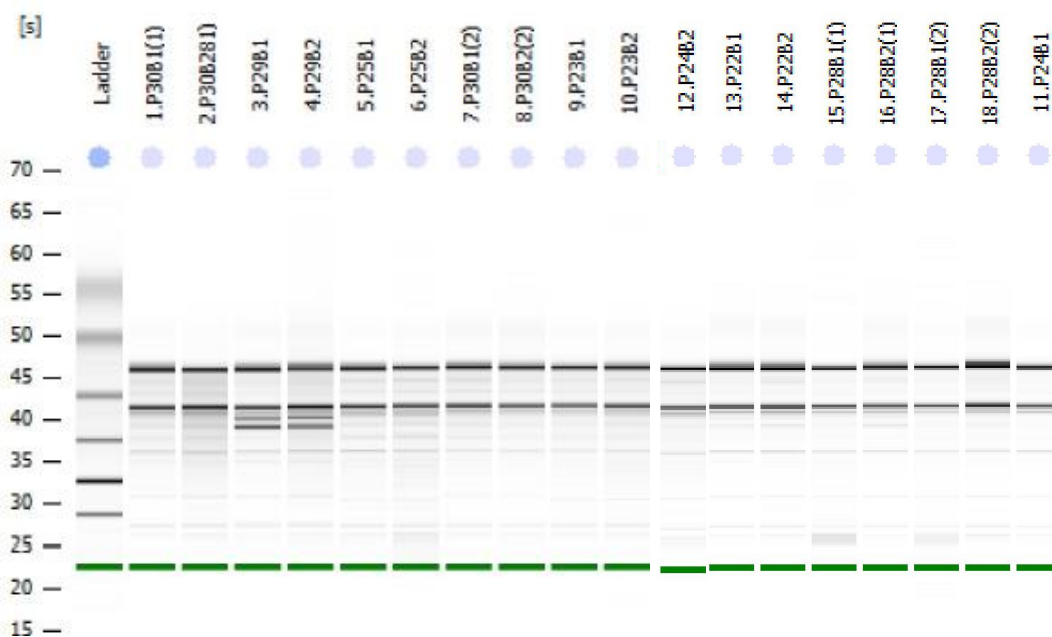


Figure A. 2. Sample RNA electrophoresis using the Agilent 2100 Bioanalyzer.

6.4 RNA-seq library construction

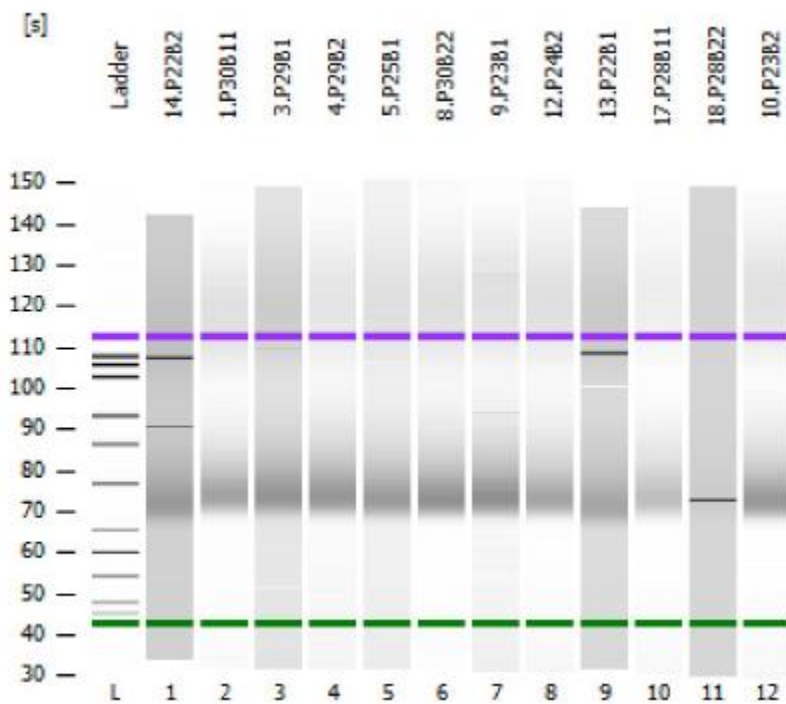


Figure A. 3. Sample library electrophoresis after adapter ligation and purification.

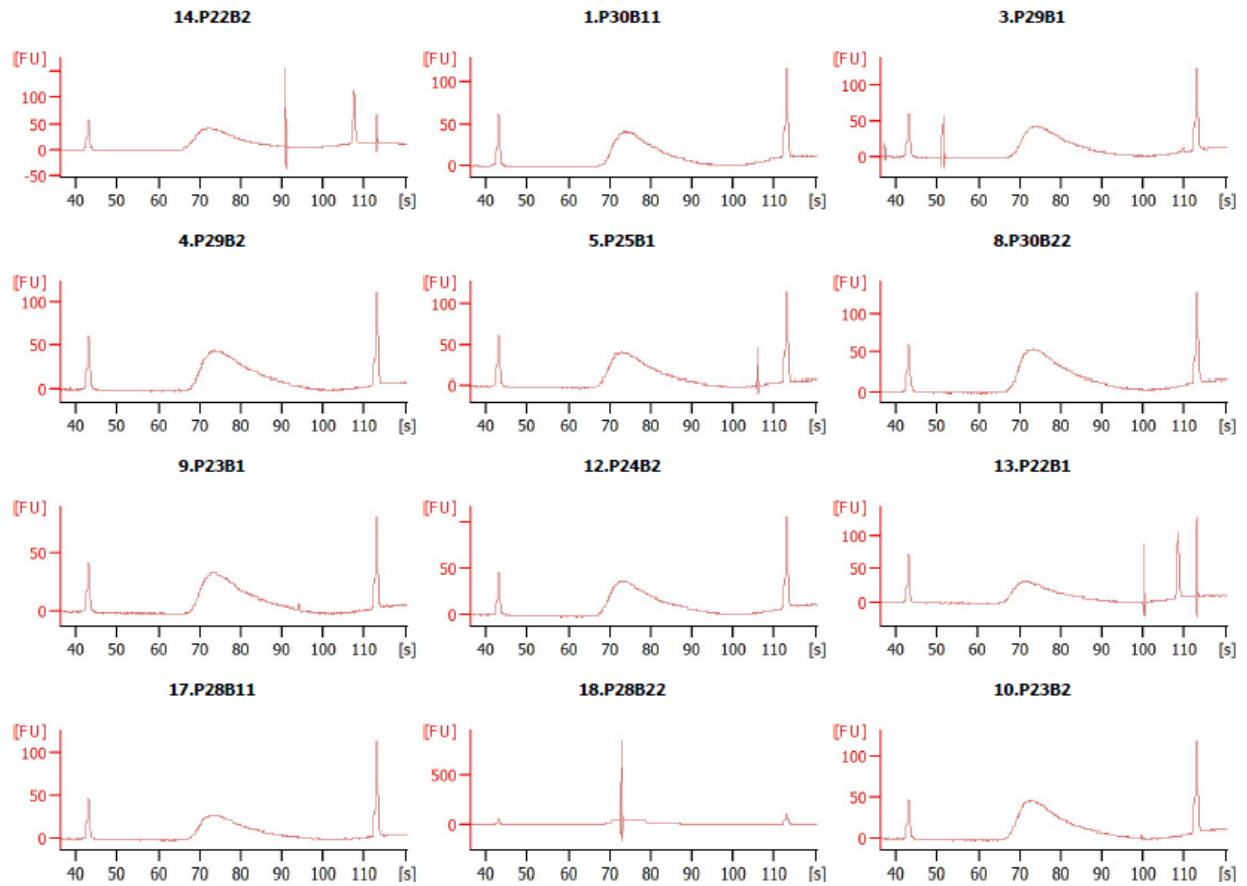


Figure A. 4. Sample library size distribution used for RNA-seq.

Table A. 2. Average size and concentration of libraries used to normalize and pool libraries.

Strain -> Gas supply	Sample ID	Average size (bp)	DNA concentration (ng/uL)	DNA concentration (nM) ^a
HCA->MFG	P25B1	286.0	29.4	155.7533376
	P23B1	298.5	28.8	146.1854728
	P23B2	287.5	27.0	142.2924901
LCA->MFG	P24B2	289.0	29.2	153.0879732
	P22B1	261.5	28.4	164.551828
	P22B2	276.5	32.6	178.6399255
LCA->Air	P29B1	297.5	37.6	191.4947797
	P29B2	303.0	31.0	155.0155016
LCA-> CO ₂	P28B1	281.5	25.8	138.8664621
	P28B2	297.0	29.4	149.9846954
LCA-> CO ₂ +CKD	P30B1	296.0	35.6	182.2276822
	P30B2	304.0	28.8	143.5406699

^aDNA concentration in nM was calculated using the formula: $\frac{[DNA]}{660 \times (pb)} \times 1000000$, where $[DNA]$ is the library

concentration in ng μL^{-1} , $660 = \frac{1 \text{ mol } pb}{660 \text{ g } pb}$ and pb the average size of the library.

6.5 Sequencing results

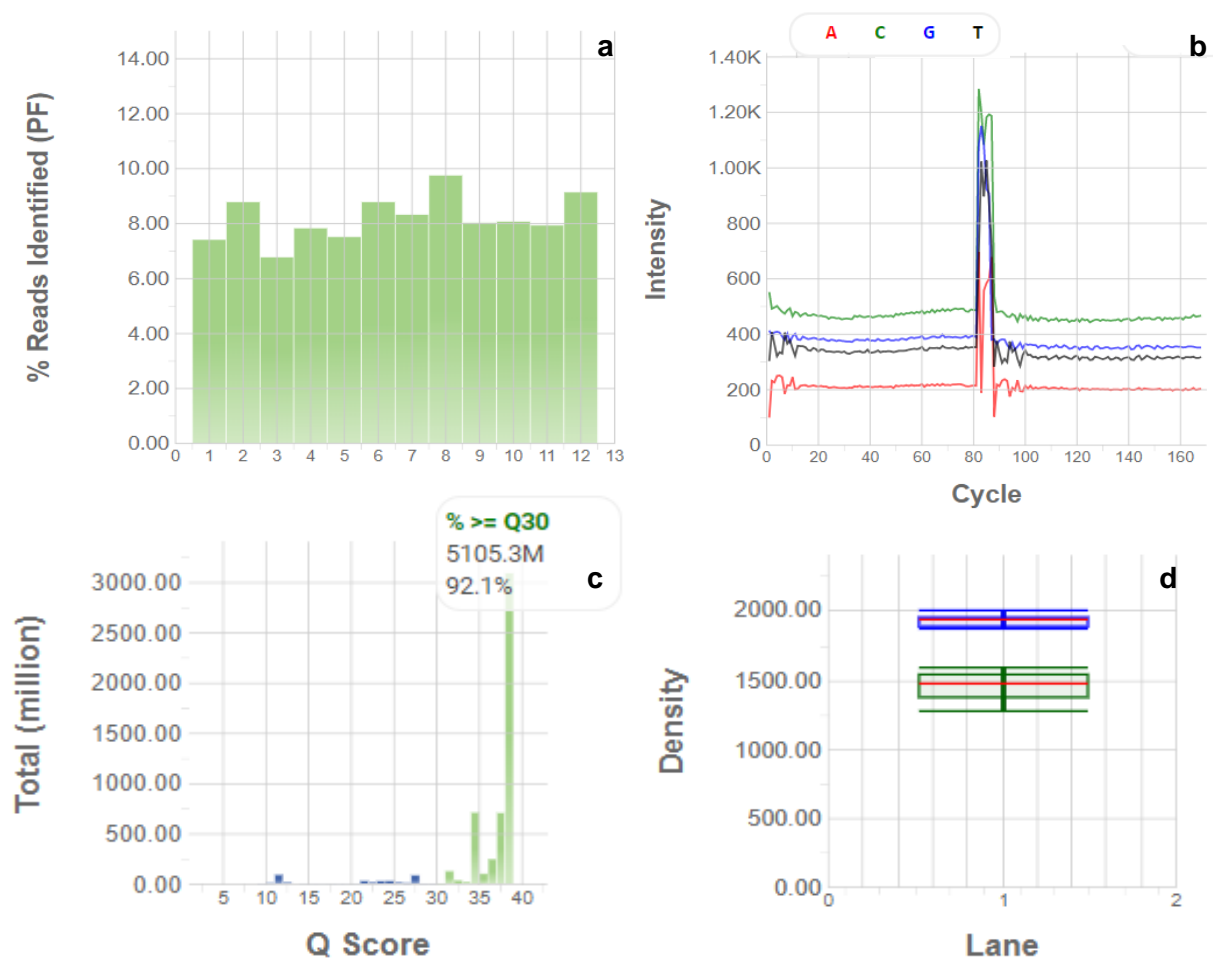


Figure A. 5. Results of the sequencing run (81 bp paired-end) using a MiSeq Illumina sequencer. a) Reads per sample passing filter (PF), b) nucleotide intensity by cycle, c) QScore distribution and d) cluster density passing filter (green box plot).

Table A. 3. Summary of results of the sequencing run (300 bp paired-end) for differential transcriptome analysis using a MiSeq Illumina sequencer.

Parameter	Value
Yield (Gbp)	2.75
% \geq Q30	78.38
Error rate (%)	2.72
Reads passing filter (PF)	9 116 486
Cluster density (k mm ⁻²)	182

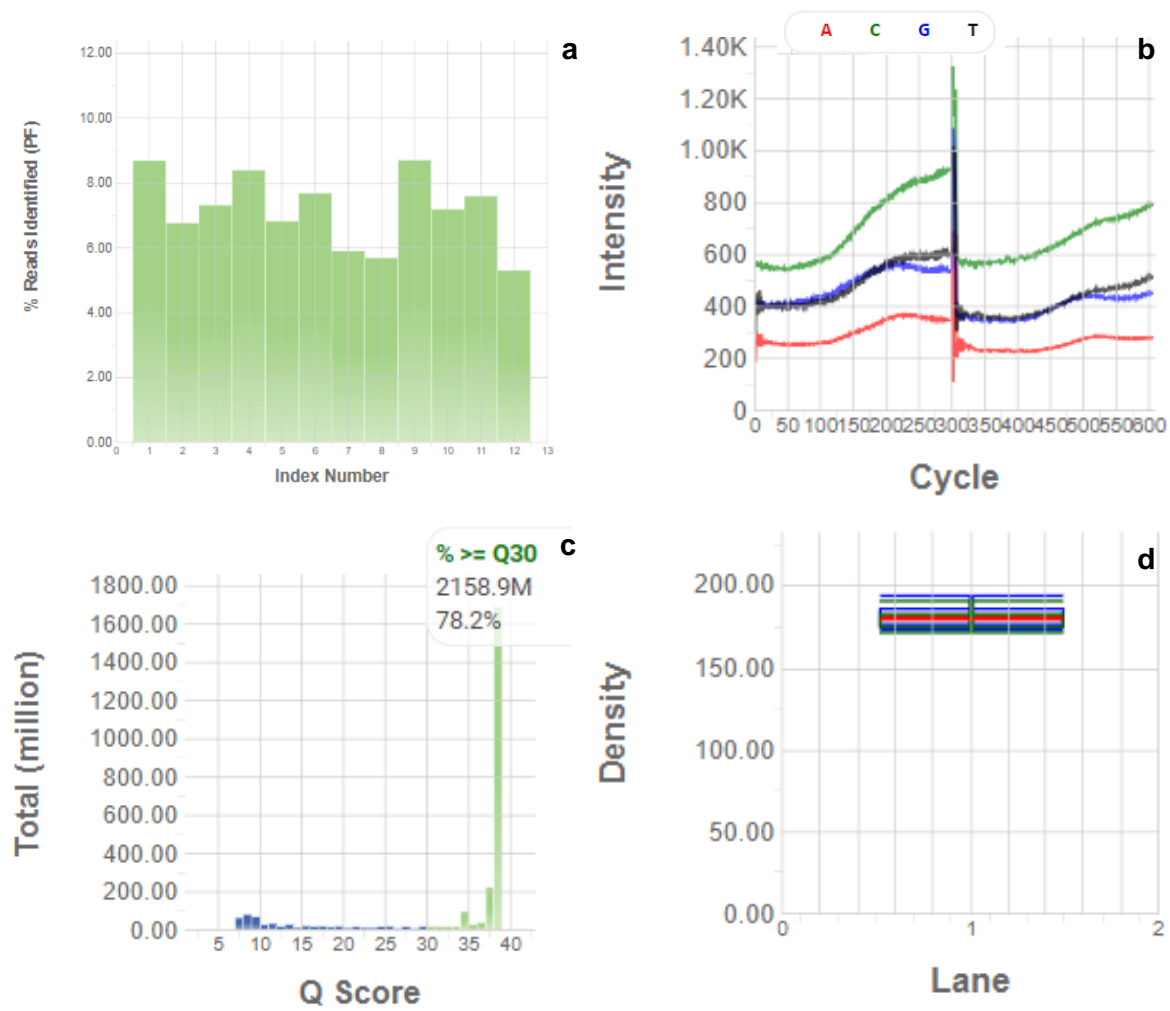


Figure A. 6. Results of the sequencing run (300 bp paired-end) using a MiSeq Illumina sequencer. a) Reads per sample passing filter (PF), b) nucleotide intensity by cycle, c) QScore distribution and d) cluster density passing filter (green box plot).

Appendix C

6.6 *de novo* assembly and functional annotations

Table A. 4. Species protein sequences used to generate the two databases for transcriptome BLAST analysis. Database 1 constructed with the blast top-hit species reported for *Scenedesmus acutus* (Sirikhachornkit *et al.*, 2018) plus *S. quadricauda* and *A. thaliana* and database 2 blast top-hit species for *Dunaliella tertiolecta* (Shin *et al.*, 2015, Rismani-Yazdi *et al.*, 2011) plus other algae, bacteria and plants.

Database 1	Database 2		
	Algae	Bacteria	Plants
<i>Monoraphidium neglectum</i>	<i>Chlamydomonas eustigma</i>	<i>Synechococcus elongatus</i>	<i>Populus trichocarpa</i>
<i>Chlamydomonas reinhardtii</i>	<i>Helicosporidium</i>	<i>Leptolyngbya boryana</i>	<i>Ricinus communis</i>
<i>Volvox carteri f. nagariensis</i>	<i>Micromonas pusilla</i>	<i>Arthrospira platensis</i>	<i>Physcomitrella patens</i>
<i>Coccomyxa subellipsoidea</i> C-169	<i>Ostreococcus sp</i> "lucimarinus"	<i>Anabaena cylindrica</i>	<i>Zea mays</i>
<i>Chlorella variabilis</i>	<i>Raphidocelis subcapitata</i>	<i>Marinobacter algicola</i>	<i>Selaginella moellendorffii</i>
<i>Auxenochlorella</i> <i>protothecoides</i>	<i>Tetraabaena socialis</i>	<i>Streptomyces hygrosopicus</i>	<i>Vitis vinifera</i>
<i>Klebsormidium nitens</i>	<i>Micractinium conductrix</i>	<i>Kordia aglicida</i>	<i>Medicago truncatula</i>
<i>Arabidopsis thaliana</i>	<i>Micromonas commoda</i>	<i>Pseudomonas fluorescens,</i> <i>putida</i>	<i>Glycine max</i>
<i>Scenedesmus quadricauda</i>	<i>Gonium pectoral</i>	<i>Algoriphagus marincola</i>	<i>Malus domestica</i>
<i>Candida orthopsilosis</i>	<i>Bathycoccus prasinus</i>	<i>Roseobacter denitrificans</i>	<i>Morus notabilis</i>
<i>Candida parapsilosis</i>	<i>Ostreococcus tauri</i>	<i>Pontibacter actinariium</i>	<i>Theobroma cacao</i>
<i>Candida parapsilosis</i>	<i>Phaeodactylum tricorutum</i>	<i>Prunus persica</i>	
	<i>Emiliana huxleyi</i>	<i>Marinobacter sp</i>	
	<i>Ectocarpus siliculosus</i>	<i>Streptomyces sp</i>	
	<i>Thalassiosira pseudonana</i>		
	<i>Nannochloropsis gaditana</i>		
	<i>Guillardia theta</i>		
	<i>Gracilaria chorda</i>		
	<i>Porphyra umbilicalis (laver)</i>		
	<i>Chondrus crispus</i> (carrageen)		
	<i>Thalassiosira pseudonana</i>		
	<i>Galdieria sulphuraria</i>		
	<i>Dunaliella viridis</i>		
	<i>Dunaliella salina</i>		

Table A. 5. Sample paired read mapping to the *de novo* transcriptome of *D. abundans* using CLC Workbench Genomics 11.0.

Strain->Gas supply	Replicate	Paired read count	Paired, mapped pairs (%)	Paired, broken pairs (%)	Paired, not mapped (%)	Total mapping (%)
HCA->MFG	1	6 032 308	78.13	12.91	8.96	91.04
	2	4 959 820	77.66	14.35	7.99	92.01
	3	5 494 488	75.24	16.10	8.66	91.34
LCA->MFG	1	4 896 498	81.38	10.35	8.27	91.73
	2	6 473 456	79.63	12.16	8.21	91.79
	3	5 303 742	78.51	13.16	8.33	91.67
LCA->Air	1	4 473 498	80.35	11.44	8.21	91.79
	2	5 170 916	78.32	13.17	8.51	91.49
LCA-> CO ₂	1	5 324 042	82.35	9.44	8.21	91.79
	2	5 235 358	79.05	12.48	8.47	91.53
LCA-> CO ₂ +CKD	1	5 798 184	81.53	9.79	8.68	91.32
	2	5 801 322	78.88	12.65	8.47	91.53

Bibliography

- APHA-AWWA-WEF. (2012). Standard Methods for the Examination of Water and Wastewater. Washington, D.C. Recovered from https://www.mwa.co.th/download/file_upload/SMWW_4000-6000.pdf
- Aslam, A., Thomas-Hall, S., Mughal, T. and Schenk, P. (2017). Selection and adaptation of microalgae to growth in 100% unfiltered coal-fired flue gas. *Bioresource Technology*, 233, 271-283. DOI 10.1016/j.biortech.2017.02.111
- Becker, EW. 1994. *Microalgae: biotechnology and microbiology*. Cambridge University Press. Cambridge, UK.
- Camargo, E. and Lombardi, A. (2017). Effect of cement industry flue gas simulation on the physiology and photosynthetic performance of *Chlorella sorokiniana*. *J Appl Phycol*. DOI 10.1007/s10811-017-1291-3
- CEMEX. (2017). CEMEX Annual Report. Recovered from <https://www.cemex.com/es/web/guest/sostenibilidad/reportes/reportes-globales>
- Cheban, L., Malischuk, I. and Marchenko, M. (2015). Cultivating *Desmodesmus armatus* (Chod.) Hegew. in recirculating aquaculture systems (RAS) waste water. *Arch. Pol. Fish*, 23, 155–162. DOI 10.1515/aopf-2015-0018
- Cheng, Y., Labavitch, J. and Gheynst, J. (2014). Elevated CO₂ concentration impacts cell wall polysaccharide composition of green microalgae of the genus *Chlorella*. *Letters in Applied Microbiology*. DOI 10.1111/lam.12320
- Chung, T.-Y., Kuo, C.-Y., Lin, W.-J., Wang, W.-L. and Chou, J.-Y. (2018). Indole-3-acetic-acid-induced phenotypic plasticity in *Desmodesmus* algae. *Scientific Reports*, 1–13. <http://doi.org/10.1038/s41598-018-28627-z>
- Conesa, A., Götz, S., García-Gómez, J.M., Terol, J., Talón, M. and Robles, M. (2005). Blast2GO: a universal tool for annotation, visualization and analysis in functional genomics research. *Bioinformatics*, 21(18), 3674-3676. DOI 10.1093/bioinformatics/bti610

- Cuellar-Bermudez, A., Garcia-Perez, J. and Rittman, B. (2015). Photosynthetic bioenergy utilizing CO₂: an approach on flue gases utilization for third generation biofuels. *Journal of Cleaner Production*, 98, 53-65. DOI doi.org/10.1016/j.jclepro.2014.03.034
- Dincer, I., Ozgur, C., & Kadioglu, F. (2013). *Causes, Impacts and Solutions to Global Warming*. Springer. New York, USA.
- Duong, V. T., Ahmed, F., Thomas-Hall, S. R., Quigley, S., Nowak, E., and Schenk, P. M. (2015). High protein- and high lipid-producing microalgae from northern australia as potential feedstock for animal feed and biodiesel. *Frontiers in Bioengineering and Biotechnology*, 3(53). DOI 10.3389/fbioe.2015.00053
- El Smary, N. (2011). The polyphasic description of a *Desmodesmus* spp. Isolate with the potential of bioactive compounds production. *Biotechnol. Agron. Soc. Environ.*, 15(2), 231-238. <https://popups.uliege.be:443/1780-4507/index.php?id=7173>.
- El-Sheekh, M., Eladel, H., Battah, M. and Abd-Elal, S. (2015). *Effect of different nitrogen sources on growth and biochemical composition of the green microalgae Scenedesmus obliquus and Chlorella kessleri*. Botany Department, Faculty of Science, Tanta University and Zagazig University. Recovered from https://www.researchgate.net/publication/269518929_Effect_of_different_nitrogen_sources_on_growth_and_biochemical_composition_of_the_green_microalgae_Scenedesmus_obliquus_and_Chlorella_kessleri
- Emanuelsson, O., Nielsen, H., Brunak, S. and Von Heijne, G., 2000. Predicting subcellular localization of proteins based on their N-terminal amino acid sequence. *Journal of molecular biology*, 300(4), 1005-1016. DOI 10.1006/jmbi.2000.3903
- Fan, J., Xu, H., Luo, Y., Wan, M., Huang, J. Wang, W. and Li, Y. (2015). Impacts of CO₂ concentration on growth, lipid accumulation, and carbon-concentrating-mechanism-related gene expression in oleaginous *Chlorella*. *Appl Microbiol. Biotechnol.*, 99, 2451-2462. DOI 10.1007/s00253-015-6397-4

- Fan, J., Ye, J., Kamphorst, J.J., Shlomi, T., Thompson, C.B. and Rabinowitz, J.D. (2014). Quantitative flux analysis reveals folate-dependent NADPH production. *Nature*, 510 (7504), 298–302.
- García-Cubero, R., Moreno-Fernández, J. and García-González, M. (2017). Modelling growth and CO₂ fixation by *Scenedesmus vacuolatus* in continuous culture. *Algal Research*, 333-339. DOI 10.1016/j.algal.2017.04.018
- Garibay-Hernández, A., Vázquez, R., Sánchez, P., Serrano, L. and Martínez, A. (2009). Biodiesel a partir de microalgas. *BioTecnología*, 13(3), 38–61. https://www.researchgate.net/publication/268207621_Biodiesel_a_partir_de_microalgas
- Gaur, V., Qureshi, I., Singh, A., Chanana, V. and Salunke, D. (2010). Crystal Structure and Functional Insights of Hemopexin Fold Protein from Grass Pea. *Plant Physiology*, 152, 1842-1850. DOI 10.1104/pp.109.150680
- Ghosh, A., Khanra, S., Mondal, M., Halder, G., Tiwari, O. N., Saini, S., Bhowmick, T-K. and Gayen, K. (2016). Progress toward isolation of strains and genetically engineered strains of microalgae for production of biofuel and other value-added chemicals: A review. *Energy Conversion and Management*, 113, 104–118. DOI 10.1016/j.enconman.2016.01.050
- Giordano, M. and Raven, J. (2014). Nitrogen and sulfur assimilation in plants and algae. *Aquatic Botany*, 118, 45-61. DOI 10.1016/j.aquabot.2014.06.012
- Global Carbon ATLAS (GCA). (2017). CO₂ emissions. Recovered from [http://www.globalcarbonatlas.org/en/CO₂-emissions](http://www.globalcarbonatlas.org/en/CO2-emissions)
- Gowik, U., and Westhoff, P. (2011). The Path from C3 to C4 Photosynthesis. *Plant Physiology*, 155:56-63. DOI 10.1104/pp.110.165308
- Guo, Y., Yuan., Xu, J., Wang, Z., Yuan, T., Zhou, W., Xu, J., Liang, G., Xu, H. and Liu, S. (2017). Metabolic acclimation mechanism in microalgae developed for CO₂ capture from industrial flue gas. *Algal Research*, 225-233. DOI 10.1016/j.algal.2017.07.029

- Hegewald, E. and Braband, (2017). A taxonomic revision of *Desmodesmus* serie *Desmodesmus* (Sphaeropleales, Scenedesmaceae). *Fottea, Olomouc*, 17(2), 191-208. DOI 10.5507/fot.2017.001
- Honaas, L., Wafula, E., Wickett, N., Der, J., Zhang, Y., Edger, P., Altman, N., Pires, J., Leebens-Mack, H. and dePamphilis, C. (2016). Selecting Superior *De Novo* Transcriptome Assemblies: Lessons Learned by Leveraging the Best Plant Genome. *PLOS ONE*, 11(1), e0146062. DOI 10.1371/journal.
- Huang, Y., Cheng, J., Lu, H., He, Y., Zhou, J. and Cen, K. (2017). Transcriptome and key genes expression related to carbon fixation pathways in *Chlorella* PY-ZU1 cells and their growth under high concentrations of CO₂. *Biotechnol Biofuels*, 10(181). DOI 10.1186/s13068-017-0868-z
- Huang, Y., Niu, B., Gao, Y., Fu, L. and Li, W. (2010). CD-HIT Suite: a web server for clustering and comparing biological sequences. *Bioinformatics*; 26(5). DOI 10.1093/bioinformatics/btq003
- IEA. (2016). CO₂ emissions from fuel combustion. Recovered from https://www.iea.org/publications/freepublications/publication/CO2EmissionsfromFuelCombustion_Highlights_2016.pdf
- Ito, T., Tanaka, M., Shinkawa, H., Nakada, T., Ano, Y., Kurano, N., Soga, T. and Tomita, M. (2013). Metabolic and morphological changes of an oil accumulating trebouxioephycean alga in nitrogen-deficient conditions. *Metabolomics*, 9, S178-S187. DOI 10.1007/s11306-012-0463-z
- Jiang, Y., Zhang, W., Wang, J., Chen, Y., Shen, S. and Liu, T. (2012). Utilization of simulated flue gas for cultivation of *Scendesmus dimorphus*. *Bioresource Technology*, 128, 359-364. DOI 10.1016/j.biortech.2012.10.119
- Johnson, M.T., Carpenter, E.J., Tian, Z., Bruskiwich, R., Burris, J.N., Carrigan, C.T., Chase, M.W., Clarke, N.D., Covshoff, S., Edger, P.P. and Goh, F. (2012). Evaluating methods for isolating total RNA and predicting the success of sequencing phylogenetically diverse

- plant transcriptomes. *PLoS one*, 7(11), p.e50226. DOI 10.1371/journal.pone.0050226.g001
- Kanehisa, M. and Goto, S. (2000). KEGG: kyoto encyclopedia of genes and genomes. *Nucleic acids research*, 28(1), pp.27-30. <https://www.ncbi.nlm.nih.gov/pmc/articles/PMC102409/pdf/gkd027.pdf>
- Katsube-Tanaka, T., Khan, N., Yamaguchi, S., Yamaguchi, T. and Iida, S. (2016). Glutelin is partially degraded in globulin-less mutants of rice (*Oryza sativa* L.). *Plant Production Science*, 19(3), 401-410. DOI: 10.1080/1343943X.2016.1168705
- Kim, S., Liu, K., Lee, S., Hong, S., Cho, B., Lee, H., Lee, C. and Choi, H. (2013). Effects of Light Intensity and Nitrogen Starvation on Glycerolipid, Glycerophospholipid, and Carotenoid Composition in *Dunaliella tertiolecta* Culture. *PLoS ONE*, 8(9), e72415. DOI 10.1371/journal.pone.0072415
- Koehler, P. and Wieser. (2013). Chapter 2, Chemistry of Cereal Grains. M. Gobbetti and M. Gänzle (eds.). *Handbook on Sourdough Biotechnology*. Springer Science+Business Media, New York. 11-45 pp. DOI 10.1007/978-1-4614-5425-0_2
- Kong, F., Romero, I., Warakanont, J. and Li-Beisson, Y. (2018). Lipid catabolism in microalgae. *New Phytologist*, 218, 1340-1348. DOI 10.1111/nph.15047
- Lara-Gil, J. A., Álvarez, M. M., and Pacheco, A. (2014). Toxicity of flue gas components from cement plants in microalgae CO₂ mitigation systems. *Journal of Applied Phycology*, 26(1), 357–368. DOI 10.1007/s10811-013-0136-y
- Lara-Gil, J. A., Senés-Guerrero, C., and Pacheco, A. (2016). Cement flue gas as a potential source of nutrients during CO₂ mitigation by microalgae. *Algal Research*, 17, 285–292. DOI 10.1016/j.algal.2016.05.017
- Li, S., Xu, J., Chen, J., Chen, J., Zhou, C. and Yan, X. (2014). The major lipid changes of some important diet microalgae during the entire growth phase. *Aquaculture*, 104-110. DOI 10.1016/j.aquaculture.2014.02.032

- Lichtenthaler, H. K. (1987). Chlorophylls and carotenoids: Pigments of photosynthetic biomembranes. *Plant Cell Membranes*, 350–382. DOI 10.1016/0076-6879(87)48036-1
- Long-range Transboundary (LRTAP) and European Environment Agency (EEA). Cement production. ISSN 1725-2237
- López, A., Schauble, S., Valenzuela, J., Imam, S., Carter, W., Bilgin, D., Yohn, C., Turkarslan, S., Reiss, D., Orellana, M., Price, N. and Baliga, N. (2015). Transcriptional program for nitrogen starvation-induced lipid accumulation in *Chlamydomonas reinhardtii*. *Biotechnology for Biofuels*, 8(207). DOI 10.1186/s13068-015-0391-z
- Lu, S., Wang, J., Ma, Q., Yang, J., Li, X. and Yuan, Y. (2013). Phospholipid Metabolism in an Industry Microalga *Chlorella sorokiniana*: The Impact of Inoculum Sizes. *PLOS ONE*, 8(8), e70827. DOI 10.1371/journal.pone.0070827
- Maehre, H., Dalheim, L., Edvinsen, G., Elvevoll, E. and Jensen, I. (2018). Protein Determination-Method Matters. *Foods*, 7(5). DOI 10.3390/foods7010005
- Malerba, M. E., Heimann, K., and Connolly, S. R. (2016). Nutrient utilization traits vary systematically with intraspecific cell size plasticity. *Functional Ecology*, 30(11), 1745–1755. <http://doi.org/10.1111/1365-2435.12662>
- Mansfeldt, C., Richter, L., Ahner, B., Cochlan, W. and Richardson, R. (2016). Use of *de novo* transcriptome libraries to characterize a novel oleaginous marine *Chlorella* species during the accumulation of triacylglycerols. *PLOS ONE*, 11(2), e0147527. DOI 10.1371/journal.pone.0147527
- Martínez García, L. (2012). *Eliminación de CO₂ con microalgas autóctonas*. Thesis presented to obtain the Doctor's degree. Universidad de León, México. Recovered from <https://buleria.unileon.es/bitstream/handle/10612/1414/2008ON-MART%25CDNEZ%20GARC%25CDA%2C%20LORENA.pdf?sequence=1>
- Matich, E., Camgoz, E., Caliskan, E., Pfeifer, B., Haznedaroglu, B. and Atilla-Gokcumen, G. (2018). Time-series lipidomic analysis of the oleaginous green microalga species *Ettlia oleoabundans* under nutrient. *Biotechnology for biofuels*, 11(29). DOI 10.1186/s13068-018-1026-y

- Matusiak-Mikulín, K., Tukaj, C. and Tukaj, Z. (2007). Relationships between growth, development and photosynthetic activity during the cell cycle of *Desmodesmus armatus* (Chlorophyta) in synchronous cultures. *European Journal of Phycology*, 41(1), 29-38. DOI 10.1080/09670260500502521
- Matyash, V., Liebisch, G., Kurzchalia, T., Shevchenko, A. and Schwudke, D. (2008). Lipid extraction by methyl-tert-butyl ether for high-throughput lipidomics. *Journal of Lipid Research*, 49, 1137-1146. DOI 10.1194/jlr.D700041-JLR200
- Medina, M. (2006). Análisis de Alimentos: Extracto etéreo. Departamento de Tecnología de Alimentos. Universidad Central de Venezuela. Recovered from <http://www.ciens.ucv.ve:8080/generador/sites/mmedina/archivos/ Practica9.pdf>
- Min, K., Lin, H. and Kun, Y. (2016). Nitrogen-induced metabolic changes and molecular determinants of carbon allocation in *Dunaliella tertiolecta*. *Scientific reports*. DOI 10.1038/srep37235
- Moroney, J. V., and Ynalvez, R. A. (2007). Proposed carbon dioxide concentrating mechanism in *Chlamydomonas reinhardtii*. *Eukaryotic Cell*, 6(8), 1251–1259. DOI 10.1128/EC.00064-07
- Muradyan, E., Klyachko-Gurvich, G., Tsoglin, L., Sergeyenko, T. and Pronina, N. (2004) Changes in lipid metabolism during adaptation of the *Dunaliella salina* photosynthetic apparatus to high CO₂ concentration. *Rus. J. Plant Physiol.*, 51, 53–62.
- Nelson, N. and Yocum, C. (2006). Structure and Function of Photosystems I and II. *Annu. Rev. Plan. Biol.*, 57, 521-65. DOI 10.1146/annurev.arplant.57.032905.105350
- Niu, Y. F., Zhang, M. H., Li, D. W., Yang, W. D., Liu, J. S., Bai, W. Bin, and Li, H. Y. (2013). Improvement of neutral lipid and polyunsaturated fatty acid biosynthesis by overexpressing a type 2 diacylglycerol acyltransferase in marine diatom *Phaeodactylum tricornutum*. *Marine Drugs*, 11(11), 4558–4569. DOI 10.3390/md11114558
- NOAA. (2016). *Trends in Atmospheric Carbon Dioxide*. Recovered from <https://www.esrl.noaa.gov/gmd/aggi/>

- Olofsson, M., Lindehoff, E., Svensson, F. and Legrand, C. (2015). Baltic Sea microalgae transform cement flue gas into valuable biomass. *Algal Research*, 11:227-233. DOI 10.1016/j.algal.2015.07.001
- Osborne, T.B. (1895). The proteins of barley 1. *Journal of the American Chemical Society*, 17, 539–567. DOI 10.1021/ja02162a008
- Ozturk, B., Asikkutlu, B., Akkoz, C. and Aitici, T. (2018). Molecular and Morphological Characterization of Several Cyanobacteria and Chlorophyta Species Isolated from Lakes in Turkey. *Turk. J. Fish. & Aquat. Sci.*, 19(8). DOI 10.4194/1303-2712-v19_8_01
- Pancha, I., Chokshi, K., George, B., Ghosh, T., Paliwal, C., Maurya, R. and Mishra, S. (2014). Nitrogen stress triggered biochemical and morphological changes in the microalgae *Scenedesmus* sp. CCNM 1077. *Bioresource Technology*, 156, 146-154. DOI 10.1016/j.biortech.2014.01.025
- Patil, L. and Kaliwal, B. (2017). Effect of CO₂ Concentration on Growth and Biochemical Composition of Newly Isolated Indigenous Microalga *Scenedesmus bajacalifornicus* BBKLP-07. *Appl. Biochemical Biotechnol.*, 182, 335-348. DOI 10.1007/s12010-016-2330-2
- PBL Netherlands Environmental Assessment Agency. (2011). Long-term trend in global CO₂ emissions, report. Recovered from http://edgar.jrc.ec.europa.eu/news_docs/C02%20Mondiaal_%20webdef_19sept.pdf
- Perrineau, M., Gross, J., Zelzion, E., Price, D., Levitan, O., Boyd, J. and Bhattacharya, D. (2014). Using Natural Selection to Explore the Adaptive Potential of *Chlamydomonas reinhardtii*. *PLOS ONE*, 9(3), e92533. DOI 10.1371/journal.pone.0092533
- Pessaraki, M. (2016). *Handbook of Photosynthesis*. CRC Press Taylor & Francis Group. Florida, USA. 385-388 pp.
- Ramanan, R., Vinayagamoorthy, N., Sivanesan, S. D., Kannan, K., and Chakrabarti, T. (2012). Influence of CO₂ concentration on carbon concentrating mechanisms in cyanobacteria and green algae: a proteomic approach. *Algae*, 27(4), 295–301. DOI 10.4490/algae.2012.27.4.295

- Randmann, E. M., Vieira, F., Duarte, T. and Vieira, J. A. (2011). Isolation and application of SO_x and NO_x resistant microalgae in biofixation of CO₂ from thermoelectricity plants. *Energy Conversion and Management*, 52(10), 3132-3126. DOI 10.1016/j.enconman.2011.04.021
- Rismani-Yazdi, Haznedaroglu, B., Bibby, K. and Peccia, J. (2011). Transcriptome sequencing and annotation of the microalgae *Dunaliella tertiolecta*: Pathway description and gene discovery for production of next-generation biofuels. *BMC Genomics*, 12, 148. <http://www.biomedcentral.com/1471-2164/12/148>
- Shahidi, F. (2003). Extraction and measurement of total lipids. *Curren Protocols in Food Analytical Chemistry*, 7(1), D1.1.1–D1.1.11. DOI 10.1002/0471142913.fad0101s07
- Shahzad, U. (2015). Global warming: Causes, effects and solutions. *Durreesamin Journal*, 1(4).
- Shin, H., Hong, S., Kim, H., Yoo, C., Lee, H., Choi, H., Lee, C. and Cho, B. (2015). Elucidation of the growth delimitation of *Dunaliella tertiolecta* under nitrogen stress by integrating transcriptome and peptidome analysis. *Bioresource Technology*, 194, 57-66. DOI 10.1016/j.biortech.2015.07.002
- Simão, F. A., Waterhouse, R. M., Ioannidis, P., Kriventseva, E. V. and Zdobnov, E. M. (2015). BUSCO: assessing genome assembly and annotation completeness with single-copy orthologs. *Bioinformatics*, 31, 3210–2. DOI 10.1093/bioinformatics/btv351
- Sirikhachornkit, A., Suttangkakul, A., Vuttipongchaikij, S. and Juntawong, P. (2018). De novo transcriptome analysis and gene expression profiling of an oleaginous microalga *Scenedesmus acutus* TISTR8540 during nitrogen deprivation-induced lipid accumulation. *Scientific reports*, 8, 3668. DOI 10.1038/s41598-018-22080-8
- Solovchenko, A. and Khozin-Goldberg, I. (2013). High-CO₂ tolerance in microalgae: Possible mechanisms and implications for biotechnology and bioremediation. *Biotechnology Letters*, 35(11), 1745–1752. DOI 10.1007/s10529-013-1274-7
- Solovchenko, A., Gorelova, O., Selyakh, I., Pogosyan, S., Baulina, O., Semenova, L., Chivkunova, O., Voronova, E., Konyukhov, I., Scherbakov, P. and Lobakova, E. (2015). A novel CO₂-tolerant symbiotic *Desmodesmus* (Chlorophyceae, Desmodesmaceae): Acclimation to

- and performance at a high carbon dioxide level. *Algal Research*, 11, 399-410. DOI 10.1016/j.algal.2015.04.011
- Sun, H., Mao, X., Li, Y., Wu, T. and Chen, F. (2018). High-value biomass from microalgae production platforms: strategies and progress based on carbon metabolism and energy conversion. *Biotechnol. Biofuels*, 11, (227). DOI 10.1186/s13068-018-1225-6
- Sun, Z., Chen, Y. F., and Du, J. (2016). Elevated CO₂ improves lipid accumulation by increasing carbon metabolism in *Chlorella sorokiniana*. *Plant Biotechnology Journal*, 14(2), 557–566. DOI 10.1111/pbi.12398
- Suzuki, S., Yamaguchi, H., Nakajima, N. and Kawachi, M. (2018). *Raphidocelis subcapitata* (= *Pseudokirchneriella subcapitata*) provides an insight into genome evolution and environmental adaptations in the Sphaeropleales. *Scientific reports*. DOI 10.1038/s41598-018-26331-6
- Talec, A., Philistin, M., Ferey, F., Walenta, G., Irisson, J., Bernard, O. and Sciandra, A. (2013). Effect of gaseous cement industry effluents on four species of microalgae. *Bioresource Technology*, 143, 353-359. DOI 10.1016/j.biortech.2013.05.104
- Valenzuela J; Mazurie, A. Carlson, R., Gerlach, R., Cooksey, K., Peyton., B., and Fields, M. W. (2012). Potential role of multiple carbon fixation pathways during lipid accumulation in *Phaeodactylum tricornutum*. *Biotechnology For Biofuels*, 5, 40. DOI 10.1186/1754-6834-5-40
- Van Den Hende, S., Vervaeren, H. and Boon, N. (2012). Flue gas compounds and microalgae: (Bio-)chemical interactions leading to biotechnological opportunities. *Biotechnology advances*, 30, 1405-1424. DOI 10.1016/j.biotechadv.2012.02.015
- Van Eynde, E., Lenaers, B., Tytgat, T., Blust, R. and Lenaerts, S. (2016). Valorization of Flue gas by combining Photocatalytic Gas Pretreatment with Microalgae Production. *Environ. Sci. Technol.*, 50(5), 2538-2545. DOI 10.1021/acs.est.5b04824
- Van Oss, H., and Padovani, A. (2003). Cement manufacture and the environment - part II: environmental challenges and opportunities, *J. Ind. Ecol.*, 7(1), 93–126. DOI 10.1162/108819803766729212.

- Wang, C., Guo, L., Li., and Wang, Z. (2012). Systematic Comparison of C3 and C4 Plants Based on Metabolic Network Analysis. *BMC Biology*, 6(2):1-14. DOI 10.1186/1752-0509-6-S2-S9
- WBSCD. (2012). *Guidelines for Emissions Monitoring and Reporting in the Cement Industry. Emissions Monitoring and Reporting. Version 2.0.* Recovered from https://www.wbcsdcement.org/pdf/CSI_TF4%20Emissions%20monitoring_Web.pdf
- Westerhoff, P., Hu, Q., Espaza-Soto, M. and Vermaas, W. (2013). Growth parameters of microalgae tolerant to high levels of carbon dioxide in batch and continuous-flow photobioreactors, *Environmental Technology*, 31(5), 523-532. DOI 10.1080/09593330903552078
- Wickham, H. (2016). *ggplot2: Elegant Graphics for Data Analysis*. Springer-Verlag. New York.
- WMO and GAW. (2017). *WMO Greenhouse Gas Bulletin*. Recovered from <https://public.wmo.int/en/resources/library/wmo-greenhouse-gas-bulletin>
- Worrell, E., Price, L., Martin, N., Hendriks, C. and Meida, O. (2001). Carbon dioxide emission from global cement industry. *Annu. Rev. Energy. Environ.*, 26, 303-29. https://www.researchgate.net/publication/228756550_Carbon_Dioxide_Emission_from_the_Global_Cement_Industry/download
- Yang, D., Song, D., Kind, T., Ma, Y., Hoefkens, J. and Fiehn, O. (2015). Lipidomic Analysis of *Chlamydomonas reinhardtii* under Nitrogen and Sulfur Deprivation. *PLOS ONE*, 10(9), e0137948. DOI 10.1371/journal.pone.0137948
- Yang, S., Wang, J., Cong, W., Cai, Z. and Ouyang, F. (2004). Effects of bisulfite and sulfite on the microalga *Botryococcus braunii*, *Enzym. Microb. Technol.*, 35 (1), 46–50. DOI 10.1016/j.enzmictec.2004.03.014.
- Yao, L., Gerde, J. A., Lee, S. L., Wang, T., and Harrata, K. A. (2015). Microalgae lipid characterization. *Journal of Agricultural and Food Chemistry*, 63(6), 1773–1787. DOI 10.1021/jf5050603

-
- Yeh, T., Tseng, Y., Chen, Y., Hsiao, Y., Lee, P., Chen, T., Chen, C., Kao, C., Chang, J., Chen, J. and Lee, T. (2017). Transcriptome and physiological analysis of a lutein-producing alga *Desmodesmus sp.* reveals the molecular mechanisms for high lutein productivity. *Algal Research*, 21, 103-119. DOI 10.1016/j.algal.2016.11.013
- Zhang, Y., Chen, H, He, C. and Wang, Q. (2013). Nitrogen Starvation Induced Oxidative Stress in an Oil-Producing Green Alga *Chlorella sorokiniana* C3. *PLOS ONE*, 8(7), e69225. DOI 10.1371/journal.pone.0069225

Curriculum Vitae

Shirley María Mora Godínez

Biotechnology Engineer

Correo electrónico: shirleymora10@gmail.com

Academic history

- From 2013 to 2016 Biotechnology Engineering, Tecnológico de Costa Rica
- From 2017 to 2018 Master of Science in Biotechnology, Tecnológico de Monterrey

Professional experience

- From 2015 to 2016 Research assistant in Biotechnology Center, Tecnológico de Costa Rica, in the projects:
- “Caracterización de germoplasma de Ricinus communis de diferentes zonas de Costa Rica”*
 - “Establecimiento de un proceso de recolección, secado y ultrasonificación de la biomasa seca algal a partir de un proceso de Chlorella vulgaris”*
 - “Establecimiento de una colección de cepas de microalgas autóctonas con potencial comercial”*
- July to December 2016 Research stay in FEMSA Biotechnology Center, Tecnológico de Monterrey in the project *“Transcriptómica de una microalga clorofita adaptada a altas concentraciones de CO₂: Validación del transcriptoma de novo mediante RT-qPCR y caracterización de lípidos de valor comercial”*.
- 2017 to 2018 Student of Master in Tecnológico de Monterrey in the project *“Differential transcriptome and lipidome analysis of Desmodesmus abundans grown under a continuous flow of model cement flue gas in a photobioreactor”*.

Relevant experiences

- 2017 Assitance to XVII Congreso Nacional de Biotecnología y Bioingeniería, 25-30 de junio, Puerto Vallarta, México.
- 2018 Assitance to The 8th International Conference on Algal Biomass, Biofuels and Bioproducts, 11-13 June 2018, Seattle, WA, USA.

This document was typed in using Microsoft Word by Shirley María Mora Godínez.